MECHANICAL PROPERTIES, ELECTRICAL AND THERMAL CONDUCTIVITIES OF MULTI-WALL CARBON NANOTUBE-REINFORCED NATURAL RUBBER AND NITRILE RUBBER BLENDS

PATTANA KUESENG

**A THESIS SUBMITTED IN PARTIAL FULFILLMENT
OF THE REQUIREMENTS FOR
THE DEGREE OF DOCTOR OF PHILOSOPHY
(POLYMER SCIENCE AND TECHNOLOGY)
FACULTY OF GRADUATE STUDIES
MAHIDOL UNIVERSITY
2014**

Thesis
entitled

MECHANICAL PROPERTIES, ELECTRICAL AND THERMAL CONDUCTIVITIES OF MULTI-WALL CARBON NANOTUBE-REINFORCED NATURAL RUBBER AND NITRILE RUBBER BLENDS

……………………………….……
Mr. Pattana Kueseng
Candidate

……………………………………….
Assoc. Prof. Chakrit Sirisinha,
Ph.D.
Major advisor

……………………………………….
Assoc. Prof. Nittaya Rattanasom,
Ph.D.
Co-advisor

……………………………………….
Mr. Pongdhorn Sae-Oui,
Ph.D.
Co-advisor

……………………………….……
Assoc. Prof. Sombat Thanawan, Ph.D.,
Acting Dean
Faculty of Graduate Studies
Mahidol University

……………………………………...
Asst. Prof. Panya Sunintaboon,
Ph.D.
Chair
Doctor of Philosophy Program
in Polymer Science and Technology
Faculty of Science
Mahidol University

Thesis
entitled

MECHANICAL PROPERTIES, ELECTRICAL AND THERMAL CONDUCTIVITIES OF MULTI-WALL CARBON NANOTUBE-REINFORCED NATURAL RUBBER AND NITRILE RUBBER BLENDS

was submitted to the Faculty of Graduate Studies, Mahidol University
for the degree of Doctor of Philosophy (Polymer Science and Technology)
on
June 2, 2014

..……………………………….………...
Mr. Pattana Kueseng
Candidate

…………………………….……….......
Assoc. Prof. Jatuphorn Wootthikanokkhan,
Ph.D.
Chair

…...…………………………….………
Assoc. Prof. Chakrit Sirisinha,
Ph.D.
Member

……………………………….……
Assoc. Prof. Nittaya Rattanasom,
Ph.D.
Member

…………………………….………….
Mr. Pongdhorn Sae-Oui,
Ph.D.
Member

……………………………….……
Assoc. Prof. Sombat Thanawan, Ph.D.,
Acting Dean
Faculty of Graduate Studies
Mahidol University

…………………..……………………
Prof. Skorn Mongkolsuk,
Ph.D.
Dean
Faculty of Science
Mahidol University

MECHANICAL PROPERTIES, ELECTRICAL AND THERMAL CONDUCTIVITIES OF MULTI-WALL CARBON NANOTUBE-REINFORCED NATURAL RUBBER AND NITRILE RUBBER BLENDS

PATTANA KUESENG 5238142 SCPO/D

Ph.D. (POLYMER SCIENCE AND TECHNOLOGY)

THESIS ADVISORY COMMITTEE: CHAKRIT SIRISINHA, Ph.D., NITTAYA RATTANASOM, Ph.D., PONGDHORN SAE-OUI, Ph.D.

ABSTRACT

In this research, the properties of 50/50 NR/NBR blends containing MWCNT/NR masterbatches prepared using the predispersing method (P) and conventional method (C) were studied. The amount of MWCNT in both blends was varied from 0 to 6 phr. Additionally, the properties of NR/NBR blends at various blend ratios prepared from the MWCNT/NR masterbatch (mNR) and MWCNT/NBR masterbatch (mNBR) were compared. The amount of MWCNT for both mNR and mNBR blends was kept constant at 4 phr. Furthermore, the properties of 50/50 NR/NBR blends filled with 4 phr of MWCNT, OH-MWCNT, and SiOH-MWCNT were determined.

The results show that modulus, tensile strength, tear strength, and electrical and thermal properties of the P blends are significantly higher than those of the C blends. This is simply due to the better MWCNT dispersion in the P blends. At 4 phr MWCNT, modulus, tensile strength, tear strength, and electrical conductivity of the P blend in the milling direction (MD) are higher than those of the corresponding transverse direction (TD) sample. Moreover, the anisotropic properties of the P blends are clearly observed when 4 phr MWCNT is loaded. This is because most of the MWCNTs in the P blends are aligned along the MD when MWCNT is not more than 4 phr as confirmed by dichroic ratio. Also, SEM images show that the number of MWCNT agglomerates increases when MWCNT is more than 4 phr.

It was also found that hardness, modulus, tensile strength, tear strength, oil resistance, and thermal and electrical conductivities of the mNR blends are superior to those of the corresponding mNBR blends. Additionally, the results show that 100% modulus, storage modulus at 30 ºC, tensile strength, tear strength, and electrical conductivity of both mNR and mNBR blends in MD are higher than those of the corresponding TD samples. Moreover, the 50/50 mNR blend gives the best overall properties. Furthermore, it can be seen that modulus, tensile strength, tear strength, and oil resistance of the 50/50 NR/NBR blend containing SiOH-MWCNT are greater than those containing OH-MWCNT and MWCNT. Also, 300% modulus, storage modulus at 30 ºC, tensile strength, tear strength, and electrical conductivity of these blends in MD are higher than those of the corresponding TD samples. However, modification of the MWCNT surface does not affect the electrical and thermal conductivities of the blends.

KEY WORDS: NR/NBR BLENDS/MULTI-WALL CARBON
NANOTUBE/MECHANICAL PROPERTIES/THERMAL
CONDUCTIVITY/ELECTRICAL CONDUCTIVITY

159 pages

สมบัติเชิงกล การนำไฟฟ้าและการนำความร้อนของยางผสมระหว่างยางธรรมชาติและยางไนไตรล์ที่มีคาร์บอนนาโนทิวบ์เป็นสารเสริมแรง

MECHANICAL PROPERTIES, ELECTRICAL AND THERMAL CONDUCTIVITIES OF MULTI-WALL CARBON NANOTUBE-REINFORCED NATURAL RUBBER AND NITRILE RUBBER BLENDS

พัฒนา เกื้อเส้ง 5238142 SCPO/D

ปร.ด. (วิทยาศาสตร์และเทคโนโลยีพอลิเมอร์)

คณะกรรมการที่ปรึกษาวิทยานิพนธ์: ชาคริต สิริสิงห, Ph.D., นิตยา รัตนโสม, Ph.D., พงษ์ธร แซ่อุย, Ph.D.

บทคัดย่อ

งานวิจัยนี้ได้ศึกษาสมบัติต่างๆของยางผสมระหว่างยางธรรมชาติและยางไนไตรล์ (NR/NBR) ที่สัดส่วนการผสม 50/50 โดยใช้มาสเตอร์แบชของยางธรรมชาติที่เตรียมจากวิธีการแตกตัว (P) และวิธีการผสมแบบดั้งเดิม (C) และทำการแปรปริมาณของ MWCNT ตั้งแต่ 0 ถึง 6 ส่วน ต่อยาง 100 ส่วน (phr) และได้เปรียบเทียบสมบัติต่างๆ ของยางผสม NR/NBR ที่สัดส่วนการผสมต่างๆ เมื่อเตรียมยางผสมจากมาสเตอร์แบช MWCNT/NR (mNR) และ MWCNT/NBR (mNR) นอกจากนี้ได้ศึกษาสมบัติต่างๆของยางผสมที่มี MWCNT, OH-MWCNT และ SiOH-MWCNT เป็นสารตัวเติม ในปริมาณ 4 phr ด้วย

ผลการทดลองแสดงให้เห็นว่า มอดูลัส ความทนต่อแรงดึง ความทนต่อการฉีกขาด สมบัติการนำความร้อนและการนำไฟฟ้า ของยางผสม P มีค่าสูงกว่ายางผสม C ที่มีปริมาณ CNT เท่ากัน เนื่องจากยางผสม P มีการกระจายตัวของ MWCNT ที่ดีกว่ายางผสม C และเมื่อเติม MWCNT ในปริมาณ 4 phr พบว่าค่ามอดูลัส ความทนต่อแรงดึง และความทนต่อการฉีกขาดของยางผสม P ในทิศตามแนวที่ยางถูกรีดออกจากลูกกลิ้ง (MD) มีค่าสูงกว่าของยางผสม P ในทิศตั้งฉากกับทิศที่ยางถูกรีดออกจากลูกกลิ้ง (TD) อีกทั้งพบว่ายางผสม P แสดงสมบัติแอนไอโซโทรปิคอย่างชัดเจนเมื่อปริมาณ MWCNT เท่ากับ 4 phr ทั้งนี้เนื่องจาก MWCNT ส่วนใหญ่เรียงตัวในทิศ MD เมื่อปริมาณ MWCNT ไม่เกิน 4 phr ซึ่งยืนยันได้ด้วยสัดส่วนไดโครอิก และภาพถ่ายจากเครื่องอิเล็กตรอนแบบส่องกราดแสดงให้เห็นว่าจำนวนของแอกโกลเมอเรตของ MWCNT เพิ่มขึ้นเมื่อเติม MWCNT ในปริมาณมากกว่า 4 phr

นอกจากนี้ยังพบว่า ความแข็ง มอดูลัส ความทนต่อแรงดึง ความทนต่อการฉีกขาด ความทนทานต่อน้ำมัน การนำความร้อนและการนำไฟฟ้า ของ mNR มีค่าสูงกว่าของ mNBR และการทดลองแสดงให้เห็นว่า 100% มอดูลัส มอดูลัสสะสมที่อุณหภูมิ 30 ºC ความทนต่อแรงดึงและความทนต่อการฉีกขาดของทั้ง mNR และ mNBR ในทิศ MD มีค่าสูงกว่าในทิศ อีกทั้งพบว่า mNR ที่สัดส่วนการผสม 50/50 ให้สมบัติโดยรวมดีที่สุด นอกจากนี้ยังเห็นได้ว่ามอดูลัส ความทนต่อแรงดึง ความทนต่อการฉีกขาด และความทนทานต่อน้ำมันของ 50/50 NR/NBR ที่มี SiOH-MWCNT เป็นสารตัวเติมมีค่าสูงกว่าในกรณีที่มี OH-MWCNT และ MWCNT เป็นสารตัวเติม อีกทั้งพบว่า 300% มอดูลัส มอดูลัสสะสมที่อุณหภูมิ 30 ºC ความทนต่อแรงดึง ความทนต่อการฉีกขาด และการนำไฟฟ้าของยางผสมเหล่านี้ ในทิศ MD มีค่าสูงกว่าในทิศ TD อย่างไรก็ตามการดัดแปรพื้นผิวของ MWCNT ไม่ส่งผลต่อการนำไฟฟ้าและการนำความร้อนของยางผสม

159 หน้า

CONTENTS

CONTENTS (cont.)

CONTENTS (cont.)

Page

CONTENTS (cont.)

CONTENTS (cont.)

CONTENTS

CONTENTS (cont.)

CONTENTS (cont.)

CONTENTS (cont.)

CONTENTS (cont.)

LIST OF FIGURES

LIST OF FIGURES (cont.)

LIST OF FIGURES (cont.)

LIST OF FIGURES (cont.)

LIST OF FIGURES (cont.)

LIST OF FIGURES (cont.)

LIST OF FIGURES (cont.)

LIST OF FIGURES (cont.)

LIST OF FIGURES (cont.)

LIST OF ABBREVIATIONS

CNT	Carbon nanotube
MWCNT	Multi-wall carbon nanotube
DWCNT	Double-wall carbon nanotube
SWCNT	Single -wall carbon nanotube
OH-MWCNT	Hydroxyl modified multi-wall carbon nanotube
SiOH-MWCNT	hydroxyl modified multi-wall carbon nanotube functionalized with Si-69
IPPD	N-isopropyl-N’-phenyl-p-phenylenediamine
TBBS	N-tert-butyl-benzothiazole sulfenamide
TBzTD	Tetrabenzylthiuram disulfide
TMTM	Tetramethylthiuram monosulphide
TBTD	Tetrabutylthiuram disulphide
MBTS	2,2'-benzothiazole disulphide
ODIP	N,N'-dioctadecyl N,N'-diisopropylthiuram disulphide
CVD	Chemical decomposition
PLV	Laser ablation
PS	Polystyrene
Si-69	Bis(3-triethoxysilylpropyl) tetrasulfide
Cu	Copper
CR	Polychloroprene rubber
CB	Carbon black
EtOH	Ethanol
EPDM	Ethylene propylene diene rubber
NR	Natural rubber
OsO4	Osmium tetroxide
SBR	Styrene butadiene rubber

LIST OF ABBREVIATIONS (cont.)

PAN	Polyacrylonitrile
PDMS	Polydimethylsiloxane
ZnO	Zinc oxide
IR	Isoprene rubber
IIR	Isobutylene isoprene rubber
NBR	Acrylonitrile butadiene rubber
HNBR	Hydrogenated acrylonitrile butadiene rubber
BR	Butadiene rubber
KBr	Potassium bromide
S_8	Sulfur
BIMS	Brominated isobutylene/p-methylstyrene copolymer
EMI	Electromagnetic interference
FTIR	Fourier transform infrared spectrometer
Tan δ	Damping factor
ρ	Volume resistivity
R	Dichroic ratio
DMTA	Dynamic mechanical thermal analysis
TMA	Thermomechanical analysis
AFM	Atomic force microscope
SEM	Scanning electron microscope
SIC	Strain-induced crystallization
DPG	Diphenyl guanidine
T_g	Glass transition temperature
MD	Machine direction
TD	Transverse direction

LIST OF ABBREVIATIONS (cont.)

mNR	NR/NBR blend containing MWCNT/NR masterbatch
mNBR	NR/NBR blend containing MWCNT/NBR masterbatch
P	50/50 NR/NBR blends containing MWCNT/NR masterbatches prepared by using predispersing method
C	50/50 NR/NBR blends containing MWCNT/NR masterbatches prepared by using conventional method
RPA	Rubber processing analyzer
ASTM	American society for testing and materials
t_{s2}	Scorch time
t_{c100}	Optimum cure time at 100% cure
MDR	Moving die rheometer
M_L	Minimum torque
M_H	Maximum torque
E'	Storage modulus

CHAPTER I
INTRODUCTION

Rubber blend is commercially important because it gives a balance of properties and cost which one rubber alone cannot provide [1]. In order to obtain the rubber having both good tensile strength and oil resistance, natural rubber (NR) and acrylonitrile butadiene rubber (NBR) are blended [2-4]. However, other mechanical properties such as tear strength and abrasion resistance have to be improved by adding reinforcing fillers [3-6]. Among reinforcing fillers, carbon nanotube (CNT) is currently attractive class of inclusions because of its excellent mechanical, thermal, and electrical properties [7, 8]. Thus, the incorporation of CNT into the rubber matrix is expected to obtain the rubber composites having the above properties [9-15]. Generally, carbon nanotube can be divided into three main types which are single-wall carbon nanotube (SWCNT), double-wall carbon nanotube (DWCNT) and multi-wall carbon nanotube (MWCNT). However, MWCNT is frequently used as reinforcing filler in the rubber composites because it gives higher electrical conductivity than other types of CNT. It is known that the degree of reinforcement is extremely dependent on the degree of filler dispersion [16-18]. Previous studies have shown that the dispersion of MWCNT in the rubber matrix is rather poor because MWCNT tend to form highly entangled agglomerates like felted thread leading to poor mechanical properties [16, 17]. However, it has been reported that the incorporation of MWCNT suspension, prepared by using ultrasonic process, into SBR/BR blends can enhance the degree of MWCNT dispersion [16, 18]. Therefore, SBR/BR blends filled with MWCNT prepared by using the above method give higher mechanical properties and electrical conductivity than those prepared by using conventional mixing method [16, 18]. In some cases, the improvement in mechanical properties of polymer composites reinforced with CNT is not remarkable due to poor adhesion which gives rise to lower stress transfer ability in the composites [19]. Recent report has been shown that modification of CNT surfaces by introducing carboxylic acid groups could provide better stabilization of CNT in polar solvents and covalently link polymers leading to improve the processability and mechanical properties of the NR composites [20]. In addition, the chemical functionalization of MWCNT using silane coupling agents has been studied by several researchers [17-19]. They found that treatment of the MWCNT surface with silane leads to improvement of modulus and tensile strength of the rubber composites [9, 21, 22]. This infers that the modification of MWCNT surfaces with silane can enhance polymer-filler interaction between the CNT and rubber matrix [9, 21, 22]. Additionally, the orientation of CNT in the polymer matrix can affect the properties of the composites. This is because CNT is considered as short fibers and CNT-filled polymer composites are always analogues of short-fiber composites [23]. Therefore, the theories for the strength and modulus of short fiber reinforced polymer composites can be extended to the case of CNT reinforced polymer composites [24]. Previous work has shown that addition of 5 %wt of MWCNT improves the storage modulus of polystyrene (PS) by 49% if MWCNT is oriented in one direction, while that of the random oriented MWCNT/PS composite increases by 10% [25].

In this research, well-dispersed MWCNT in NR/NBR blends was prepared by mixing the dispersed MWCNT suspension with the blends. Then, the morphology mechanical, dynamic mechanical, thermal and electrical properties of NR/NBR vulcanizates having various MWCNT contents and blend ratios are investigated. The effect of milling direction on tear strength, tensile, dynamic mechanical and electrical properties and of the vulcanizates is also studied. Additionally, the properties of 50/50 NR/NBR blends filled with hydroxyl modified MWCNT functionalized with silane coupling agent (Si-69) are compared with those of 50/50 NR/NBR blends filled with unmodified MWCNT and hydroxyl modified MWCNT.

CHAPTER II

OBJECTIVES

The main objectives of this research are as follow;

1. To study the morphology, mechanical, dynamic mechanical, thermal, electrical and dielectric properties of 50/50 NR/NBR vulcanizates having various MWCNT contents prepared from MWCNT/NR masterbatches

2. To determine the mechanical, dynamic mechanical, thermal and electrical properties of 4 phr MWCNT-filled NR/NBR vulcanizates at various blend ratios prepared from MWCNT/NR masterbatch and MWCNT/NBR masterbatch

3. To study the mechanical, dynamic mechanical, electrical and thermal properties of 50/50 NR/NBR vulcanizates filled with 4 phr SiOH-MWCNT and OH-MWCNT.

4. To investigate the effect of MWCNT alignment on tensile, tear, dynamic mechanical and electrical properties of various NR/NBR vulcanizates.

CHAPTER III

LITERATURE REVIEW

3.1 Natural rubber (NR)

Natural rubber (NR) is an elastomer that is commercially produced from *Hevea brasiliensis* tree [26]. It has been reported that NR is a high molecular weight polymer with a molecular weight of 10^4 to 10^6 [27]. The chemical structure of NR is cis 1,4-polyisoprene as shown in Figure 3.1. The double bond of NR in each isoprene unit can react with sulfur via vulcanization reaction [28]. Moreover, its double bond can react with oxygen and ozone leading to the degradation of NR [28]. Additionally, NR has poor oil resistance because its molecule contains only carbon and hydrogen [27]. This problem can be reduced by modifying surface of NR or blending with other rubber such as chloroprene rubber (CR) and acrylonitrile butadiene rubber (NBR). It is well-known that NR is classified as an amorphous rubber. However, NR can behave as a crystalline polymer when it is stretched or cooled [29]. It has been reported that the strain-induced crystallization (SIC) of NR is an important phenomenon which brings about its excellent mechanical properties [29]. Apart from superior strength, NR has high resilience, very good low temperature flexibility, excellent dynamic properties and low heat build-up [30-31]. Therefore, it is widely used in the rubber industries. In addition, these properties can be improved when NR reacts with sulfur known as vulcanization reaction. This reaction converts the plastic and viscous nature of raw rubber into elastic rubber. Vulcanized NR generally has higher hardness, tensile strength and abrasion resistance but lower elongation relative to raw NR. Since the vulcanized NR has very low electrical conductivity, it is not suitable for using in the electronic applications such as electromagnetic interference (EMI) shielding products and strain sensors [32-33]. However, its electrical conductivity can be improved by adding conductive fillers such as conductive carbon black, graphite, graphene and carbon nanotube (CNT). In general, the main use of NR is in automobiles. It has been reported that sixty percent of all rubber consumed is for automobile tyres [34].

Additionally, NR is widely used in engineering products such as conveyor belt and bearing for bridge. Other utilizations of NR include hoses, footwear, battery boxes, foam mattresses, balloons and toys [35].

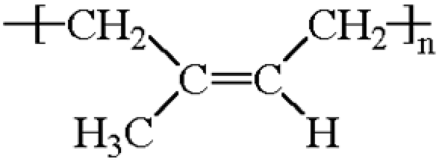

Figure 3.1 Chemical structure of NR [28]

3.2 Acrylonitrile butadiene rubber (NBR)

Acrylonitrile butadiene rubber is also known as nitrile rubber. It is produced from a copolymer of acrylonitrile and butadiene monomers. The basic structure of NBR is shown in Figure 3.2 [3]. Normally, the amount of acrylonitrile presented in the final copolymer varies from 15 to 50 percents [36]. It has been reported that the increase of acrylonitrile concentration improves the polarity and gas permeability of NBR but limits its low temperature properties [36-37]. Since NBR is a polar rubber, it has excellent resistance to non-polar oils such as petroleum oils, mineral oil and vegetable oil [36-37]. Therefore, it is mainly used where high oil resistance is required, as in automotive seals, gaskets, or other items which contact with hot oils [38]. In addition, it is used to produce hoses for oil products and the rolls for spreading ink in printing. Moreover, it is used to make protective gloves for the nuclear industry. An ability of NBR to resist temperature ranging from -40 °C to +108 °C makes it an ideal material for aeronautical applications [3]. NBR is also employed to produce moulded goods, footwear, adhesives, sealants, sponges, expanded foams, and floor mats [38]. In some applications, NBR is blended with other rubbers to get a balance in properties. For example, blending of natural rubber (NR) and nitrile rubber (NBR) imparts the blend with a balance in tensile strength, abrasion resistance and oil resistance [2-4].

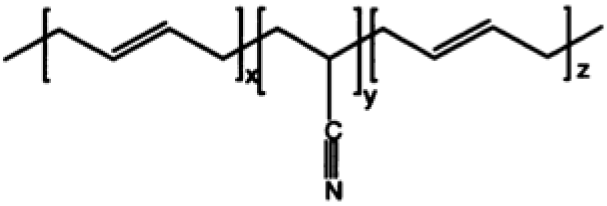

Figure 3.2 Chemical structure of NBR [3]

3.3 Rubber blend

Blending of two or more types of rubbers is a useful technique for developing materials with balanced properties of the individual constituents. Additionally, blending of different rubbers can improve the processing properties and reduce the production cost. Generally, the blends can be divided into two types, heterogeneous and homogeneous blends. If the blend is made of two rubbers, two glass transition temperatures can be observed for the heterogeneous blend. In contrast, homogeneous blend exhibits a single-phase structure and one glass transition temperature. Blending of two rubbers having different polarity causes lack of miscibility leading to poor mechanical properties. Tinker and Jones illustrate a model vulcanized blend of two rubbers containing various ingredients as shown in Figure 3.3 [39]. The blend ratio between rubber A and B for this model is 3:1. Many factors such as polymer ratio, interfacial tension, distribution of compounding ingredients and crosslink density can affect the properties of the blends and are taken into the consideration. [39-41].

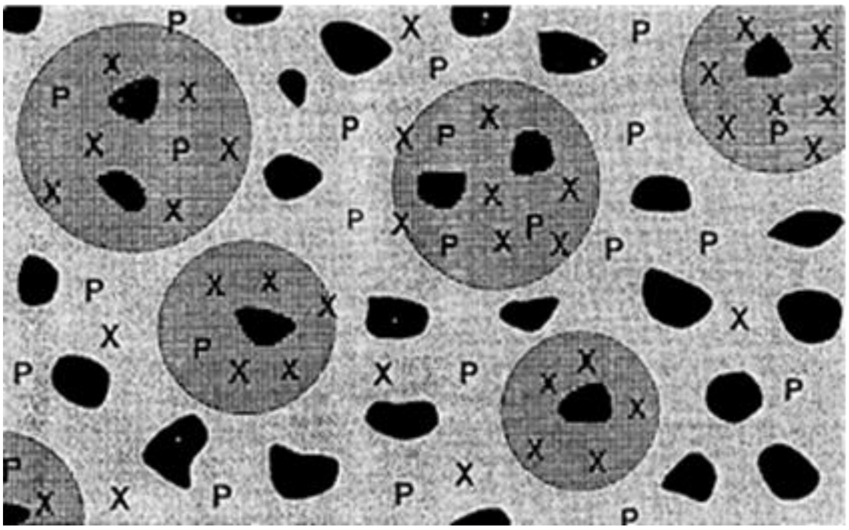

Figure 3.3 Schematic for a model blend of two rubbers (A □ and B ◍) containing filler ⬬ , plasticizer (P) and crosslink (X) [39]

3.3.1 Polymer ratio

Polymer ratio is an important factor controlling phase morphology of rubber blend. Generally, phase morphology of the rubber blend can be divided into two cases whether one phase is dispersed within another phase as depicted in Figure 3.4a (NR phase dispersed in NBR phase) or whether both are continuous phases as shown in Figure 3.4b [39]. The latter case is known as co-continuous phase morphology [39]. Ali and co-workers found that 50/50 HNBR/NR blend exhibits co-continuous phase morphology where both HNBR (grey domains) and NR (white domains) are continuous phases as displayed in Figure 3.5 [42]. It is well known that the properties of polymer blend are dominated by the continuous phase. In addition, the smaller phase size of the dispersed phase indicates the better blend compatibility of the system leading to the improved properties of the blends. For example, NR/NBR blend with smaller size of the NR dispersed in NBR matrix has oil resistance closed to that of the NBR vulcanizates [43]. Furthermore, Botos and co-workers reported that the 25/75 and 50/50 NR/ethylene-propylene-diene rubber (EPDM) blends give the best resistance against thermal ageing and UV irradiation, respectively [44]. This is because EPDM is continuous phase for both blend ratios. Moreover, Sae-oui and co-workers showed that increasing CR content in the CR/NR blends helps to improve oil, thermal and ozone resistance of the blends [45]. Varkey and co-workers studied the thermal degradation of NR/polybutadiene-co-styrene (SBR) latex blends using thermogravimetric method. They found that an increase of SBR content leads to improvement in the thermal stability of the blends [46].

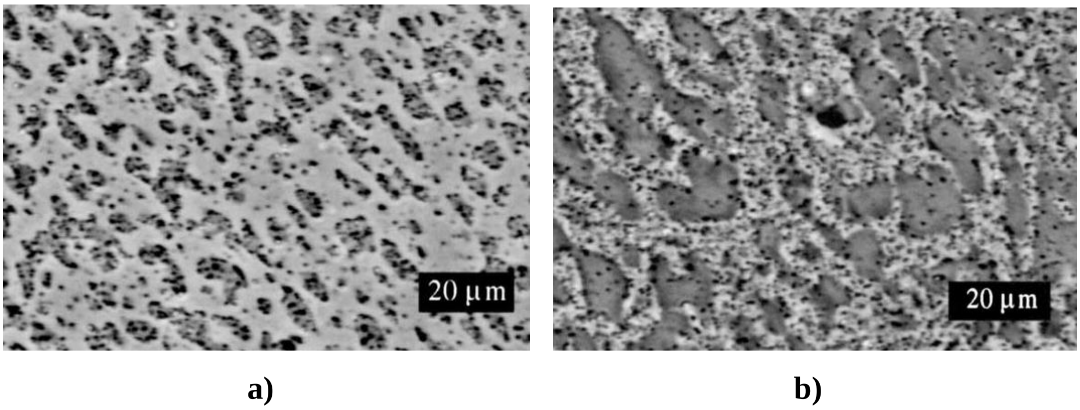

a) b)

Figure 3.4 Phase morphology of NR/NBR blends; a) NR dispersed in NBR phase and b) co-continuous phase (darker phase is NR, white phase is NBR) [39]

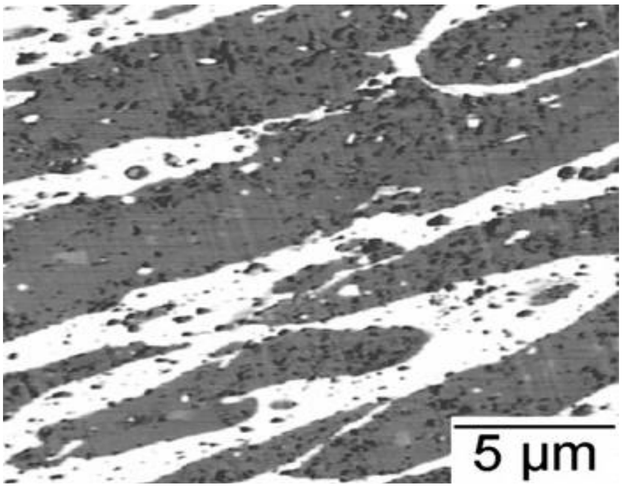

Figure 3.5 AFM image of blend morphology of 50/50 HNBR/NR; grey domains are NBR, white domains are NR [42]

3.3.2 Interfacial tension

Interfacial tension is another important factor influencing the morphology of the rubber blend [39]. Generally, the solubility parameter is one of the most important factors affecting on the interfacial tension. For example, blending of non-polar rubbers having similar solubility parameters such as NR, polybutadiene (BR) and SBR results in lower interfacial tension [39]. At lower interfacial tension, the smaller size of dispersed phase can be obtained. In contrast, blending of two rubbers having large difference in solubility parameters such as CR (polar rubber) and NR (non-polar rubber) causes higher interfacial tension leading to larger dispersed phase [39]. Additionally, interfacial tension plays a role in controlling the interfacial adhesion and crosslinking between interfaces of the two rubber phases. When the interfacial tension is high, there is slight mixing of the two rubber phases at the interface [39]. Consequently, the chance for crosslinking between the two phases is reduced leading to a weakness at the interface and poor mechanical properties of the blend. However, this problem can be solved by adding the compatibilizing agents to reduce the interfacial tension. It has been reported that phase size of HNBR in the NR matrix of nanoclay-filled 50/50 HNBR/NR blends decreases due to the reduction of the interfacial tension causing by compatibilization effect of the surfactant released from clay [42]. Additionally, it is found that the amount of the surfactant released from clay increases with increasing mixing time, resulting in smaller phase size of HNBR with increasing mixing time from 25 to 40 min as shown in Figure 3.6 [42].

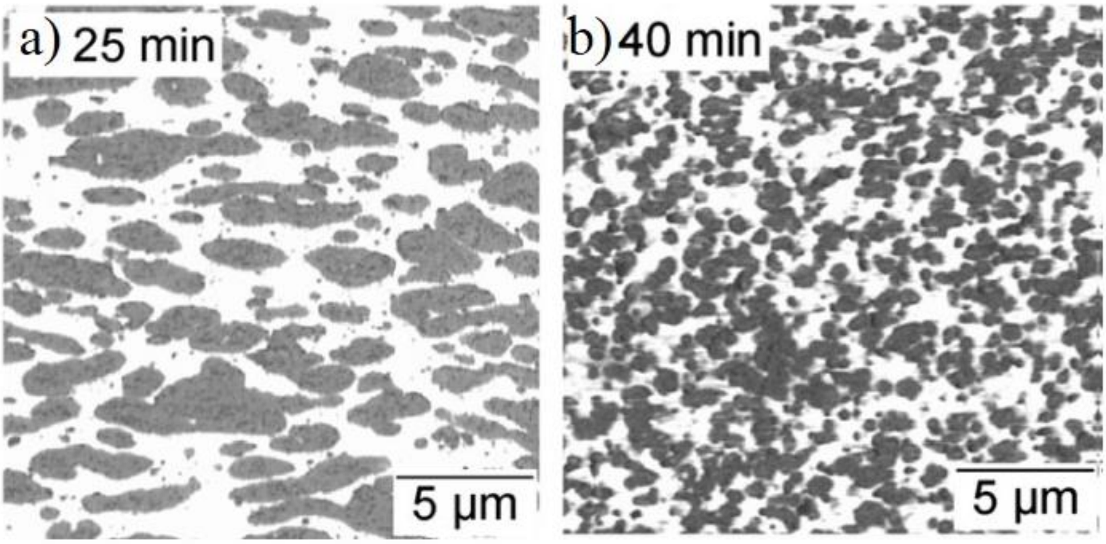

Figure 3.6 AFM image of blend morphology of 50/50 HNBR/NR in dependence of mixing time; grey domains are NBR, white domains are NR [42]

3.3.3 Distribution of filler between the elastomers

A balance of filler distribution in the blends has been shown to affect the properties of the blend [42]. However, it is difficult to control the distribution and dispersion between two rubber phases, especially when two rubbers having large difference in solubility parameter are blended. This is because filler favors to migrate into the rubber phase having similar solubility parameter [39]. Previously, the selective localization of silica within NR/SBR/NBR blend has been studied by means of FTIR spectroscopy [47]. The results indicate that silica migrates from SBR phase to NBR phase because of the stronger affinity of silica to NBR. Additionally, Edirisinghe and co-workers studied the selective localization of carbon black (CB) in NR/NBR blend by using transmitted light microscope under bright field illumination [48]. They found that carbon black migrates into NR phase due to the similar solubility parameter of carbon black to NR [48]. Besides, Callan and co-workers investigated the distribution of CB in 50/50 blends of different elastomers by using TEM technique [49]. They observed that the CB affinity decreases in the order of BR, SBR, CR, NR and EPDM [49]. Furthermore, Ali and co-workers prepared 50/50 HNBR/NR blend by using clay/NR masterbatch and examined the distribution of clay by using AFM technique [42]. They observed that nanoclay particles transfer from NR into the

HNBR phase when mixing time is more than 2 min as depicted in Figure 3.7 [42]. Additionally, it can also be seen in Figure 3.8 that 50/50 HNBR/NR blend containing 5 phr nanoclay exhibits the highest tensile modulus when the mixing time is 15 min. The explanation is given to the balance of filler distribution in each phase [42]. Moreover, it has been reported that the distribution of fillers can be determined from the Raman micro-imaging and dynamic mechanical thermal analysis (DMTA) results [50-54]. Zerda et al. applied Raman micro-imaging technique to investigate silica distribution in BR/BIMS/NR blends [50]. They observed that silica was localized in the interphase of the NR and BIMS domains and no silica was found in the BR phase [50]. Meier and co-workers attempted to study the amount of silica in each phase of a ternary BR/SBR/NR blend from the DMTA results [51]. They found that the selective localization of silica within the BR/SBR mix-phase could not be determined because of the overlapping of the glass transition temperatures (T_g) of these rubbers. In addition, Sirisinha et al. studied the distribution of CB in BR/NBR blends by using the DMTA technique [52]. The results showed that CB preferred to reside in the BR phase relative to the NBR due to the higher affinity of CB to BR. In this research, the DMTA results are also used to determine the distribution of CNT in NR/NBR blends. This method is based on the difference in damping factor (tan δ) of the gum and filled rubber vulcanizates. Basically, tan δ at peak (tan δ_{max}) decreases when the fillers such as CNT and silica are incorporated into a rubber matrix [16, 54]. This is because rigid filler restricts molecular chains of viscous rubber matrix. In cases of rubber blends, if the filler preferentially migrates from one phase to the others, the change of tan δ_{max} for each rubber phase would be observed. Therefore, the distribution of filler in each phase of the blends can be estimated by using the relationship between the magnitude of reduction in tan δ_{max} of gum and filled blends [51-54].

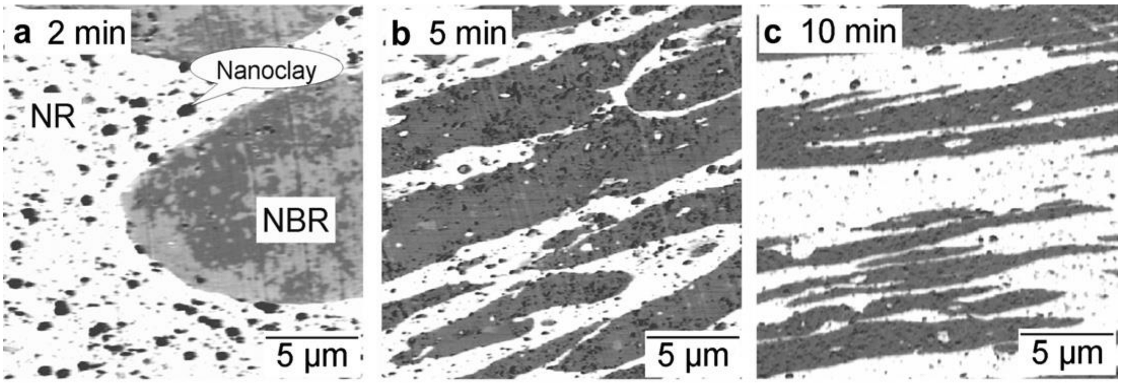

Figure 3.7 AFM images of the morphology of 50/50 HNBR/NR blend at various mixing times; dark dots = clay, grey domains = NBR, white matrix = NR [42]

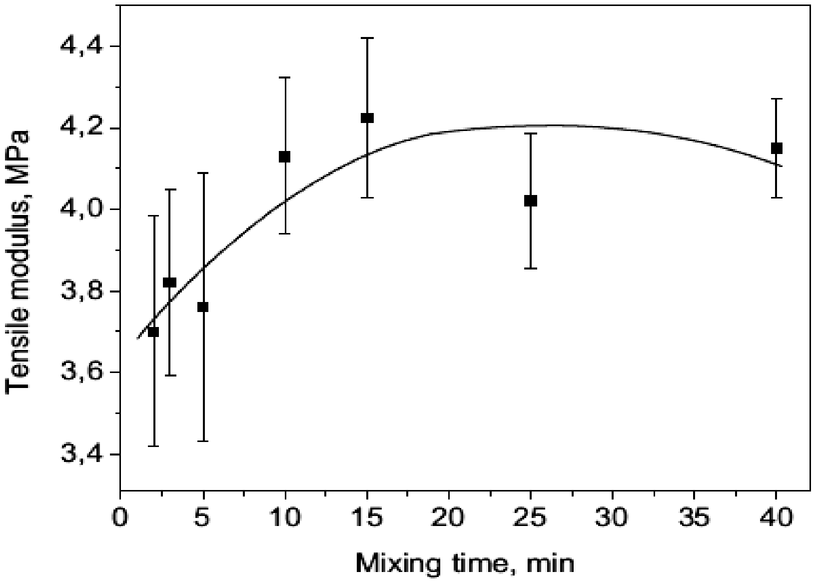

Figure 3.8 Tensile modulus of 50/50 HNBR/NR blends containing 5 phr of clay [42]

3.3.4 Distribution of crosslink between the elastomers

Sulfur-based curing system is widely used to vulcanize the general purpose diene elastomers such as NR, isoprene rubber (IR), NBR, SBR and the rubber blends prepared by using these rubbers. It is well known that the vulcanization rate with sulfur alone is slow. A faster process can be achieved by adding small amounts of accelerators and activators which are ZnO and fatty acid [55-56]. For rubber blends cured with sulfur-based system, poor distribution of crosslink density between two rubber phases readily takes place due to the poor distribution of curing agents in each phase. This leads to poor mechanical properties. Gardiner and co-worker have previously demonstrated that sulfur transfer from NR to SBR is gradual while its transfer from NR to isobutylene isoprene rubber (IIR) is sharp at the interface. This is because there is larger difference in sulfur solubility between NR and IIR than that between NR and SBR [57]. Additionally, it has been reported that blending of highly unsaturated elastomers such as NR and BR with the elastomers containing a low level of unsaturation such as EPDM and IIR leads to an imbalance of crosslinks [58]. However, the distribution of crosslinks can be controlled by using suitable accelerators [39]. Andrew and co-worker employed various accelerators to investigate the distribution of crosslinks in both phases of 50/50 NR/NBR blends [39]. They used *N*-*t*-butylbenzothiazole-2-sulphenamide (TBBS) as a main accelerator while the secondary accelerators chosen were tetramethylthiuram monosulphide (TMTM), diphenyl guanidine (DPG), tetrabutylthiuram disulphide (TBTD), 2,2'-benzothiazole disulphide (MBTS) and N,N'-dioctadecyl N,N'-diisopropylthiuram disulphide (ODIP). As can be seen in Figure 3.9, TBBS, TBBS/DPG, TBBS/MBTS and TBBS/TBTD give a balance of crosslink distributions between two rubber phases. However, they also observed that the use of only TBBS for preparing the blend rather gives lower cure rate. Therefore, the addition of the secondary accelerators such as DPG, TBTD and MBTS is essential for improving the cure rate without adversely affecting crosslink distribution. As a consequence, a balance in tensile strength of the blends would be achieved. For the other mechanical properties such as tear strength and abrasion resistance of the blends, they can be improved by the addition reinforcing fillers [3-6].

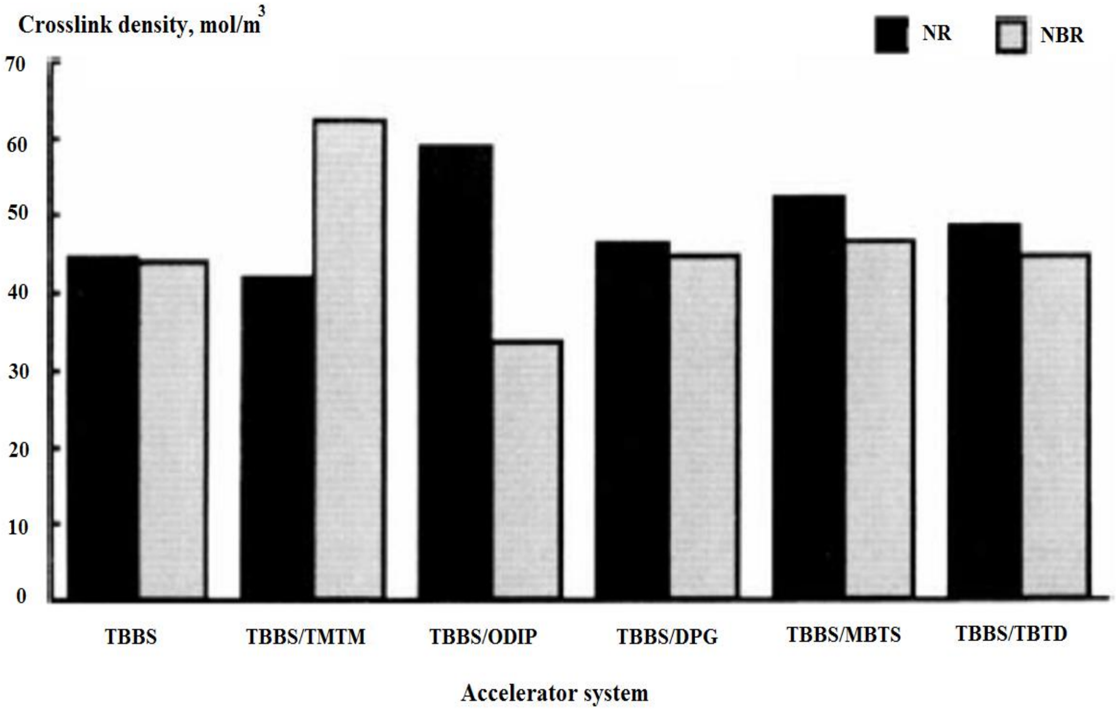

Figure 3.9 Crosslink density distributions of 50/50 NR/NBR blend cured at 150 °C [39]

3.4 Rubber reinforcement

Reinforcement is defined as improvement in properties of rubber such as modulus, tear strength, tensile strength, cracking resistance, fatigue resistance and abrasion resistance [59]. Commercial application of elastomers often requires the use of filler to obtain the desired properties. The fillers used in the rubber industry are mainly classified into reinforcing, semi-reinforcing and non-reinforcing fillers. The choice of filler is usually dictated by the end-application of elastomer and economics. Generally, the effects of filler on the properties of rubber vulcanizates depend on particle size, surface area, particle shape, surface activity and filler-matrix interaction. It is well known that the rubber vulcanizates containing smaller particle size or larger specific surface area of filler exhibit the higher reinforcing efficiency [59-62]. For filler shape, it can be characterized by their aspect ratio into sphere, cube, needle, block, plate and fiber as shown in Figure 3.10 [63]. The aspect ratio is the ratio of mean length to mean diameter of filler [63]. It has been reported that the filler having higher aspect ratio give rise to the higher reinforcing efficiency for the rubber composites [2, 42]. Among reinforcing fillers, carbon nanotube and nano-clay are classified as fiber and plate, respectively because they have high aspect ratio which is able to enhance the mechanical properties of the rubber composites [2, 42]. However, good interfacial adhesion between rubber matrix and filler is necessary to achieve high reinforcement [21, 63]. In the rubber composites, the applied stress is basically transferred from the rubber matrix to the strong and stiff filler. If there is good interfacial adhesion between rubber matrix and filler, the better stress transfer from matrix to filler would occur and lead to the improvement of the mechanical properties [9, 21-22]. On the other hand, poor adhesion between rubber matrix and filler results in lower stress transfer ability and consequently gives rise to insignificant improvement in mechanical properties of the rubber composites [19]. Therefore, modification of filler surfaces is necessary in order to improve the interaction between the rubber matrix and filler surface.

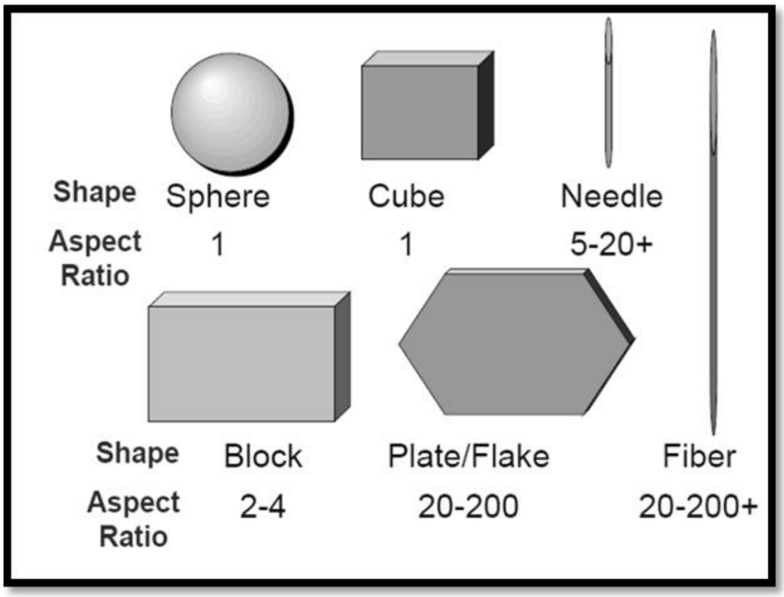

Figure 3.10 Aspect ratios of fillers having different shapes [63]

3.5 Carbon nanotubes (CNT)

3.5.1 Structure of CNT

In 1991, Sumio Iijima used a high resolution transmission electron microscope to study the soot created in an electrical discharge between two carbon electrodes [64]. He observed that the soot contains structures that consist of several concentric tubes of carbon. These are later known as carbon nanotube (CNT). CNT is long cylinder of covalently bonded carbon atoms as shown in Figure 3.11 [64]. Typically, the length is significantly greater than the width resulting in a large aspect ratio. CNT has a similar structure to a fullerene, but instead of forming a sphere like the fullerene atom, the atoms form a cylindrical tube that may (or may not) be capped off at each end by half a fullerene molecule [64].

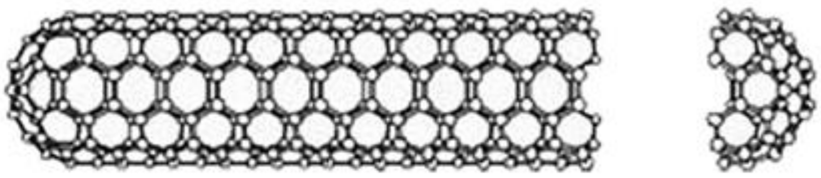

Figure 3.11 Structure of CNT [64]

3.5.2 Types of CNTs

In general, there are three different types of CNTs which are single-wall carbon nanotube (SWCNT), double-wall carbon nanotube (DWCNT), and multi-wall carbon nanotube (MWCNT) as illustrated in Figure 3.12 [65]. A SWCNT contains one graphene sheet that rolls up to form a cylinder. For DWCNT, it contains two graphene sheets that one sheet is within another sheet and both sheets is rolled up to form a cylinder. In case of MWCNT, it consists of several concentric cylinders. the MWCNT is used as a reinforcing filler in NR/NBR blends.

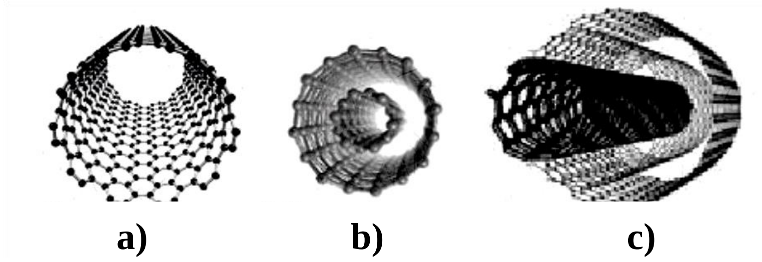

Figure 3.12 Three different types of carbon nanotubes; a) single-wall, b) double-wall and c) multi-wall carbon nanotube [65]

3.5.3 Synthesis of CNTs

Nowadays, CNTs are produced by three techniques which are arc discharge, laser ablation and chemical decomposition (CVD) [66]. For the arc discharge method, arc plasma is generated between the two carbon electrodes in an inert atmosphere. The inert atmosphere used is generally helium gas. A fibrous deposit forms on the cathode as the anode is consumed. The deposit generally consists of 50% by volume MWCNT. It is also possible to grow SWCNT by the arc discharge method using hydrogen gas instead of helium gas. For the laser ablation process, a graphite target containing small amounts of a metal catalyst is used. The target is placed in a furnace under 1200°C in an inert atmosphere followed by evaporation using a high power laser. The carbon nanotube develops on the cooler surface of the reactor, as the vaporized carbon condenses. The yield of MWCNT synthesized by this process is about 70% by volume of MWCNT. However, the overall production costs of the laser ablation process are high. Therefore, chemical vapor deposition (CVD) method is generally used to avoid the limitations of the other synthetic methods. For CVD method, a substrate is prepared with a layer of metal catalyst particles, most commonly nickel, cobalt, iron, or a combination of these materials. The diameter of the grown nanotubes is related to the size of the metal particles. The substrate is heated to approximately 700°C. To initiate the growth of nanotubes, two types of gases are blended into the reactor. Gases used in this process can be ammonia, nitrogen or hydrogen. It is well known that disadvantage of this method is the formation of entangled CNT. However, more aligned CNT can be generated by using the conditions which lead to rapid and dense nucleation on the substrates [66-67]. In addition, MWCNT in the length range of millimeters can be synthesized by extending the growth time. Table 3.1 summarizes the methods used for synthesizing CNTs [66-67]. Normally, the quality and yield of the generated CNT are significantly affected by technique and the synthesis conditions used.

Table 3.1 A summary of the methods for the synthesis of CNTs [66-67]

Method	Technology of preparation	Typical mean diameter (nm)	Product description
Are discharge	- First reported production - Modified Kratschmer reactor is used	1.5(0.9-3.1)	- Lesser quality - CNT packed as bundle
Laser ablation (PLV)	- Ablation from graphite doped with Fe, Co and Ni catalysts	1.4(1-1.8)	- High quality - Good diameter control
Chemical vapour deposition (CVD)	- Catalytic chemical vapour deposition - Supported metal catalysts are used	1.5(1.3-2)	- Cheapest - Commercial - Upscalable

3.5.4 Properties of CNTs

3.5.4.1 Mechanical properties of CNTs

It is well known that the chemical bonding of CNTs is composed entirely of sp^2 bond which is similar to that of graphite. This bond is stronger than the sp^3 bond found in alkanes and diamond, providing CNTs with their unique strength. It has been reported that the modulus of CNTs is in the same range as graphite fiber and the strength is at least an order of magnitude higher than the graphite fiber [68-69]. Eitan and co-worker reported that the SWCNT has Young's modulus of about 1 TPa as compared to 300-800 GPa for graphite fiber [70]. In addition, Tu and co-worker reported that the Young's modulus of the MWCNT is about 4.7 TPa, which is much higher than any other known fillers [68-69]. However, some computational studies show that the true modulus of the MWCNT are below the estimated value obtained from the graphene sheet [71]. This could be explained by the presence of defect namely Stone Wales defect on its surface [72]. The Stone Wales defect is the rearrangement of the six membered rings into pentagons and heptagons [72]. This rearrangement is a result of 90° rotation of C-C bond leading to the formation of defect on the wall of CNT as depicted in Figure 3.13(a). When the stress is applied along the MWCNT axis direction, this defect is propagated as shown in Figure 3.13(b) resulting in the decrease of the mechanical properties of the MWCNT [72]. In addition, mechanical behaviour of the MWCNT under tensile load can be another reason for the lower of its true modulus relative to the estimated value obtained from the graphene sheet [71]. This is because the inner walls of the MWCNT are not effective in bearing tensile loads applied at both ends. This means that it is only the outmost layer of the MWCNT which takes the entire load. [71]. Therefore, failure resulting from the Stone Wales defect occurs only at the outer wall of the MWCNT by breaking the bonds among carbon atoms as demonstrated in Figure 3.14 [71]. Additionally, it has been reported that the mechanical response of MWCNT is different from that of conventional fibers or other reinforcing materials due to its hollow morphology. Therefore, the MWCNT can sustain even 40% strain without showing any brittle behaviour [71].

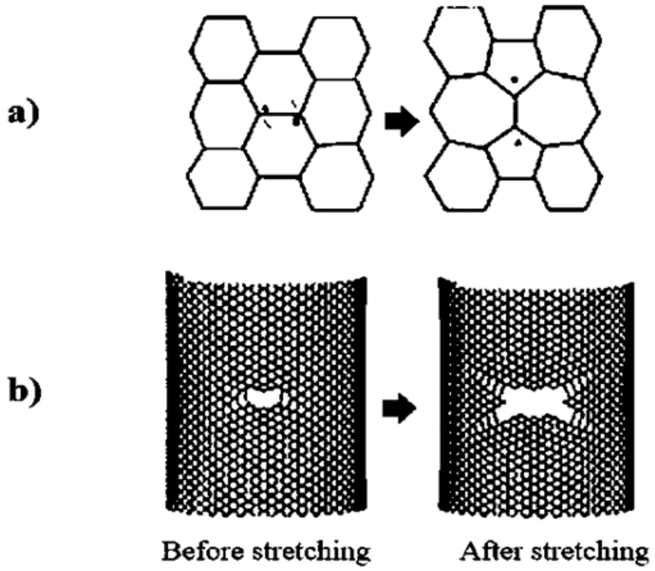

Figure 3.13 Spontaneous formation of Stone-Wales defect in CNT; a) formation Stone-Wales defect and b) propagation of Stone-Wales defect under tension [72]

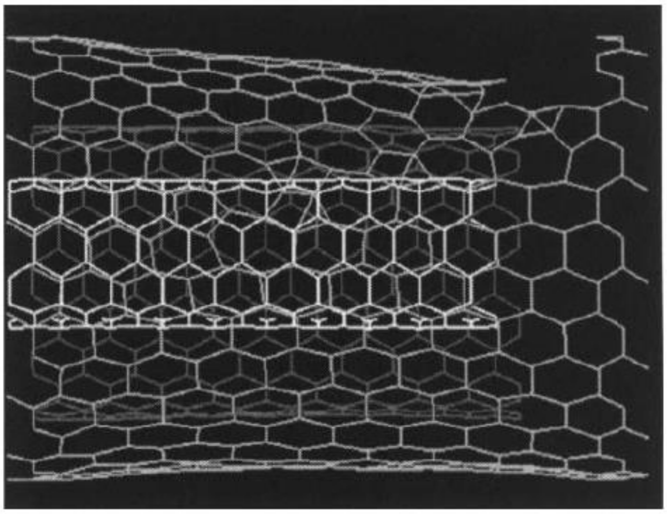

Figure 3.14 Breaking the bonds of outmost wall of MWCNT under stretching process [71]

3.5.4.2 Electrical properties of CNTs

The sidewall of CNTs generally consists of only hexagonal carbon rings, whereas the end caps are made of pentagons and hexagons in order for curvature to exist [66]. Due to the carbon-carbon bond symmetry of the cylindrical tube, CNT has a number of orientations known as chirality that can form a closed cylinder [66]. The *(m,n)* indices determine the diameter and chirality, which are key parameters of a nanotube. Depending on the chirality, CNTs can be either metals or semiconductors. Folding of a) graphene sheet in the (8,8), (8,0), and (10,-2) vectors leads to b) armchair, c) zigzag, and d) chiral tubes, as depicted in Figure 3.15, respectively [66]. The electrical properties of CNTs depend on how the hexagons are orientated along the axis of the tube. If a sheet is rolled in direction of zigzag, the CNTs would have electronic properties as a semiconductor. Additionally, when a sheet is rolled in the direction of chiral, the CNT would give electronic properties as metal. Furthermore, if the hexagons orientate in the configuration labeled armchair (hexagons are lined up parallel to the axis of the nanotube), the CNT would have electrical properties similar to metal. When voltage is applied between two ends of an armchair nanotube, a current will flow. It appears that an armchair carbon nanotube gives a better electrical conductivity than a copper (Cu) normally used in an electrical wire, or any other metals [64, 66]. Also, the electrical conductivity of the CNT obtained from sheet rolled in direction of armchair is higher than that of the CNT obtained from sheet rolled in direction of chiral. It has been reported that electron transport in CNTs only along the axis of tube [66]. In addition, intrinsic superconductivity in CNTs has been reported by several researchers [64, 71]. However, many other experiments found no evidence of superconductivity. Thus, the validity of the claims about intrinsic superconductivity in CNTs remains a subject of debate [64]. Four probe measurements have been previously developed to generate the information on transport property of individual MWCNT [73]. Interestingly, it is found that MWCNT represents more complex transport property because of the presence of cylinders of different chirality. On the other hand, the transport property of SWCNT is more uniform in nature. It has been reported that the electrical conductivity of individual SWCNT at room temperature is about 10^6 S/m for sheet rolled in direction of armchair and 10 S/m for sheet rolled in zigzag direction [66]. In case of MWCNT, its electrical conductivity of about 2×10^7 S/m was reported [18]. It is well established that MWCNT can consist of mixed chiralities, and there are indications that the overall electronic behavior is determined by the external shell [64, 66]. Souier and co-workers also suggested that the conductivity in CNTs can also be adjusted by suitably doping them resulting in the alteration of their original lattice structure [71]. In addition, it is found that CNTs have similar nature of the conductivity behavior as conducting polymers [71].

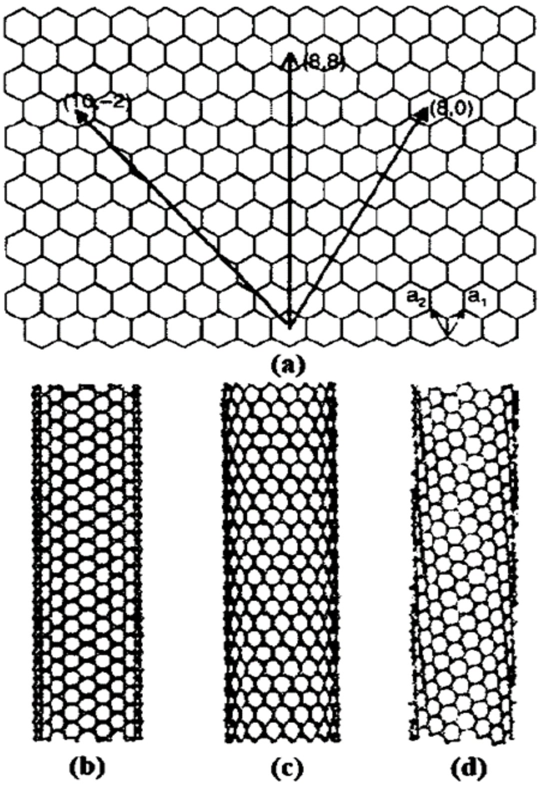

Figure 3.15 Schematic honeycomb structure of a) a graphene sheet can be formed by folding the sheet along lattice vectors into b) armchair, c) zigzag and d) chiral [66]

3.5.4.3 Thermal properties of CNTs

Normally, CNTs have low-temperature specific heat. Therefore, it shows high thermal conductivity. The thermal conductivity of CNTs has been examined both theoretically and experimentally. It is found that theoretical thermal conductivity of CNTs at room temperature is larger than graphite or diamond. Measurements show that the thermal conductivity at room temperature is over 200 W/mK for bulk samples of SWCNT and over 3000 W/mK for individual MWCNT [18]. In addition, it is found that SWCNT has higher thermal conductivity than copper which is well known for good thermal conductivity. Besides, it has been reported that the addition of only 1 wt% SWCNT to epoxy resin can double the thermal conductivity, showing that nanotube composites may be useful for thermal management applications. Moreover, the temperature stability of CNTs is estimated to be up to 2800 °C in vacuum and about 750 °C in air [7].

3.6 CNTs/polymer composite

CNTs are considered as ideal reinforcing fillers in a wide range of composite systems [7-9, 74]. This is due to their high aspect ratio and exceptional mechanical properties, very small diameter, low density, high electrical and thermal conductivities as mentioned previously. Many researchers reported that the incorporation of CNTs into polymer matrix brings about improving mechanical, electrical and thermal properties of polymer composites by orders of magnitude. In addition, CNT-filled polymer composites are widely used in many applications such as nanotube reinforced materials, field-effect transistors, field emitters and tips for scanning probe microscopy [71, 74]. Figure 3.16 shows some of the applications emerging from CNT-reinforced composites [74]. Several researchers have extensively studied to develop the high performance CNT/polymer composites [2, 17, 75]. The key points to achieve the high performance CNT/polymer composites are homogeneous dispersion of CNT in the polymer matrix and great alignment of CNT in the polymer matrix as well as good interfacial interaction between the filler and matrix [16, 17, 25].

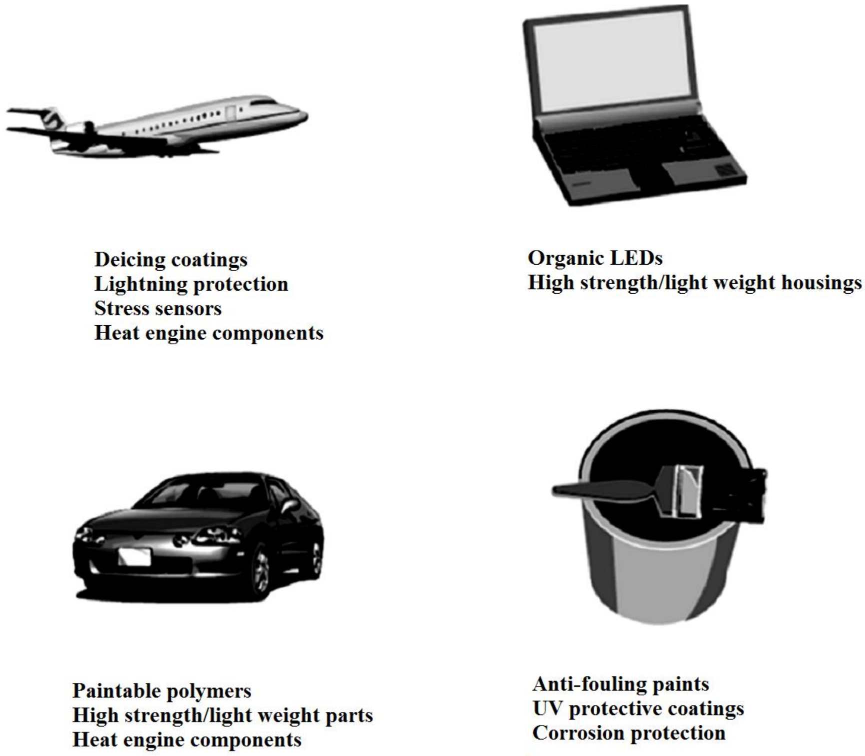

Figure 3.16 Applications for CNT/polymer composites [74]

3.6.1 Dispersion of CNTs

It is known that the degree of reinforcement is extremely dependent on the degree of filler dispersion [16-18]. Previous studies have shown that the dispersion of MWCNT in the rubber matrix is rather poor because MWCNT tends to form highly entangled agglomerates like felted thread leading to poor mechanical properties [16-17]. Several different methods have been attempted to disperse the CNT [16-18]. It has been shown previously that CNT can be dispersed by using ultrasonic process. By using this method, the surface of the dispersed CNT in aqueous medium is treated by dispersing agents to reduce the Van der Waals forces after the CNT is deagglomerated. This means that the dispersing agents can separate the CNT to prevent re-aggregation [76-77]. However, ultrasonic process can cause the breakage of the CNT leading to low aspect ratio [78]. Several researchers have studied the effect of various surfactants on the dispersion of CNT suspension. Matarredonna and co-workers found that the dispersion of CNT in the suspension is improved by adding sodium dodecylbenzene sulfonate, an anionic surfactant [79]. This is because the adsorption of the surfactant molecules at the CNT surface leading to stabilization of the nanotube via steric repulsion [80-81]. In addition, Moore and co-workers observed that the utilization of a polymeric surfactant which is a Pluronic (polyethylene oxide – polypropylene oxide – polyethylene oxide, PEO-PPO-PEO) gives rise to an improvement in CNT dispersion in aqueous medium, especially at high CNT content [82]. This is due to the fact that its hydrophilic groups extending into the water can obstruct the CNT aggregation [83]. In other words, it increases distance between the CNT causing the reduction of the van der Waals forces. However, charge repulsion is taken place instead of this type of stabilization when ionic surfactant is used. [82]. When well-dispersed CNT in aqueous medium is obtained, it is also important to keep well-CNT dispersion after it is added into the polymer matrix. Therefore, many methods have been adopted to improve dispersion of CNT in the polymer matrices [16-18, 84]. Villmow and coworkers attempted to enhance dispersion of the MWCNT in a poly(lactic acid) matrix by using a twin-screw mixer having high mechanical shear [84]. However, this process brings about a serious breakage of the MWCNT leading to a decrease in its length and effective aspect ratio, and a consequent decrease in electrical conductivity of the composite [84]. Yue and co-worker dispersed the MWCNT in organic solvent using ultrasonic process, before mixing the CNT suspension with the HNBR. They found a significant improvement in the mechanical and electrical properties when only 2 phr MWCNT is added [85]. In addition, an incorporation of MWCNT suspension, prepared by using ultrasonic process, into 50/50 SBR/BR blend gives higher mechanical properties and electrical conductivity than the corresponding blend prepared by conventional mixing method due to an improvement of MWCNT dispersion [16, 18].

3.6.2 Alignment of CNTs

Since CNTs are considered as short fiber, the CNT-filled polymer composites are analogous to the polymer composites filled with short fiber [23]. Therefore, the theories for the strength and modulus of short fibers reinforced polymer composites can be extended to the case of CNTs reinforced polymer composites [24]. In order to control the alignment of CNT in the polymer matrix, many methods have been adopted [25, 86-87]. Kim and co-workers aligned the MWCNT in EPDM using dragged shear force from milling process [86]. They found that the aligned MWCNT in EPDM matrix brings about the enhancement in elastic modulus, thermal conductivity, electrical conductivity, and electromagnetic shielding property [86]. Additionally, Sharma and co-workers reported that the mechanical properties and electrical conductivity of the PC composites containing the CNTs aligned by using magnetic alignment method are higher than those of PC composites containing the randomly aligned CNTs. [87]. Other methods can be used to create the alignment of CNT are electrospinning and solution spinning. Chae and co-workers showed that utilization of electrospinning method to prepare the SWCNT/polyacrylonitrile (PAN) composites gives the alignment of SWCNT up to 99% when 1 wt% SWCNT is added into the PAN [88]. As a result, its storage modulus at 25 °C increases by 6.6 GPa relative to that of the unfilled one [88]. In addition, Kim et al. observed the improvement in modulus of the MWCNT/PC composites prepared using electrospinning method because of the improvement of the MWCNT alignment [89]. Furthermore, Ci et al. determined the modulus in the longitudinal and transverse directions of the aligned MWCNT/PDMS composite prepared by using infiltration process [90]. As can be seen in Figure 3.17, the moduli of the PDMS composites determined under compression for the longitudinal and transverse directions are 18.87 and 7.95 MPa, respectively. Additionally, melt spinning and drawing methods have been used to align the CNT in PAN composites [91]. However, it is found that the mechanical, electrical and thermal properties of the obtained composites prepared by these methods are much lower than those of the theoretical estimates [92]. Although, numerous methods have been used to achieve alignment of CNTs in polymer matrix, these methods give much lower physical properties compared to the theoretical properties predicting by computer simulation [71]. The variation in mechanical properties of CNTs, perfection of the carbon nanotube structure, and adhesion between the matrix and the carbon nanotube may be the reason for the incapability to create a strong material even with well aligned CNTs [71].

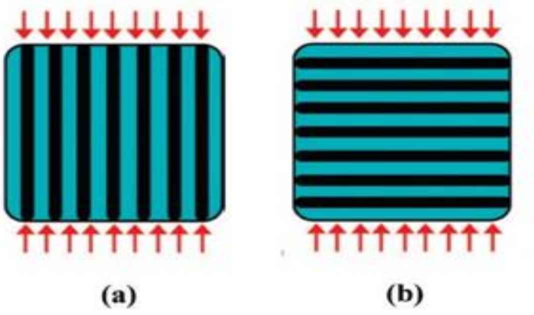

Figure 3.17 Schematics of different CNT-filled PDMS samples tested under compression; a) longitudinal direction and b) transverse direction [90]

3.6.3 Modification of CNTs

It has been reported that CNTs have a considerable reinforcing effect but they exhibit relatively poor interfacial adhesion with rubber matrices such as NR, SBR and NBR resulting in an insignificant improvement in the mechanical properties [19, 20-21, 93]. This is because there is weak van der Waals forces between rubber molecule and CNTs surface [93]. Many researchers have attempted to modify the CNT surfaces in order to improve the interfacial adhesion between rubber and the CNTs surface. [9, 20-22]. For instance, carboxylic acid groups are introduced to the CNTs surface by using acid treatment and oxidation reaction methods as displayed in Figures 3.18(a) and 3.18(b), respectively. It appears that these methods could provide better stabilization of CNTs in polar solvents and covalently link polymers leading to the improvement of the processability and mechanical properties of the NR and PS composites [9, 20]. Additionally, Shanmugharaj and co-workers reported that the MWCNT modified by using oxidation reaction exhibits better dispersion in water than the unmodified MWCNT due to the presence of carboxyl and hydroxyl groups on nanotube surface [9]. Furthermore, Feng et al. found that the storage modulus of CR composite filled with MWCNT containing carboxyl groups is higher than that of CR composite containing unmodified MWCNT [94]. This is because carboxyl groups on MWCNT surface can form a hydrogen bonding with CR resulting in enhancing interfacial adhesion and hence improvement of mechanical properties [94]. On the other hand, the polar functional groups on CNT surfaces cannot improve the mechanical properties of the non-polar rubbers such as NR and SBR due to the difference in their polarity [2, 9]. Therefore, another method has been attempted by grafting with silane coupling agents as illustrated in Figure 3.18(c) [9, 21-22, 95]. Shanmugharaj et al. found that treatment of the MWCNT surface with silane results in improving the modulus and tensile strength of the CNT/NR composites [9, 95]. This is because the modification of MWCNT surfaces with silane can enhance the interfacial adhesion via covalent bonding interaction between the MWCNT and NR matrix [9, 95].

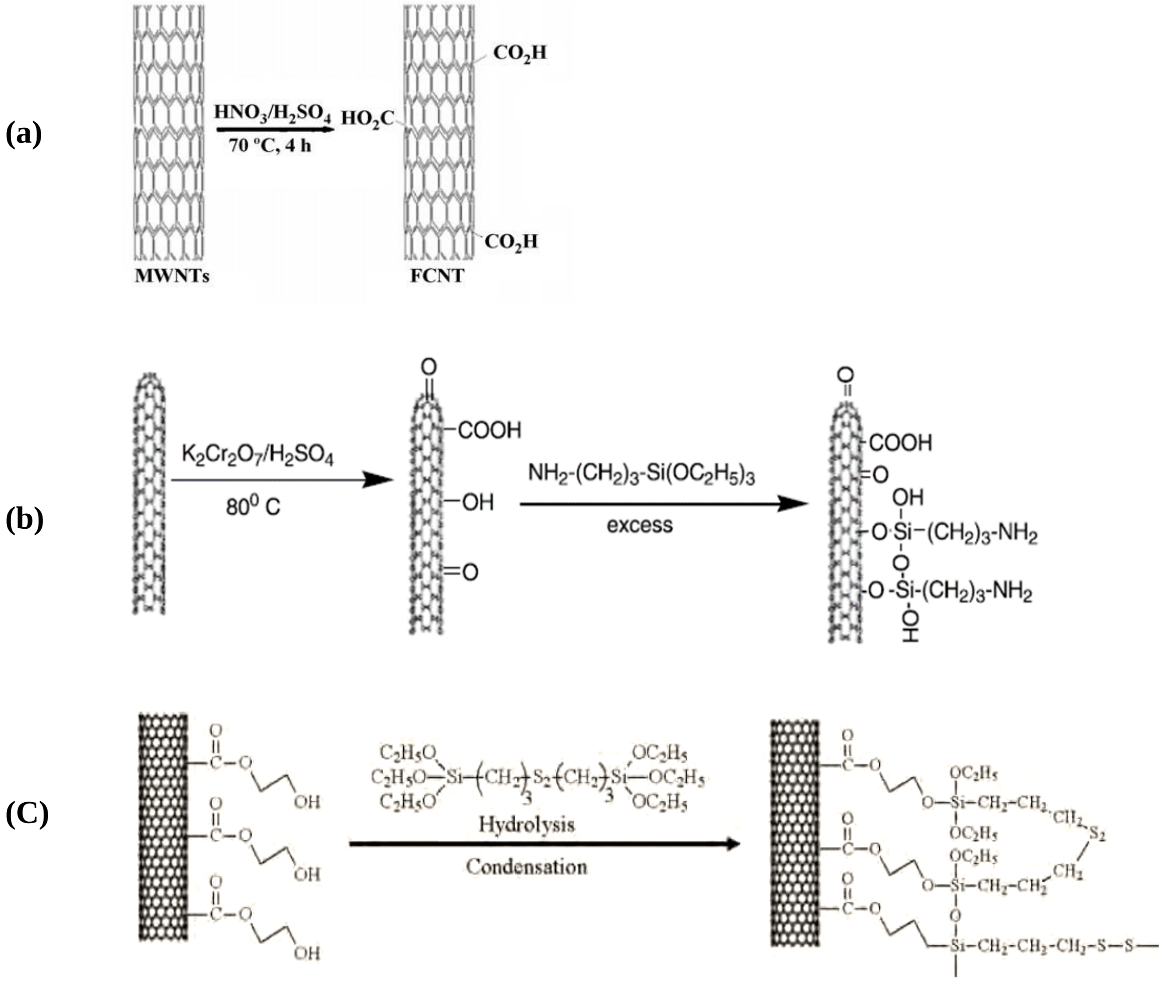

Figure 3.18 Chemical modification of CNT; a) acid treatment, b) oxidation reaction and c) grafting with silane-coupling agent [9, 20-21]

CHAPTER IV
MATERIALS AND METHODS

4.1 Materials

The materials used in the present study were rubbers, fillers, chemicals and reagents as shown in Tables 4.1-4.3.

4.1.1 Rubbers

Table 4.1 List of rubbers used in the present study

Rubbers	Trade name/Grade	Manufacturer
Natural rubber (NR)	STR 5L	Thai Rubber Latex Corporation Public Co., Ltd., Thailand
Nitrile rubber (NBR)	KRYNAC® 3345 F	Caldic Co., Ltd., Thailand

4.1.2 Fillers

Table 4.2 List of fillers used in the present study

Fillers	Trade name/Grade	Manufacturer
Multi-wall carbon nanotube (MWCNT)	NC7000	Nanocyl S.A. In., Belgium
Hydroxyl modified multi-wall carbon nanotube (OH-MWCNT)	NTP3020	Shenzhen Nanotech port Co., Ltd., China

4.1.3 Chemicals and Reagents

Table 4.3 List of chemicals and reagents used in the present study

Chemicals and Reagents	**Trade name/Grade**	**Supplier**
Zinc oxide (ZnO)	Commercial	Chemmin Co., Ltd., Thailand
Stearic acid	Commercial	Chemmin Co., Ltd., Thailand
Sulfur (S_8)	Commercial	The Siam Chemical Public Co., Ltd., Thailand
N-tert-butyl-benzothiazole sulfenamide (TBBS)	Commercial	Reliance Technochem Co., Ltd., Thailand
Tetrabenzylthiuram disulfide (TBzTD)	Commercial	Reliance Technochem Co., Ltd., Thailand
N-isopropyl-N’-phenyl-p-phenylenediamine (IPPD)	Commercial	MDR International Co., Ltd., Thailand
Ethyl alcohol (EtOH)	Commercial	RCI Labscan Co., Ltd., Thailand
Non-ionic surfactant	Nonidet P40	RCI Labscan Co., Ltd., Thailand
Silane coupling agent (Bis(3-triethoxysilylpropyl) tetrasulfide)	Si-69	JJ-Dequssa Co., Ltd., Thailand
Osmium tetroxide	Commercial	Becthai Co., Ltd., Thailand
Toluene	Commercial	RCI Labscan Co., Ltd., Thailand

4.2 Instruments

The instruments used in the present study are summarised in Table 4.4.

Table 4.4 List of instruments used in the present study

Instrument	Model	Manufacture
Ultrasonic bath	B2510-MTH	Branson ultrasonic corporation
Brabender plasticorder	R 2000	Brabender Mix Germany
Laboratory 2-roll mill	LRM150 Nishimura NS76	Labtech engineering
Moving die rheometer	rheoTECH MD+	Tech-Pro
Electrical hydraulic hot press	G 30H	Wabash Genesis Series Hydraulic Press
Instron extensometer	5566	Instron Universal
Hardness durometer Shore A	H17A	Wallace
Din abrasion tester	6102	Zwick
BF Goodrich flexometer	TP/N 2602	Goodrich
Scanning electron microscope	S-5000	Hitachi
Scanning electron microscope	JSM-5410	JEOL
Scanning electron microscope	JSM-6301F	JEOL
Dynamic mechanical thermal analyser (DMTA)	Explexor TM 25 N	Gabo Qualimeter
Rubber process analyzer (RPA)	RPA2000	Alpha Technologies
Rubber cutting machine	-	Chaicharoen Karnchang
Microtome	1400	Leitz
Hot Disk thermal analyzer 2500	TPS 2500	Kyoto Electronics
HP4284A precision LCR meter	4284A	Agilent Technologies

Table 4.4 List of instruments used in the present study (cont.)

Instrument	**Model**	**Manufacture**
Raman spectrometer	NTEGRA Spectra	NT-MDT
Four-point probe	2400	Keithley
Fourier transform infrared spectrometer (FTIR)	Equinox 55	Brucker
Impedance analyzer	4192A	Hewlett Packard

4.3 Preparation of dispersed MWCNT suspension

MWCNT was dispersed in ethanol (EtOH) and the ratio of MWCNT:EtOH is 1:20. Thereafter, 15 %w/w_{MWCNT} of the non-ionic surfactant was added to a mixture of MWCNT and ethanol. Then, the mixture was sonicated gently by using an ultrasonic bath for approximately 2.5 h. The obtained MWCNT suspension was subsequently mixed with the dry rubber for preparing MWCNT/rubber masterbatches in the next step.

4.4 Preparation of hydroxyl modified multi-wall carbon nanotube functionalized with Si-69

0.2 g of hydroxyl modified multi-wall carbon nanotube (OH-MWCNT) was added in 100 ml of toluene and stirred with a magnetic stirrer for 3 min. Subsequently, the OH-MWCNT suspension was sonicated using ultrasonic bath at room temperature for 10 min. Thereafter, Si-69 was added into the OH-MWCNT suspension and vigorously stirred with mechanical stirrer using rotor speed 400 rpm for 6 h at 75 °C. The Si-69 concentration used in this study was varied from 0 to 6 %w/v. Later, the mixture was filtered using nylon membrane filter. Then, the OH-MWCNT modified with Si-69 (SiOH-MWCNT) was washed several times with methanol in order to remove the physical interaction between OH-MWCNT and non-reactive Si-69 [95]. Thereafter, SiOH-MWCNT was dried at 80 °C for 12 h. The grafting index of the obtained SiOH-MWCNT was characterized using FTIR. In addition, the obtained SiOH-MWCNT was used for preparing the SiOH-MWCNT/NR masterbatch in the next step.

4.5 Preparation of MWCNT/rubber masterbatches

4.5.1 Preparation of MWCNT/NR masterbatches using predispersing and conventional methods

MWCNT/NR masterbatches containing various MWCNT contents (from 4 to 12 phr) were prepared by using the predispersing and conventional methods. For the predispersing method, the dispersed MWCNT suspension prepared as described previously in section 4.3 was mixed with the masticated NR on a two-roll mill at 80 ºC for 15 min. For MWCNT/NR masterbatches prepared by using the conventional method, the MWCNT powder was mixed directly into NR on the two-roll mill using the same mixing conditions. The MWCNT/NR masterbatches obtained from these two methods were then used to prepare 50/50 NR/NBR blends. Also, MWCNT/NR masterbatches prepared by using predispersing were used to prepare NR/NBR compounds at various blend ratios.

4.5.2 Preparation of MWCNT/NBR masterbatch prepared by using predispersing method

The MWCNT suspension prepared as described in the section 4.3 was mixed with a masticated NBR on a two-roll mill at 80 ºC for 15 min in order to prepare the MWCNT/NBR masterbatch. The obtained MWCNT/NBR masterbatch was then used for preparing 4 phr MWCNT-filled NR/NBR compounds (mNBR) at various blend ratios.

4.5.3 Preparation of MWCNT/NR, OH-MWCNT/NR and SiOH-MWCNT/NR masterbatches prepared by using predispersing method

The MWCNT/NR, OH-MWCNT/NR and SiOH-MWCNT/NR masterbatches having 8 phr MWCNT were prepared by using the predispersing method as described previously in section 4.5.1. The obtained MWCNT/NR, OH-MWCNT/NR and SiOH-MWCNT/NR masterbatches were then used for preparing the 50/50 NR/NBR compounds containing 4 phr of MWCNT, OH-MWCNT and SiOH-MWCNT, respectively.

4.6 Preparation of MWCNT-filled 50/50 NR/NBR compounds using MWCNT/NR masterbatch prepared from predispersing and conventional methods

The formulations of 50/50 NR/NBR compounds at various MWCNT contents are shown in Table 4.5. 50/50 NR/NBR blends containing the MWCNT/NR masterbatches prepared by using the predispersing and conventional methods (see section 4.5.1) were denoted as “P” and “C”, respectively. The number following the letters indicates the amount of MWCNT in the blends. Each MWCNT/NR masterbatch and other ingredients, except the curatives, were mixed with NBR by using a laboratory-size internal mixer at a temperature of 50ºC, a rotor speed of 50 rpm and a fill factor of 0.7. The total mixing time was 8 min. After discharging, the compound was further mixed on a two roll-mill for 1 min. Then, the curatives were added into the compound. Thereafter, the compound was further mixed for 5 min and was finally passed through the smallest nip gap of the 2-roll mill ten times in the same direction before sheeting off.

Table 4.5 Formulation of NR/NBR compounds containing various MWCNT loading

Ingredient	**Amount (phr[a])**									
	P0	**P2**	**P4**	**P5**	**P6**	**C0**	**C2**	**C4**	**C5**	**C6**
NR	50	-	-	-	-	50	-	-	-	-
NBR	50	50	50	50	50	50	50	50	50	50
MWCNT/NR masterbatch[b]	-	52	54	55	56	-	52	54	55	56
Stearic acid	1	1	1	1	1	1	1	1	1	1
Zinc oxide	3	3	3	3	3	3	3	3	3	3
IPPD	1	1	1	1	1	1	1	1	1	1
TBBS	1.2	1.2	1.2	1.2	1.2	1.2	1.2	1.2	1.2	1.2
TBzTD	0.4	0.4	0.4	0.4	0.4	0.4	0.4	0.4	0.4	0.4
Sulfur	2	2	2	2	2	2	2	2	2	2

[a] Parts per hundred parts of rubber

[b] Masterbatches prepared from the predispersing and the conventional methods were used to prepare P and C compounds, respectively.

4.7 Preparation of MWCNT-filled NR/NBR compounds at various blend ratios using MWCNT/NR masterbatch and MWCNT/NBR masterbatch

In order to study effect of MWCNT/rubber masterbatch types on the properties of the MWCNT-filled NR/NBR blends, the MWCNT/NR and MWCNT/NBR masterbatches were used to prepare NR/NBR blends at various blend ratios. The formulations of all NR/NBR compounds are shown in Table 4.6. The NR/NBR blends having 4 phr MWCNT and containing the MWCNT/NR masterbatch and MWCNT/NBR masterbatch were denoted as “mNR” and “mNBR”, respectively. The MWCNT/NR and MWCNT/NBR masterbatches used in this experiment were prepared as described previously in section 4.5. In order to prepare 70/30, 50/50 and 30/70 mNRs, the NBR was masticated on a two-roll mill at 80 °C for 15 min. Then, the MWCNT/NR masterbatch was masticated for 2 min by using a laboratory-size internal mixer before blending with the masticated NBR for another 2 min at a setting temperature of 50 ºC with a rotor speed of 50 rpm and a fill factor of 0.7. Thereafter, various chemicals, except the curatives were added and mixed for 4 min. The total mixing time in the internal mixer was 8 min. After discharging, the compound was further masticated on a two roll-mill for 1 min before adding the curatives and mixing for 5 min. Finally, the mNR compound was passed through the smallest nip gap of the 2-roll mill ten times in the same direction before sheeting off.

For preparing 70/30, 50/50 and 30/70 mNBRs, the NR was masticated on a two-roll mill at 80 ºC for 15 min. Then, the MWCNT/NBR masterbatch was masticated for 2 min by using a laboratory-size internal mixer before blending with the masticated NR for another 2 min. The same procedure and conditions used for preparing mNR blend were applied to prepare the mNBR blends.

In addition 100/0 NR/NBR and 0/100 NR/NBR compounds containing 4 phr MWCNT were also prepared for using as the control. 100/0 NR/NBR containing 4 phr MWCNT or 100/0 mNR was prepared by mixing the dispersed MWCNT suspension having 4 phr MWCNT with the masticated NR on a two-roll mill at 80ºC for 15 min. Then, the NR containing 4 phr MWCNT was mixed with other ingredients by using the same equipment and conditions as those used for preparing the other mNR compounds. For preparing 0/100 NR/NBR containing 4 phr MWCNT or 0/100 mNBR, the dispersed MWCNT suspension containing 4 phr MWCNT was mixed with the masticated NBR on a two-roll mill at 80ºC for 15 min. Then, the NBR containing 4 phr MWCNT was mixed with other ingredients by using the same equipment and conditions as those used for preparing the 100/0 mNR compound.

Table 4.6 Formulation of NR/NBR compounds at various blend ratios

Ingredient	**Amount (phr)**							
	mNR				**mNBR**			
	100/0	**70/30**	**50/50**	**30/70**	**70/30**	**50/50**	**30/70**	**0/100**
NR	100	-	-	-	70	50	30	-
NBR	-	30	50	70	-	-	-	100
MWCNT/NR masterbatch	-	74	54	34	-	-	-	-
MWCNT/NBR masterbatch	-	-	-	-	34	54	74	-
MWCNT in MWCNT suspension	4	-	-	-	-	-	-	4
Stearic acid	1	1	1	1	1	1	1	1
Zinc oxide	3	3	3	3	3	3	3	3
IPPD	1	1	1	1	1	1	1	1
TBBS	1.2	1.2	1.2	1.2	1.2	1.2	1.2	1.2
TBzTD	0.4	0.4	0.4	0.4	0.4	0.4	0.4	0.4
Sufur	2	2	2	2	2	2	2	2

4.8 Preparation of 50/50 NR/NBR compounds containing unmodified carbon nanotube, hydroxyl modified multi-wall carbon nanotube and hydroxyl modified multi-wall carbon nanotube functionalized with silane coupling agent (Si-69)

The MWCNT/NR, OH-MWCNT/NR and SiOH-MWCNT/NR masterbatches were used to prepare the 50/50 NR/NBR blends containing 4 phr of MWCNT, OH-MWCNT and SiOH-MWCNT, respectively. The mixing procedure of these masterbatches is described in section 4.5.3. The formulations of all NR/NBR compounds are depicted in Table 4.7. The 50/50 NR/NBR blends containing MWCNT, OH-MWCNT and SiOH-MWCNT were denoted as "B_{MWCNT}", "$B_{OH-MWCNT}$" and "$B_{SiOH-MWCNT}$", respectively. The mixing procedure for preparing the blends was the same as that previously described in section 4.7. After adding the curatives, the compound was further mixed for 5 min and was finally passed through the smallest nip gap of the 2-roll mill 10 times in the same direction before sheeting off.

Table 4.7 Formulation of NR/NBR compounds containing MWCNT, OH-MWCNT and SiOH-MWCNT

Ingredient	**Amount (phr)**		
	B_{MWCNT}	**B_{OH-MWCNT}**	**B_{SiOH-MWCNT}**
NBR	50	50	50
MWCNT/NR masterbatch	54	-	-
OH-MWCNT/NR masterbatch	-	54	-
SiOH-MWCNT/NR masterbatch	-	-	54
Stearic acid	1	1	1
Zinc oxide	3	3	3
IPPD	1	1	1
TBBS	1.2	1.2	1.2
TBzTD	0.4	0.4	0.4
Sulfur	2	2	2

4.9 Determination of cure characteristics

Apparatus: Moving die rheometer (RheoTECH MD+)

Cure temperature: 150 ^{o}C

Test time: 30 minutes

Procedure:

Cure characteristics of rubber compounds were measured by using moving die rheometer (MDR) according to ASTM D5289-95. Approximately 5 g of uncured rubber, stored at room temperature at least 16 hours after compounding, was placed on the die of the rheometer cavity under oscillating arc of 0.5^{o}. The rheometer showed the increase in torque as a function of test time (Figure 4.1). The vulcanization characteristics such as minimum torque (M_L); maximum torque (M_H); scorch time (t_{s2}), time for the torque to rise 2 units from the minimum value and optimum cure time (t_{c100}) were determined from the cure curve. The t_{c100} was calculated according to the following equation 4.1.

$$t_{c100} = M_L + (M_H - M_L) \quad (4.1)$$

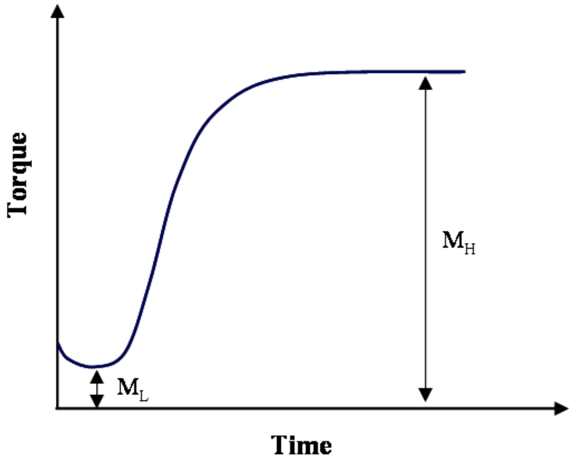

Figure 4.1 Characteristics of cure curve of rubber compound

4.10 Preparation of rubber vulcanizates

Apparatus: Electrical hydraulic hot press

Vulcanization temperature: 150 °C

Procedure:

Rubber compounds were compression molded at 150°C under pressure of 15 MPa using hydraulic hot press according to their respective optimum cure time (t_{c100}) as determined from the MDR. After the vulcanization, the specimen was kept at room temperature for at least 16 hours before testing.

4.11 Mechanical property measurements

4.11.1 Hardness

Apparatus: Hardness durometer Shore A (H17A)

Procedure:

The standard procedures for measuring hardness of rubber vulcanizates was described in ASTM D2240-97. The square specimen having 6 mm of thickness and smooth surfaces was placed on the platform of hardness tester. Then, measurements were made at different positions on the specimen. An average of these six positions was taken as the hardness value of the tested sample.

4.11.2 Tensile and tear properties

Apparatus: Universal tester (Instron 5566)

Procedure:

In this work, it was expected that the MWCNT in the rubber compounds sheeted out using a two-roll mill at a tight nip gap would be aligned in the milling direction. Thus, the test pieces for tensile and tear tests were punched from the vulcanized sheets having thickness of about 1 mm in two directions, i.e., machine direction (MD) and transverse direction (TD) as depicted in Figures 4.2A and 4.2B, respectively. In addition, the dimensions of tensile and tear specimens are shown in Figures 4.3 and 4.4, respectively. Tensile and tear properties of the specimens were determined by using a universal tester (Instron 5566) in accordance with ASTM D412-98 and D624-98, respectively. The specimens were tested by using a 1 kN load cell and a crosshead speed of 500 mm/min. The values of tensile and tear properties were the average of 4–5 specimens. In case of tensile test, the specimen was pulled in tension until rupture. Tensile data for the samples that failed outside of the gauge region were discarded. The 100% modulus, 300% modulus, elongation at break and tensile strength were calculated from equations 4.2, 4.3, 4.4 and 4.5, respectively. For tear strength, the test was involved measuring the maximum force per unit of thickness required to completely rupture the specified test specimen. Then, tear strength was calculated using equation 4.6.

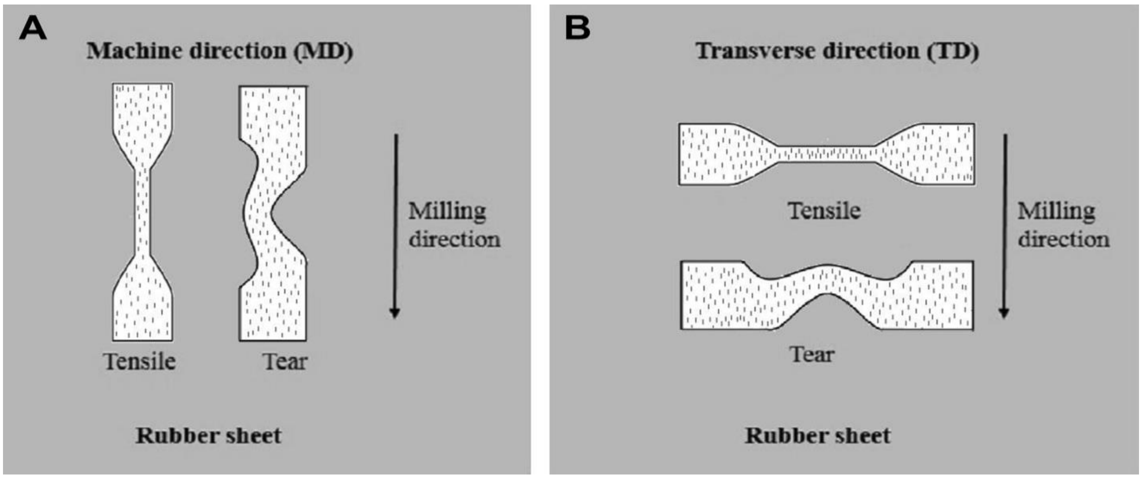

Figure 4.2 Specimen preparation for investigating the effect of milling direction; (A) MD and (B) TD

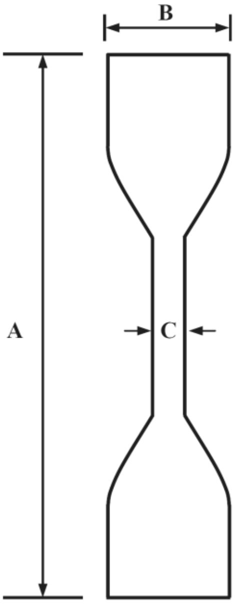

Figure 4.3 Specimen dimensions: A = 115 mm, B = 25 mm and C = 6.35 mm

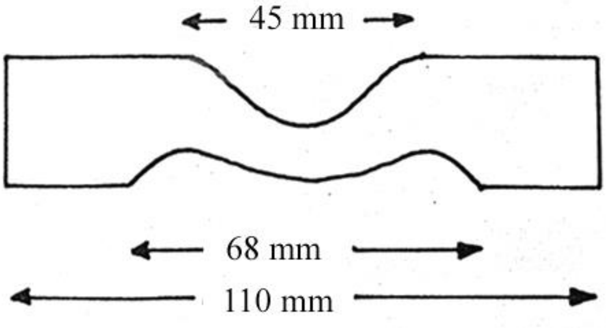

Figure 4.4 Dimensions of the tear specimen

1. 100% modulus = stress at 100% strain (4.2)

2. 300% modulus = stress at 300% strain (4.3)

3. % Elongation at break

$$\text{\% Elongation at break} = \frac{(L - L_0)}{L_0} \times 100 \qquad (4.4)$$

where L = observed distance between grips of the extended specimen

L_0 = original distance between the extensometer

4. Tensile strength

$$\text{Tensile strength} = \frac{F}{A} \qquad (4.5)$$

where F = observed force, N

A = cross-sectional area of unstrained specimen, mm^2

4. Tear strength

$$\text{Tear strength} = F/d \qquad (4.6)$$

where F = maximum force (N)
d = specimen thickness (mm)

4.11.3 Abrasion resistance

Apparatus: Zwick abrasion tester (Model 6102)
Procedure:

Abrasion loss which is reciprocal to abrasion resistance of rubber vulcanizates was determined following ASTM D5963-97. In this research, the cylindrical shape specimens having diameter of 16.0 ± 0.2 mm and height of 12 mm were used to determine abrasion loss. During testing, the specimen was abraded across an abrasive paper with corundum (grain size = 60) at constant loaded force of 10 N and constant speed of 0.32 m/s at room temperature. The volume loss of sample was calculated by using equation 4.7. At least 6 specimens were tested and the average value was taken as the test result.

$$A = \frac{\Delta m_t \times S_0}{d_t \times S} \qquad (4.7)$$

where A = abrasion loss (mm^3)
Δm_t = mass loss of the test piece (mg)
d_t = density of the test piece (mg/mm^3)
S_0 = normal abrasiveness (200 mg in this work)
S = abrasiveness of the abrasive sheet used (mg)

4.12 Dynamic mechanical property measurements

4.12.1 Heat build-up and dynamic compression set

Apparatus: Goodrich flexometer (model II™)

Procedure:

Determination of heat build-up of the vulcanizates was performed by using a Goodrich flexometer following ASTM D623-97. The dynamic compression set value could be also obtained from the same specimens using for heat build-up testing. The dynamic compression set was calculated using equation 4.8. The original height (H_0) of the specimens was measured prior to heat build-up testing. After the heat build-up testing was completed and the specimen was left at room temperature for 1 h, the final height (H_f) of the specimen was measured.

$$\text{Dynamic compression set (\%)} = [(H_0 - H_f)/H_0] \times 100 \tag{4.8}$$

4.12.2 Dynamic mechanical thermal analysis (DMTA)

Apparatus: Dynamic mechanical thermal analyzer (Explexor TM 25N)

Procedure:

The dynamic properties were determined using a dynamic mechanical thermal analyzer (DMTA). The test was performed in tension mode with static and dynamic strain amplitudes of 1% and 0.1%, respectively. The frequency used was 10 Hz. The temperature was scanned from -80ºC to 40ºC with a heating rate of 2 ºC/min. The relationship between the magnitude of reduction in tan δ_{max} (R) of gum and filled blends can be used to estimate the distribution of MWCNT in each phase of the blends by using equation 4.9 [51-54].

$$R = \frac{(\tan\delta_g)_{\max} \times (\tan\delta_f)_{\max}}{(\tan\delta_g)_{\max}} \qquad (4.9)$$

where, subscripts "*g*" and "*f*" are gum and filled blends, respectively. The term "*R*" can be related to the filler-to-rubber weight fraction (*w*) by multiplying with the rubber-filler interaction parameter (α) as given in equation 4.10.

$$R = \alpha w \qquad (4.10)$$

In case of binary blends, it can be separated to single and blend systems by the following relation;

$$R_1 = \alpha_1 w,\ R_2 = \alpha_2 w,\ R'_1 = \alpha'_1 w'_1,\ R'_2 = \alpha_2' w_2' \qquad (4.11)$$

where, subscripts "*1*" and "*2*" correspond to each single rubber system, and the "′" indicates the blend system. Additionally, *w´* denotes the weight fraction of filler to total rubber matrix in the blend as given in equation 4.12.

$$w = w'_1 + w_2' \qquad (4.12)$$

The ratio of weight fraction of filler in each phase component of the blends (w_1'/w_2') can be calculated by using equation 4.13.

$$\frac{w'_1}{w'_2} = \frac{R_1' R_2}{R_2' R_1} \qquad (4.13)$$

The equations 4.11 and 4.12 can be rearranged and then expressed as shown in equation 4.14 [51-54].

$$w_1' = \frac{R_1' R_2 w}{R_1' R_2 + R_2' R_1} \qquad (4.14)$$

The multiplication of w_1' and w_2' by 100 gives the amount of filler incorporated in rubber *1* and *2*, respectively. Consequently, it is expressed in percentage on the basis of total filler in the blend.

4.13 Dichroic ratio measurement

Apparatus: Raman spectrometer (NT-MDT)

Procedure:

The alignment degree of all types of MWCNT in the blends was investigated by determining the dichroic ratio obtained from Raman spectroscopy results. Raman spectrometer with a power of 10 mW was operated with 2 min of accumulation time. The excitation source used was a He/Ne laser with the wavelength of 632.8 nm. Each test piece with dimensions of 20 x 20 x 1 mm^3 cut from the tensile sheet in MD was arranged in parallel and perpendicular to the polarized light and the spectra data were collected. The dichroic ratio was calculated by using equation 4.15 [96-97].

$$\text{Dichroic ratio (R)} = I_{//}/I_{\perp} \qquad (4.15)$$

where, $I_{//}$ and $I_{\perp}$ are intensities of the G-band of MWCNT at 1570 cm^{-1} when the MD sample was arranged in parallel and perpendicular to polarized light, respectively. Arrangement of the MD sample for measuring the intensity of the G-band using Raman spectrometer is shown in Figure 4.5

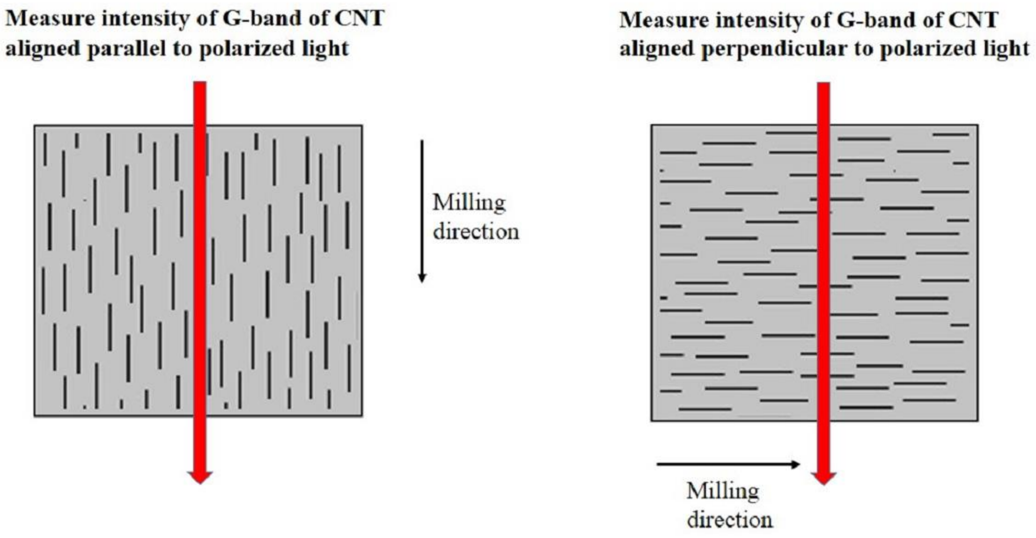

A B

Figure 4.5 Arrangement of the test piece in MD for measuring the intensity of the G-band using Raman spectrometer; (A) parallel to polarized light and (B) perpendicular to polarized light.

4.14 Electrical property measurements

4.14.1 Volume resistivity

Apparatus: HP4284A precision LCR meter (Model 4284A)

Procedure:

Specimens having dimensions of 50 x 50 x 8 mm^3 were used to determine their electrical resistivity between two conductive rubber electrodes with voltage of 1 V at room temperature by using a HP4284A precision LCR meter. The measured electrical resistance *(R)* was then converted into volume resistivity *(ρ)* by using equation 4.16.

$$\rho = \frac{RS}{d} \tag{4.16}$$

where, S is the cross-sectional area perpendicular to the current and d is the thickness of the specimens.

4.14.2 Electrical conductivity

Apparatus: Four-point probe (Model 2400)

Procedure:

The electrical conductivity was measured at room temperature using a four-point probe with a digital multi-meter having two outer current probes and two inner voltage ones. The test piece with the dimensions of 20 x 20 x 1 mm^3 was placed on the four-point probe apparatus. The current (I) was applied in the range of 0.05–500 mA and the voltage was measured. The electrical conductivity (σ) of the blends was evaluated by using equation 4.17 [98].

$$\sigma = \left(\frac{1}{(\mathrm{V/I}) * \mathrm{C.F.}_1 * \mathrm{C.F.}_2 * \mathrm{T}} \right) \tag{4.17}$$

where, T is thickness of the test piece and V is the voltage between inner probes. $C.F._1$ and $C.F._2$ are the resistance correction factors depending on the width and thickness of test piece, respectively [98].

4.15 Thermal conductivity measurement

Apparatus: Hot Disk thermal analyzer (Model 2500)

Procedure:

Thermal conductivity was measured using a hot disk thermal analyzer. A sensor was sandwiched between two slabs of sample having dimensions of 50 x 50 x 8 mm^3. Then, a heat pulse of 0.08 W was supplied to the sample for 5 s. The change in temperature as a function of time was recorded and the data obtained was converted into the thermal conductivity. The precision of the thermal conductivity measurement was ±3%.

4.16 Determination of morphology

4.16.1 Abraded surface examination

Apparatus: Scanning electron microscope (Hitachi (S-5000))

Procedure:

To investigate the abraded surfaces of the specimens used for abrasion testing, the specimens were mounted on the stubs and abraded surfaces of the samples were sputtered with gold to prevent charging on the surface before examining under SEM.

4.16.2 MWCNT dispersion and alignment examination

Apparatus: Scanning electron microscope (JEOL (JSM-6301F))

Procedure:

To investigate the degree of MWCNT dispersion and MWCNT alignment in MD and TD, rubber pieces with the dimensions 2 x 50 x 1 mm^3 were cut from the vulcanized sheets in both directions, as depicted in Figure 4.6. Then, they were immersed in liquid nitrogen for at least 3 min prior to fracture at their middle part. Later, they were mounted on the stubs and the newly exposed surfaces of the samples were sputtered with platinum–palladium to prevent charging on the surface before examining under SEM.

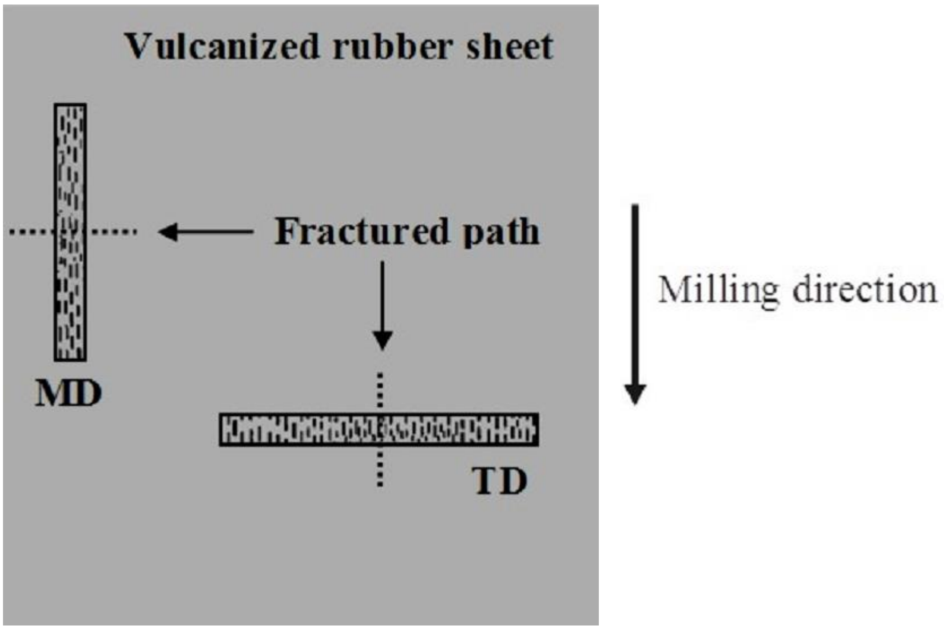

Figure 4.6 Preparation of fractured surfaces of the blends in MD and TD

4.16.3 Phase morphology examination

Apparatus: Scanning electron microscope (JEOL (JSM-5410))

Procedure:

To investigate phase morphology of NR/NBR blends, the rubber samples with the dimensions 2 x 50 x 1 mm^3 were immersed in liquid nitrogen for 6 min, and then fractured. Thereafter, the fractured surfaces were stained with osmium tetroxide (OsO_4). Then, they were mounted on the stubs and the newly exposed surface of the samples was sputtered with platinum–palladium to prevent charging on the surface before examining under SEM.

4.17 Dielectric properties

Apparatus: Impedance analyzer (Model 4192A)

Procedure:

The dielectric properties were measured with an impedance analyzer. The investigations have been performed on test piece with dimensions of 10 x10 x 1 mm^3. The samples were placed between two gold plated brass electrodes of 20 mm diameter. In the frequency range between 0.01 Hz to 10 MHz, real part of permittivity was obtained.

4.18 Fourier transform infrared spectroscopy (FTIR)

Apparatus: Fourier transform infrared spectroscopy (Equinox 55)

Procedure:

The expected silanization reaction between OH-MWCNT and Si-69 was investigated using FTIR. In order to obtain the spectra of the samples, the samples were prepared as KBr pellets. The spectra were recorded in the region 4,000-500 cm^{-1}. In this case, the grafting onto the OH-MWCNT surface could be confirmed by the presence of the established Si–O–C bonds at 1100 cm^{-1}. The intensity of the peak at 1576 cm^{-1} which was associated with the typical signal of MWCNT and not involved in the grafting reaction was used to normalize the intensity of the peak at 1100 cm^{-1} in order to determine the grafting index or the amount of grafting taken place. The grafting index can be written as equation 4.18.

$$\text{Grafting index} = I_{1100}/I_{1576} \qquad (4.18)$$

where, I_{1100} and I_{1576} are intensities of the peaks at 1100 and 1576 cm^{-1}, respectively.

4.19 Swelling ratio measurement

Procedure:

In this study, swelling ratio of the vulcanizates in the gasohol 95 and hydraulic oil is determined to estimate their resistance to the oils. Vulcanized rubber was weighed approximately 0.8 g using an electrical balance and this was considered to be an original weight. Each test piece was immersed in 80 ml oil (gasohol 95 oil or hydraulic oil) and stored in dark cabinet at room temperature for seven days. Then, the swollen specimen was removed from the oil and the excess oil was blotted using towel paper. Thereafter, the sample was put in the weighing bottle and weighed accurately. Oil resistance was presented in terms of a reciprocal swelling ratio as shown in equation 4.19. The value of swelling ratio (Q) of each vulcanizate was the average of three specimens.

$$Q = (W_s - W_u)/W_u \qquad (4.19)$$

where W_u = weight of unswollen rubber (g)

W_s = weight of swollen rubber (g)

4.20 Determination of rheological properties

Apparatus: Rubber process analyzer (RPA2000)

Procedure:

Approximately 5 g of the CR dipped sample was placed in the testing chamber. The experiment was carried out at the frequency and temperature of 3.14 rad/s and 90 °C, respectively. The strain deformation was ranged from 0.28% to 1200%. The results of elastic modulus (G´) and loss modulus (G´´) were recorded.

CHAPTER V
RESULTS AND DISCUSSION

In this study, the results and discussion of this thesis are divided into three main parts. In the first part, the properties of MWCNT-filled 50/50 NR/NBR blends containing MWCNT/NR masterbatch prepared from predispersing and conventional methods at various MWCNT loadings are focused. Then, the properties of NR/NBR blends at various blend ratios prepared from MWCNT/NR masterbatch or MWCNT/NBR masterbatch by using predispersing method under optimum conditions are compared. Finally, the effect of hydroxyl modified multi-wall carbon nanotube functionalized with silane coupling agent on the properties of 50/50 NR/NBR blend containing SiOH-MWCNT/NR masterbatch prepared by using predispersing method at optimum conditions is discussed in the third part.

5.1 The properties of MWCNT-filled 50/50 NR/NBR blends prepared from MWCNT/NR masterbatch

5.1.1 The effect of preparation methods on the properties of 50/50 NR/NBR blends filled with MWCNT

In this part, the properties such as cure characteristics, mechanical and electrical properties of the 50/50 NR/NBR blends prepared by utilizing MWCNT/NR masterbatch mixed by predispersing method (P) and conventional method (C) are compared. Also, the morphology of the P and C vulcanizates is presented.

5.1.1.1 Cure characteristics and viscoelastic properties of 50/50 NR/NBR coumpounds

Cure curves of both P and C blends are depicted in Figure 5.1

and, their maximum torque (M_H), minimum torque (M_L) and torque difference (M_H-M_L) as a function of MWCNT loading are compared in Figure 5.2. In addition, their scorch time (t_{s2}) and cure time (t_{c100}) are summarized in Table 5.1. It is evident that the scorch and cure times of both P and C blends gradually reduce with increasing MWCNT loading as displayed in Table 5.1. The reductions of scorch and cure times may result from the dilution effect and thermal conductivity enhancement of MWCNT [16]. It is interesting that the scorch and the cure times of the P blends are shorter than those of the C blends. This may be explained by the improved MWCNT dispersion bringing about the better formation of a continuous MWCNT network leading to greater thermal conductivity, and hence faster onset of crosslinking [16]. Additionally, the results reveal that the minimum torque, maximum torque and torque difference of all compounds tend to increase with increasing MWCNT loading as shown in Figure 5.2. The increase in minimum torque could be explained by the dilution effect while the increases in maximum torque and torque difference could be explained by the increased curative concentration in the mobilized rubber portion. Similar observation is also found in carbon black filled NR compounds as previously reported by Choi and co-workers [99]. As the torque difference is directly proportional to the cure state, the results reveal that crosslink density of the blends tends to increase with increasing MWCNT content. Compared to the C blends, the P blends exhibit higher torque difference and, therefore, higher crosslink density.

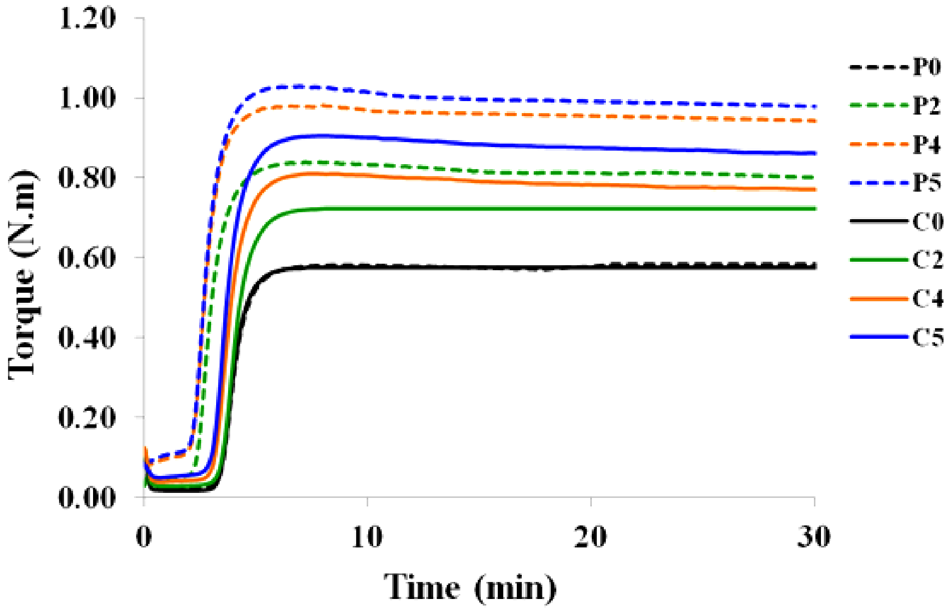

Figure 5.1 Cure characteristics of the P and C compounds at various MWCNT loadings.

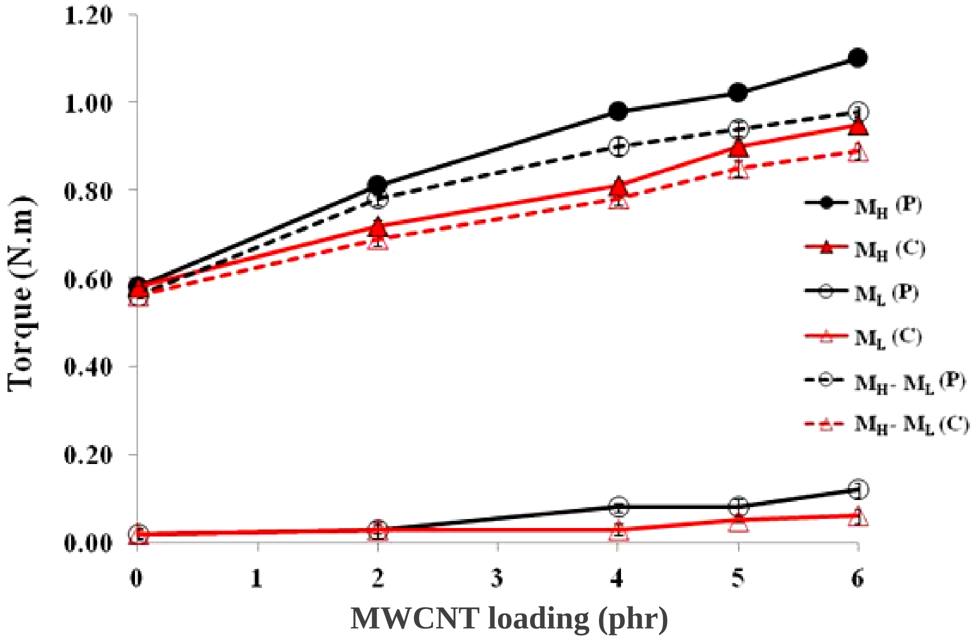

Figure 5.2 Minimum (M_L) torque, maximum (M_H) torque and torque difference (MH-ML) as a function of MWCNT loading of the P and C compounds.

Table 5.1 Scorch (t_{s2}) and cure (t_{c100}) times of the P and C compounds

Blend	MWCNT content (phr)	t_{s2} (min)	t_{c100} (min)
P	0	3.08±0.02	7.63±0.11
	2	2.24±0.05	6.40±0.09
	4	1.92±0.01	6.20±0.07
	5	1.87±0.08	6.14±0.13
	6	1.80±0.03	6.10±0.02
C	0	3.14±0.06	7.75±0.05
	2	3.11±0.01	7.26±0.01
	4	2.80±0.01	7.17±0.08
	5	2.72±0.04	7.05±0.13
	6	2.61±0.07	6.77±0.02

Figures 5.3a and 5.3b present storage modulus as a function of deformation strain of the P and C blends, respectively. As can be seen, the storage modulus at low strain of both P and C blends increases remarkably when MWCNT loading is increased. This is because the strong van der Waals interaction between MWCNTs promoting the formation of MWCNT agglomerates at high MWCNT loading gives rise to the increase in filler-filler interaction. However, it is evident that such MWCNT networks can be disrupted at high strain leading to the sharp drop in the storage modulus. Also, it can be seen that filler-filler interaction in the C blends is stronger than that for the corresponding P blends.

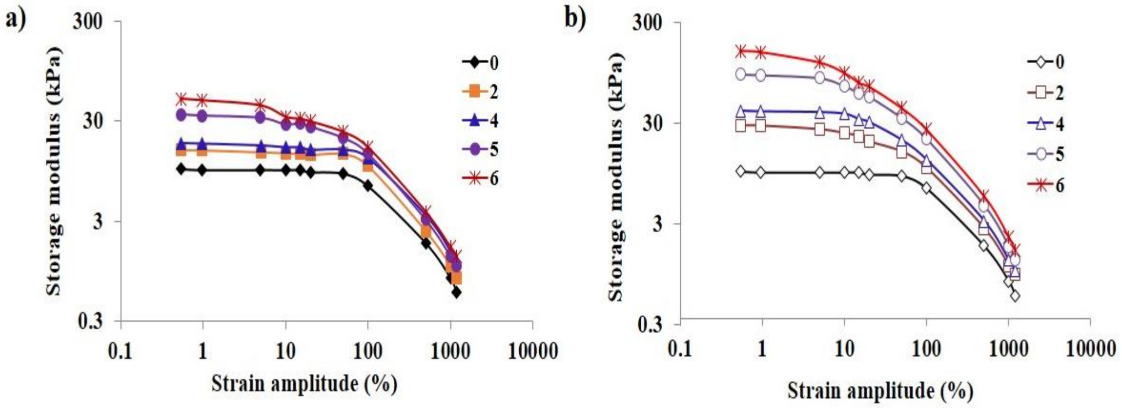

Figure 5.3 Storage modulus as a function of deformation strain of the P and C blends at various MWCNT contents; (a) P and (b) C blends

5.1.1.2 Morphology

The degree of MWCNT dispersion in the P and C blends having various MWCNT loadings was examined using SEM and the micrographs are given in Figures 5.4 and 5.5, respectively. As can be seen in Figure 5.4, good dispersion of MWCNT is observed in the P blends having 2 and 4 phr of MWCNT. Agglomeration of MWCNT is found when the amount of MWCNT is increased to 6 phr. The results also reveal that the average diameter of the small MWCNT agglomerates for the P blend having 5 phr and 6 phr of MWCNT is about 267 nm and 270 nm, respectively. For the C blends as displayed in Figure 5.5, poor MWCNT dispersion is observed when only 2 phr of MWCNT is added and the average size of the agglomerate is about 2.6 µm. Also, the agglomerate size tends to increase with increasing MWCNT content. At 6 phr of MWCNT, the average diameter of the large MWCNT agglomerates for the C blend is about 6 µm which is significantly larger than that of the corresponding P blend. From these results, it can be stated that improvement of MWCNT dispersion can be achieved by using the predispersing method. However, the formation of MWCNT agglomerates cannot be avoided when MWCNT loading is high.

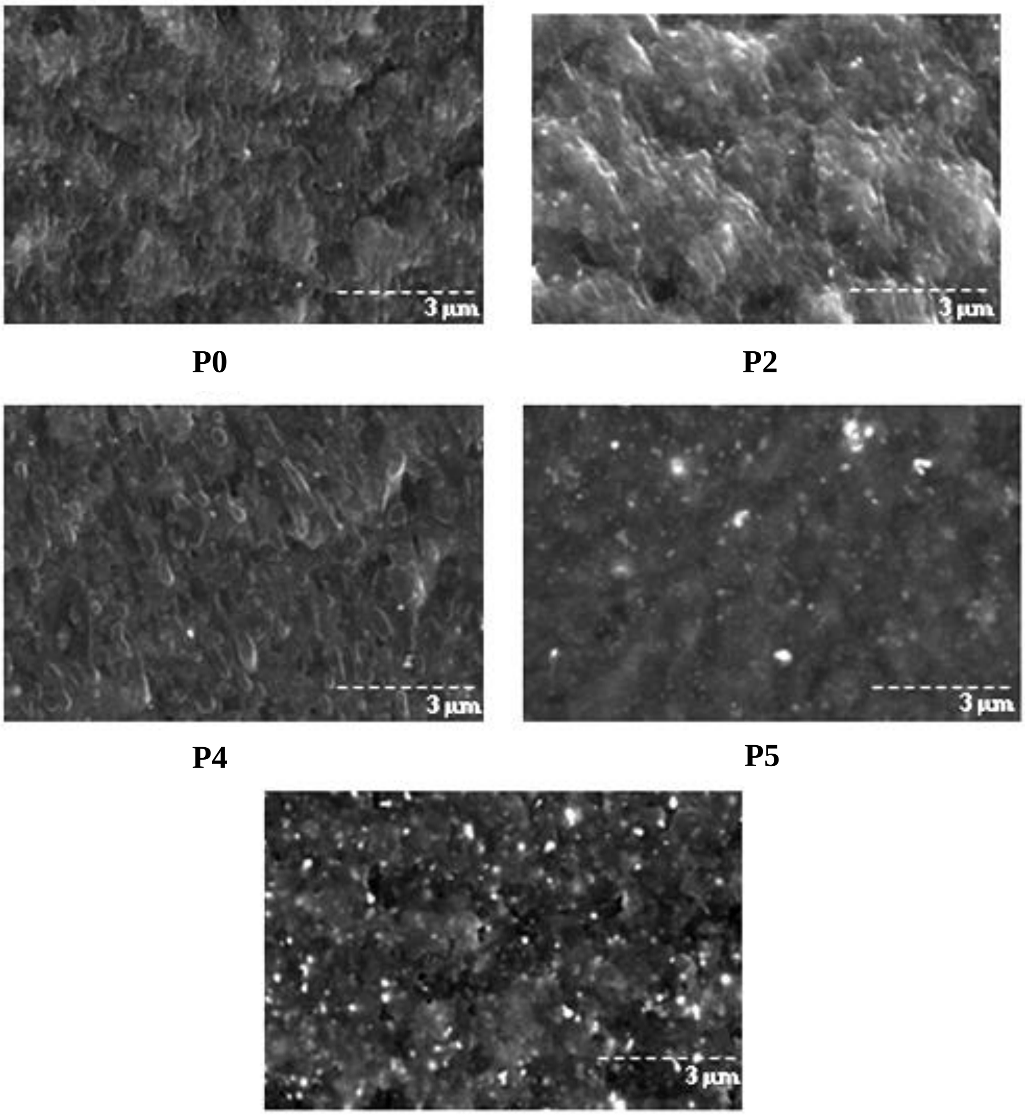

P0 **P2**

P4 **P5**

P6

Figure 5.4 SEM micrographs of fractured surface of MWCNT-filled NR/NBR vulcanizates containing the masterbatch prepared from predispersing method at various MWCNT contents.

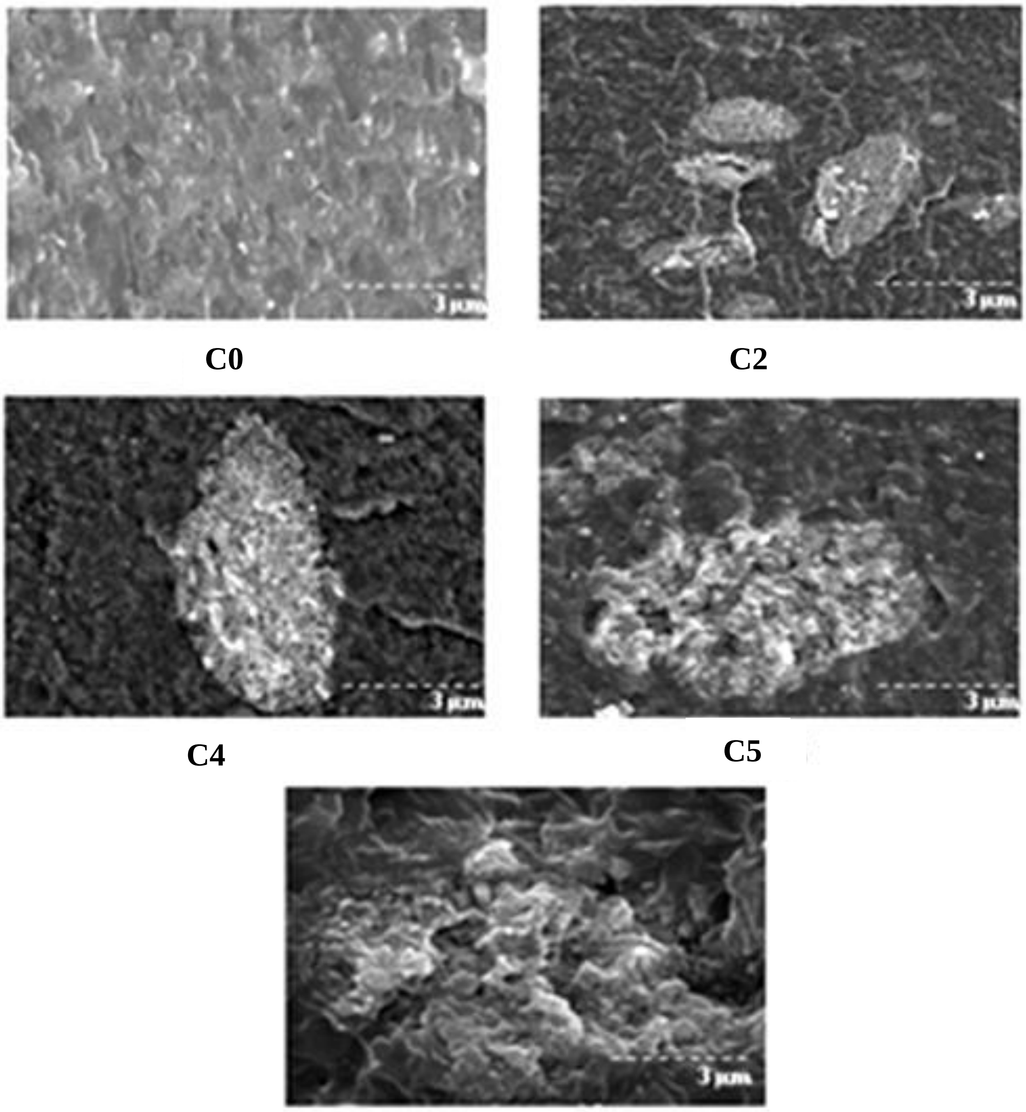

C0 **C2**

C4 **C5**

C6

Figure 5.5 SEM micrographs of fractured surface of MWCNT-filled NR/NBR vulcanizates containing the masterbatch prepared from conventional method at various MWCNT contents.

5.1.1.3 Mechanical properties

Hardness and moduli (100% and 300%) as a function of MWCNT loading of both P and C blends are compared in Figures 5.6 and 5.7, respectively. All samples exhibit increases in hardness and moduli when MWCNT loading is increased. In contrast, their elongation at break, displayed in Figure 5.8, shows the opposite trend. The increases of hardness and moduli and the decrease of elongation at break are attributed to the combination of dilution effect and increased crosslink density. It is also found that hardness and moduli of the P blends are superior to those of the C blends. Explanation is given by the greater crosslink density of the P blends. Despite its higher crosslink density, it is found that the P blends also possess greater elongation at break, compared to the C blends. It is thought that the low elongation at break of the C blends arises from the poor MWCNT dispersion. It is interesting to observe the difference in tensile strength trend as shown in Figure 5.9 when the different preparation methods were utilized. As can be seen, the tensile strength of the P blends markedly increases with increasing MWCNT loading up to 4 phr and then decreases. The reduction of tensile strength at high MWCNT loading is attributed to the formation of MWCNT agglomerates, as previously depicted in Figure 5.4. On the contrary, tensile strength of the C blends decreases continuously with increasing MWCNT loading. Poor MWCNT dispersion, particularly at high loading, is used to explain the results. These results agree well with SEM images as depicted in Figure 5.5. At a particular MWCNT loading, tensile strength of the P blends is greater than that of the C blends. Additionally, it appears in Figure 5.10 that tear strength of both P and C blends increases with increasing MWCNT content and, again, the P blends have higher tear strength than the corresponding C blends. The greater strengths of the P blends are thought to be a consequence of better MWCNT dispersion. The result also indicates that MWCNT agglomerates having diameter of 6 µm is still able to resist tear but these agglomerates could act as defects in the tensile sample [100].

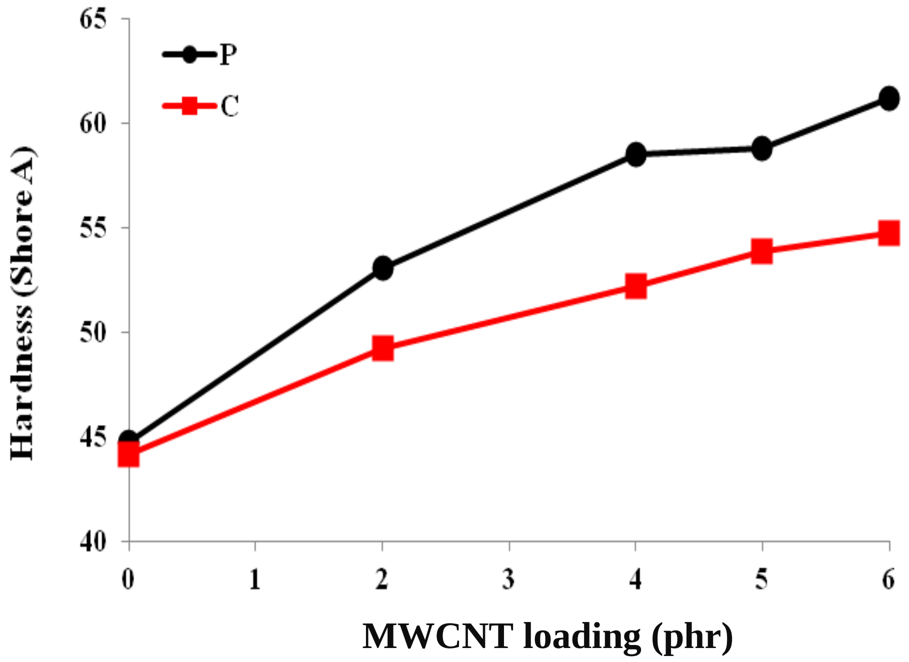

Figure 5.6 Hardness of the vulcanizates containing the masterbatch prepared from different methods.

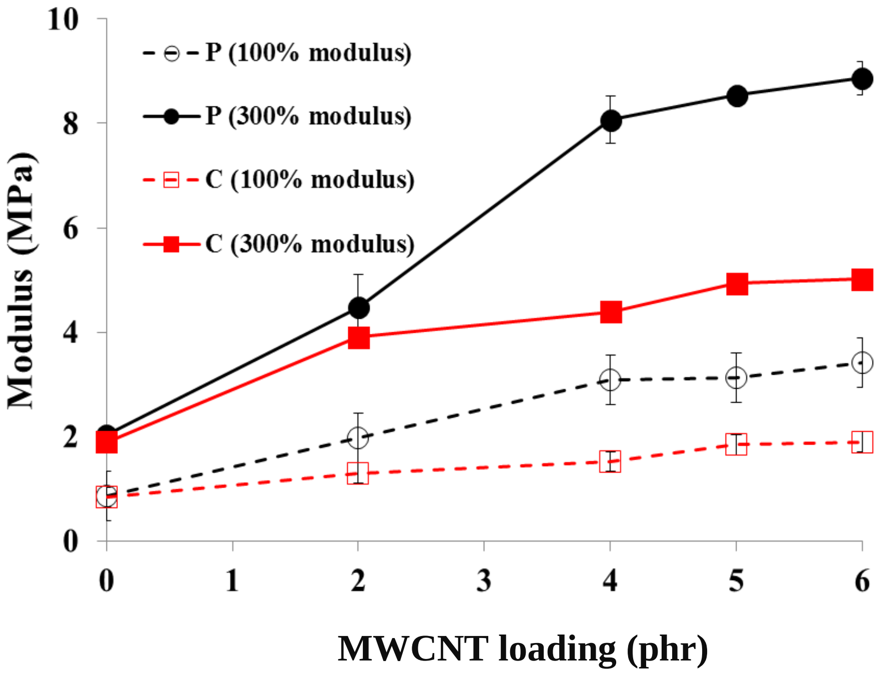

Figure 5.7 100% and 300% moduli of the vulcanizates containing the masterbatch prepared from different methods.

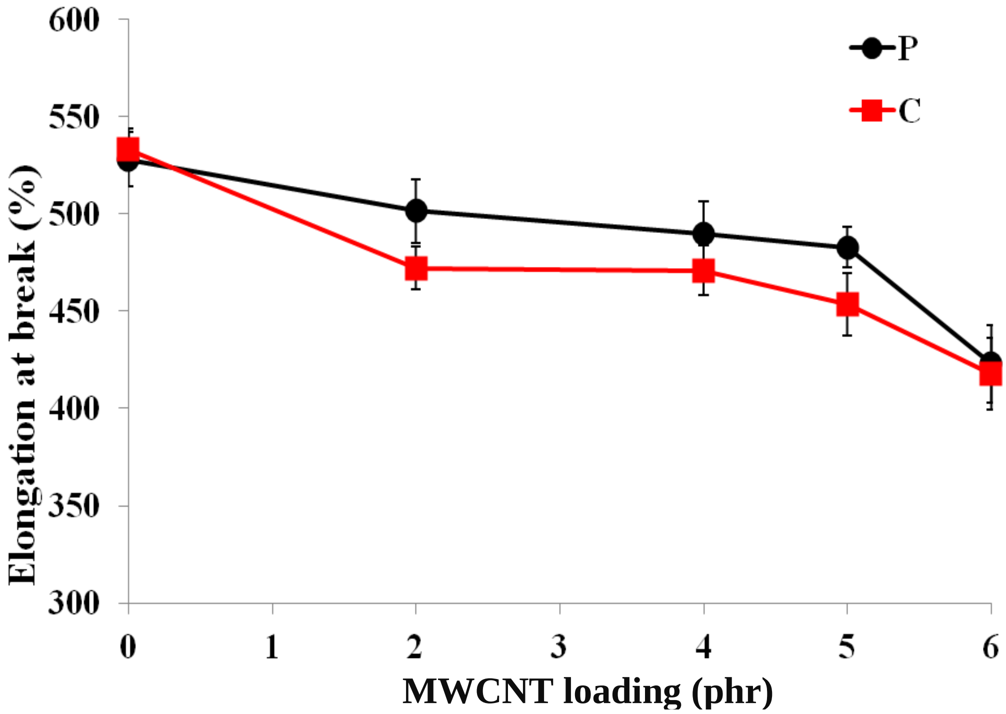

Figure 5.8 Elongation at break of the vulcanizates containing the masterbatch prepared from different methods.

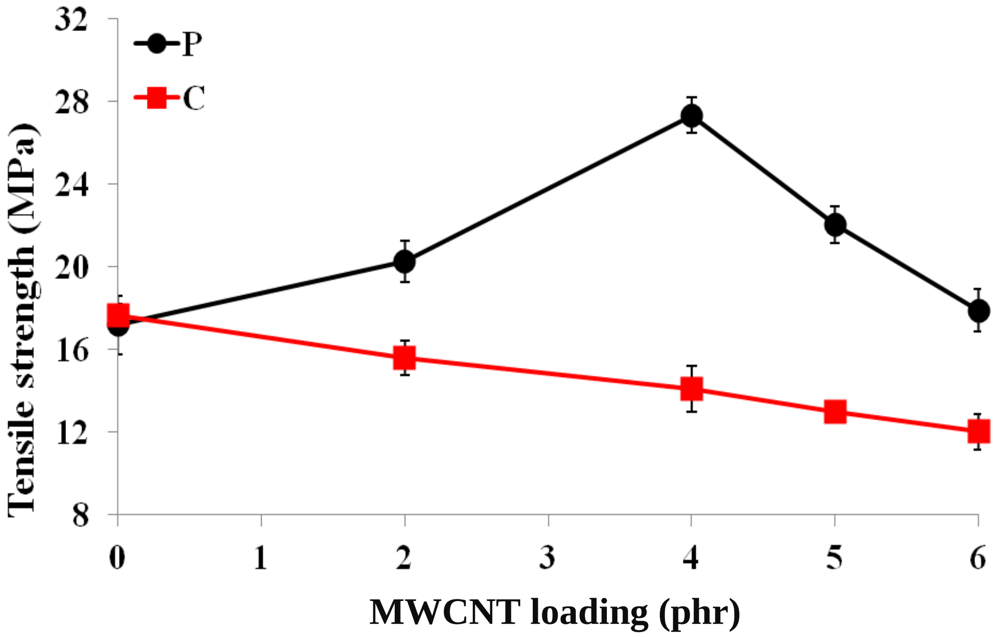

Figure 5.9 Tensile strength of the vulcanizates containing the masterbatch prepared from different methods.

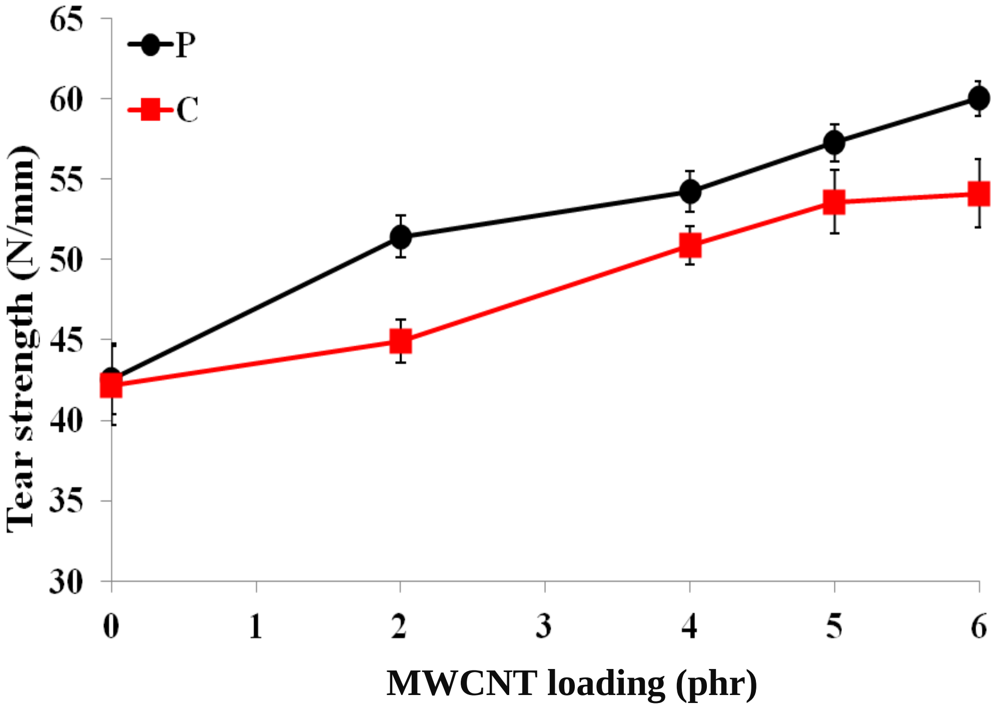

Figure 5.10 Tear strength of the vulcanizates containing the masterbatch prepared from different methods.

Abrasion resistance, inversely proportional to the volume loss, as a function of MWCNT content of all composites is displayed in Figure 5.11. It can be seen that abrasion resistance of both P and C blends rapidly increases when only 2 phr of MWCNT is added. However, enhancement in abrasion resistance of the P blend is greater than the C blends when MWCNT is further incorporated into the rubber matrices. This can be attributed to the increasing of crosslink density and better dispersion for the P blends. It has been reported that the blend with good filler dispersion exhibits better abrasion resistance than that with poor filler dispersion [101]. The improvement in their abrasion resistance coincides with the appearance of the series of parallel ridges known as Schallamach ridges on the abraded surfaces of both P and C blends as illustrated in Figures 5.12 and 5.13, respectively [102]. The formation of these ridges on abraded surfaces can protect the surface lying behind the ridges from further abrasion by the decrease of contact area resulting in the reduction of the abrasion loss [102-103]. It is found that the spacing between the ridges on the abraded surfaces of the P blend is narrower than that of the corresponding C blend.

Also, this is because the P blend has better MWCNT dispersion and higher crosslink density leading to its higher stiffness compared to the C counterpart. Therefore, the P blend possesses relatively greater abrasion resistance compared with the C blend.

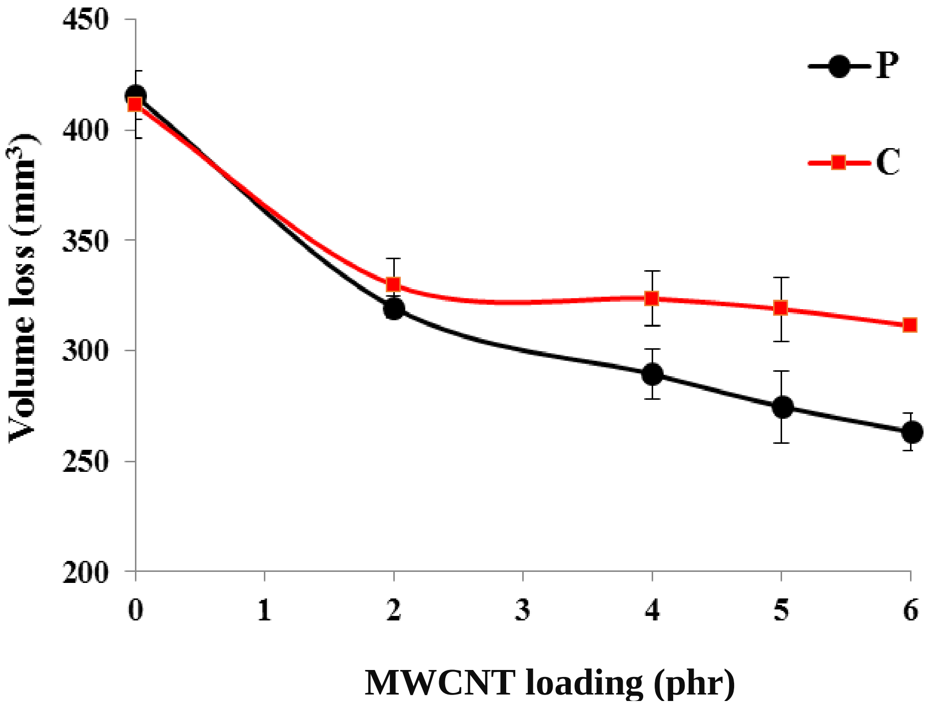

Figure 5.11 Volume loss of the vulcanizates containing the masterbatch prepared from different methods.

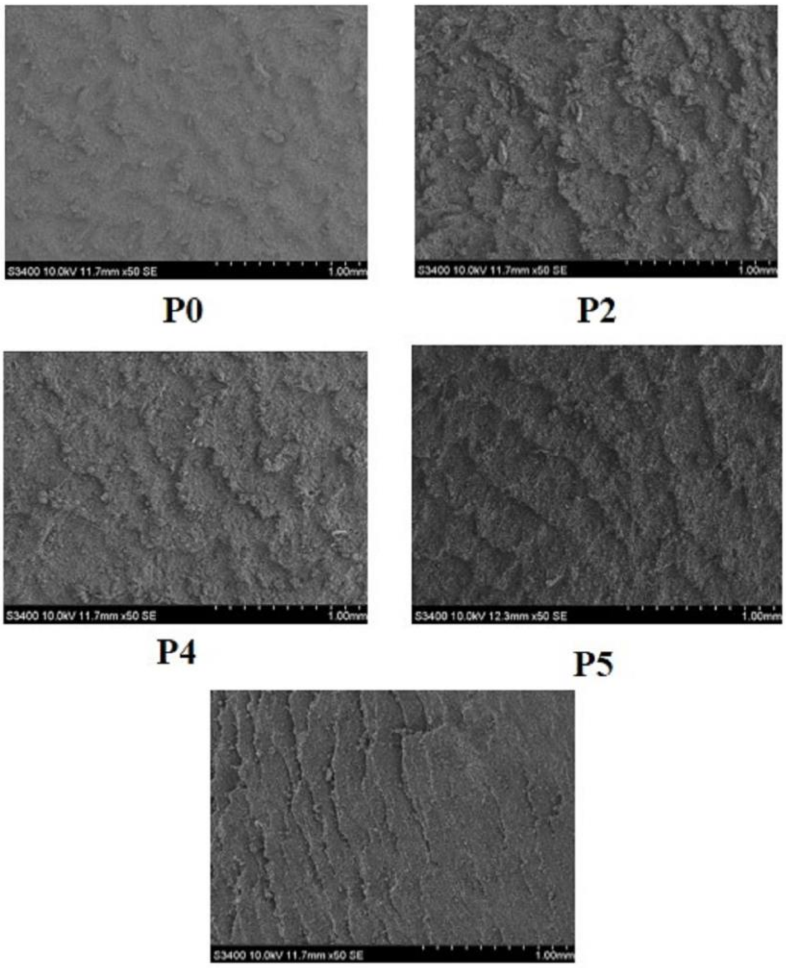

P0 **P2**

P4 **P5**

P6

Figure 5.12 SEM images of abraded surfaces of MWCNT-filled NR/NBR vulcanizates containing the masterbatch prepared from predispersing method at various MWCNT contents.

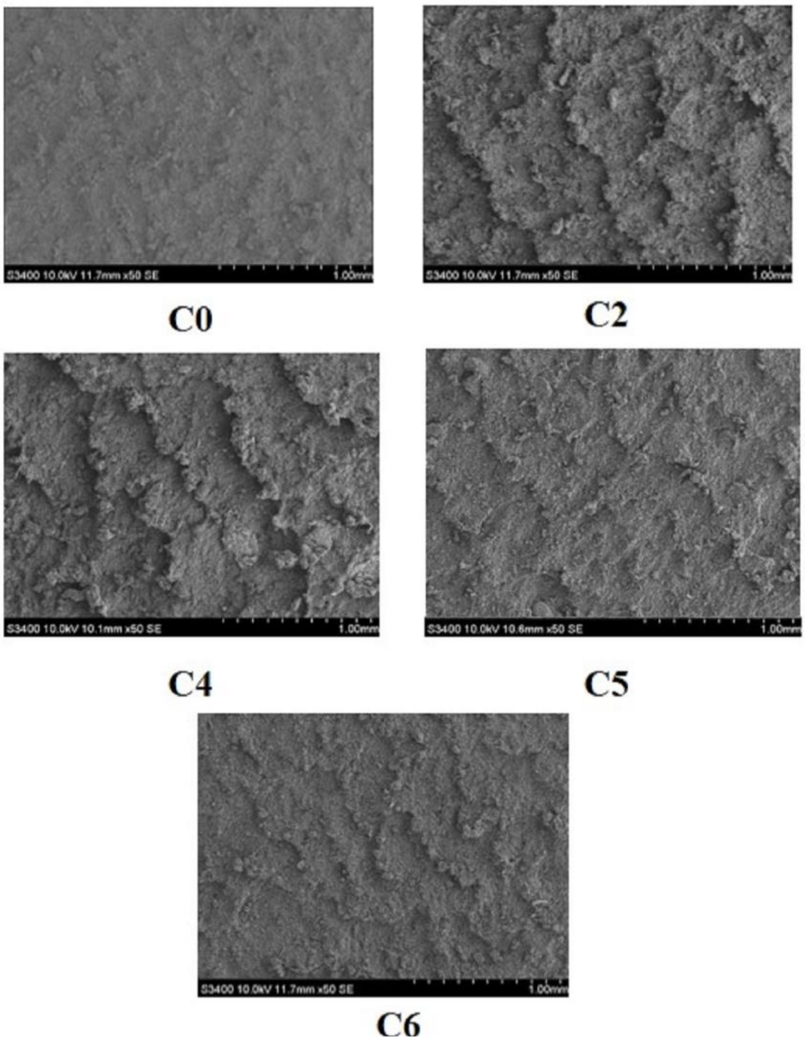

C0 **C2**

C4 **C5**

C6

Figure 5.13 SEM images of abraded surfaces of MWCNT-filled NR/NBR vulcanizates containing the masterbatch prepared from conventional method at various MWCNT.

5.1.1.4 Dynamic mechanical properties

Heat build-up and dynamic compression set of the P and C blends are presented in Figures 5.14 and 5.15, respectively. Both heat build-up and dynamic compression set of all blends tend to increase when MWCNT loading is increased due to the dilution effect. Additionally, the C blends give higher heat build-up and dynamic compression set than the P blends. The higher energy loss during the dynamic test found in the C blends is thought to arise from poor MWCNT dispersion and, therefore, greater friction between the highly entangled MWCNTs. It is also found that the compression set of the P blends sharply increases when MWCNT content is higher than 4 phr. The result coincides with the formation of MWCNT agglomerates in the P blends as previously illustrated in Figure 5.4.

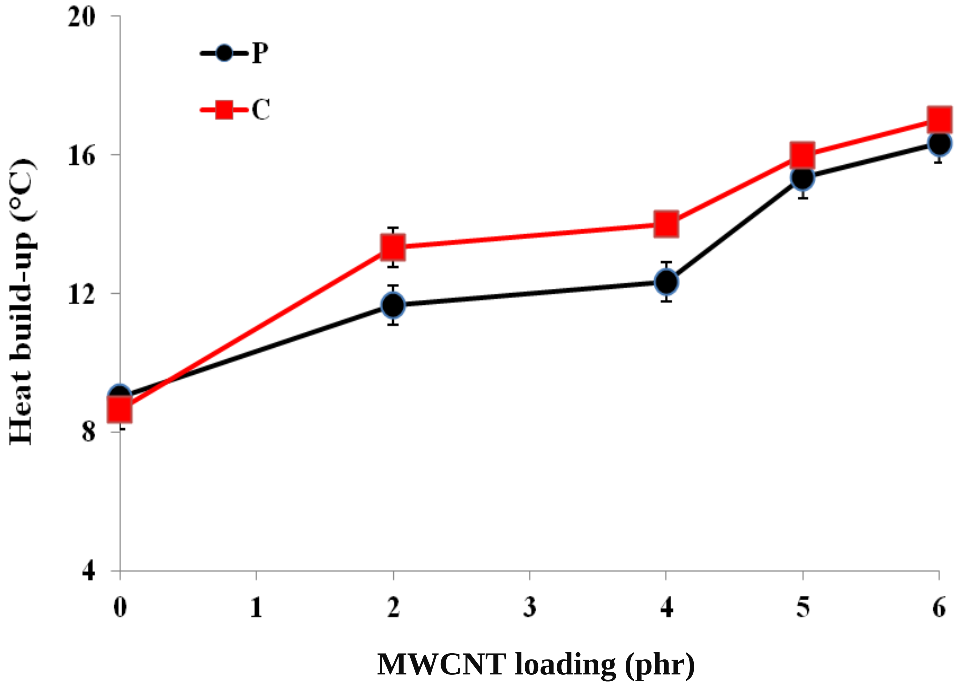

Figure 5.14 Heat build-up of the MWCNT-filled NR/NBR vulcanizates containing the masterbatch prepared from different methods.

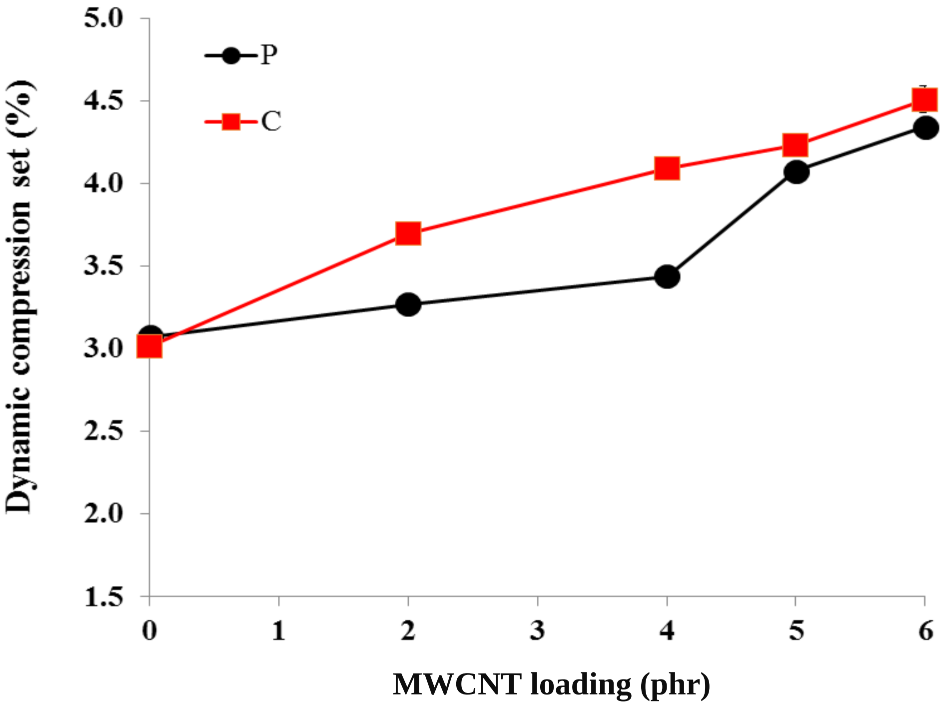

Figure 5.15 Dynamic compression set of the MWCNT-filled NR/NBR vulcanizates containing the masterbatch prepared from different methods.

Figure 5.16 depicts loss tangent (tan δ) as a function of the temperature of both P and C blends containing the masterbatch prepared from different methods. Also, their glass transition temperatures (T_g), maximum tan δ (tan δ_{max}) and storage modulus (E´) are summarized in Table 5.2. It is evident that there are two T_gs around -56 ºC and -4.5 ºC corresponding to NR and NBR phases, respectively. The difference in preparation method does not affect T_gs of both phases. In addition, T_gs of both phases do not significantly change with increasing MWCNT loading. However, the tan δ_{max} of both phases reduces when MWCNT loading is increased for all cases. This is simply due to the dilution effect. Additionally, it is found that tan δ_{max} of both phases for the P blends is lower than that of the corresponding C blends. This indicates the greater reinforcement of MWCNT in the P blends due to the better dispersion of MWCNT in the rubber matrices [16]. This result corresponds well with the mechanical properties of the composites. Also, storage modulus (E´) at 30 °C for P and C blends having various MWCNT loadings is compared in Table 5.2. It is obvious that the E´ of both P and C blends tends to increase with increasing MWCNT loading. At specific MWCNT loading, the E´ of the P vulcanizate is higher than that of the C samples due to stronger reinforcement between MWCNT and rubber chain. This result agrees well with hardness and modulus depicted previously in Figures 5.6 and 5.7.

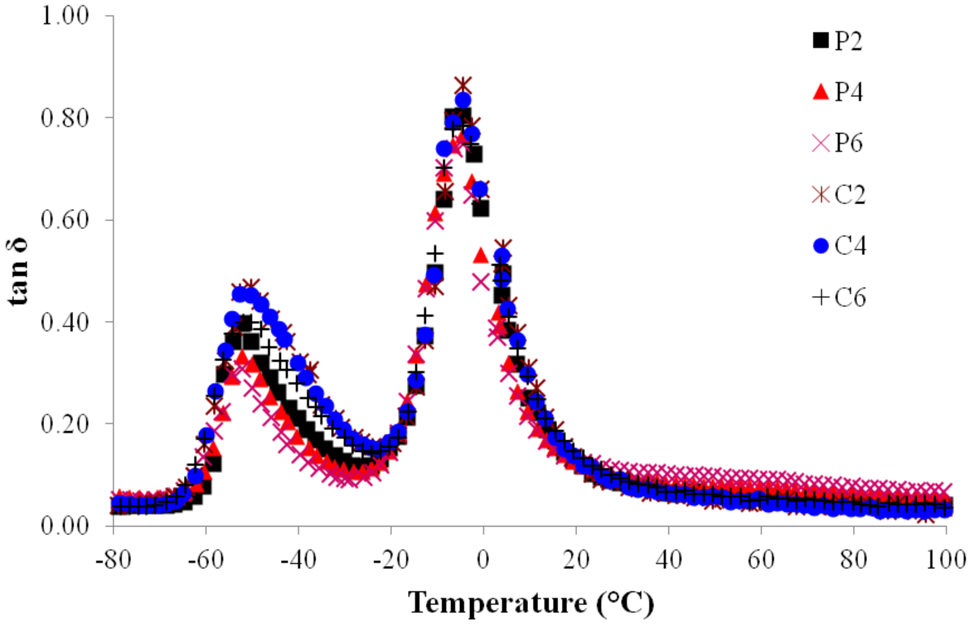

Figure 5.16 Loss tangent (tan δ) as a function of the temperature for the MWCNT-filled NR/NBR vulcanizates containing the masterbatch prepared from different methods.

Table 5.2 Effect of MWCNT loading on dynamic mechanical properties.

Blend	MWCNT content (phr)	NR		NBR		E' (MPa) at 30 °C
		T_g (°C)	tan δ_{max}	T_g (°C)	tan δ_{max}	
P	0	-56.3	0.48	-4.5	0.93	2.11
	2	-56.1	0.39	-4.6	0.80	4.96
	4	-56.4	0.33	-4.7	0.75	8.38
	5	-56.7	0.31	-4.5	0.73	9.75
	6	-56.6	0.30	-4.6	0.71	10.18
C	0	-56.2	0.48	-4.4	0.94	2.09
	2	-55.9	0.46	-4.5	0.87	3.09
	4	-56.7	0.44	-4.6	0.83	3.82
	5	-56.3	0.41	-4.5	0.81	4.46
	6	-56.4	0.39	-4.6	0.78	4.88

5.1.1.5 Oil resistance

In this section, swelling ratio of the vulcanizates in the gasohol 95 and hydraulic oil is determined to estimate their resistance to the oils. The swelling ratio of the P and C blends as a function of MWCNT loading in the gasohol and hydraulic oil are presented in Figures 5.17 and 5.18. It is found that both P and C blends exhibit a decreasing trend of swelling ratio in both gasohol and hydraulic oil with increasing MWCNT loading. This indicates that the penetration of the gasohol and hydraulic oil into MWCNT-filled NR/NBR blend is reduced by increasing MWCNT loading. The reduction of swelling ratio can be explained by the dilution effect. However, the swelling ratio of the P and C blends in the gasohol is higher than those of their corresponding samples in the hydraulic oil. This result indicates that the solubility parameter of 50/50 NR/NBR blend used in this work is closer to that of the gasohol having higher polarity than the hydraulic oil. It should be noted that gasohol oil is polar oil because it is the mixture of 10% ethanol mixed with gasoline [104]. It is also apparent that the swelling ratio of the P blends are lower than those of the C blends. The explanation is given by the higher crosslink density of P blends. Also, the better dispersion of MWCNT in the P blends thus promoting better interaction between MWCNT and rubber matrices can be another reason for the obtained results.

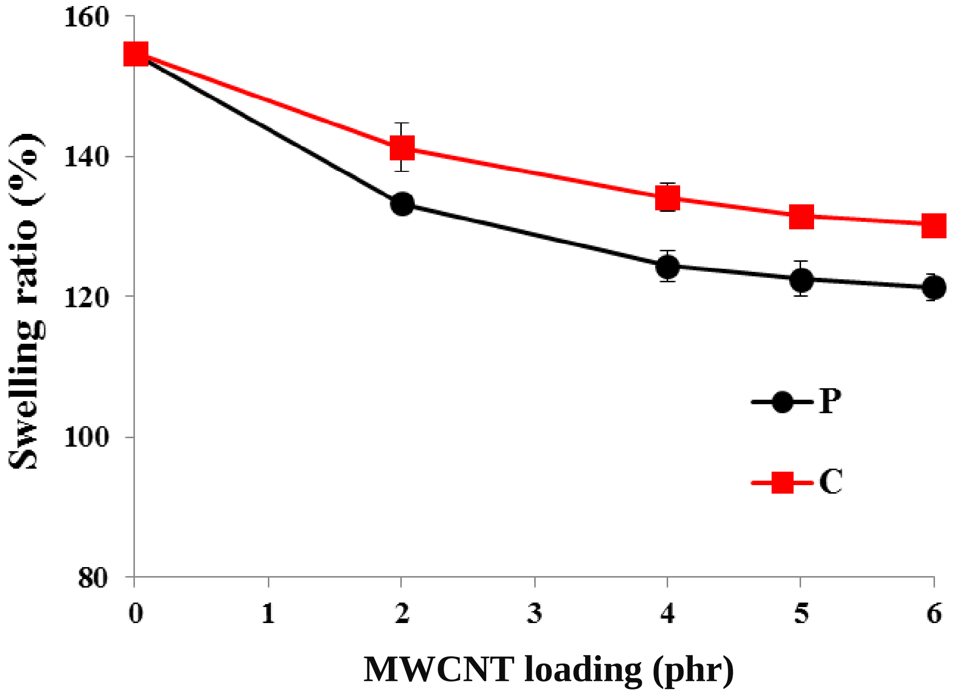

Figure 5.17 Swelling ratio of MWCNT-filled NR/NBR vulcanizates containing the masterbatch prepared from different methods in gasohol 95.

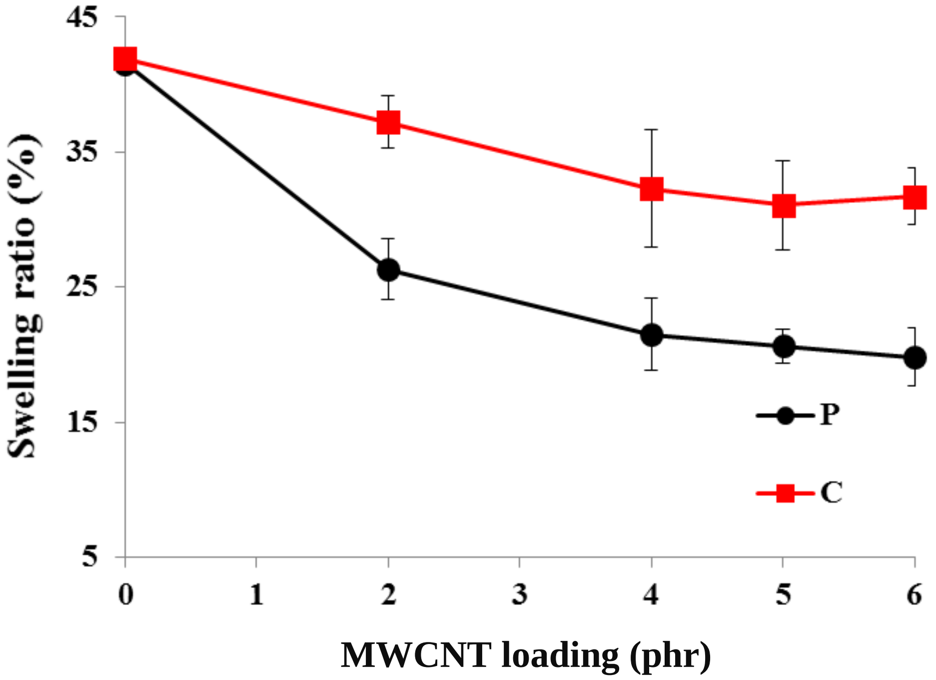

Figure 5.18 Swelling ratio of MWCNT-filled NR/NBR vulcanizates containing the masterbatch prepared from different methods in hydraulic oil.

5.1.1.6 Electrical and thermal properties

The volume resistivity of the P and C blends at various MWCNT loadings is shown in Figure 5.19. It is apparent that the volume resistivity of the unfilled 50/50 NR/NBR blend is in the order of 10^{10} ohm.cm. This value is much lower than the volume resistivity of pure NR reported to possess the intrinsic volume resistivity of about 10^{15} ohm.cm. [100]. Therefore, it can be stated that the electrical resistivity of NR can be markedly reduced by blending with NBR. It is also shown in Figure 5.19 that a reduction of volume resistivity of both P and C samples can be observed when only 2 phr of MWCNT is added. The abrupt decrease in the resistivity results from the formation of a continuous MWCNT network. A sharp change in electrical resistivity from the insulating range to the conducting range is known as the percolation threshold [16]. At a given MWCNT loading, the P blends possess lower volume resistivity than the C blends due to better MWCNT dispersion and, therefore, are better able to form a continuous MWCNT network. As can be seen in Figure 5.19, P and C blends containing 2 phr of MWCNT give resistivity of the order of 10^4 and 10^6 ohm.cm, respectively. In other words, the volume resistivity of the P and C blends decreases by about 6 and 4 orders of magnitude with respect to the unfilled rubber. This result confirms the better dispersion of MWCNT in the P blend when using the masterbatch prepared by predispersing method. Therefore, it can be stated that the dispersion of MWCNT is significantly improved when the masterbatch is prepared by predispersing method, leading to the better formation of interconnecting MWCNT network. At loadings higher than 2 phr, the conductivity of the composite mainly depends on the conductivity of the continuous conductive network formed through agglomeration. As can be seen in Figure 5.19, the volume resistivity is slightly decreased after 2 phr of MWCNT is loaded. This effect may be considered as very similar to the effect of increasing the diameter of a conducting wire on its conductivity [37].

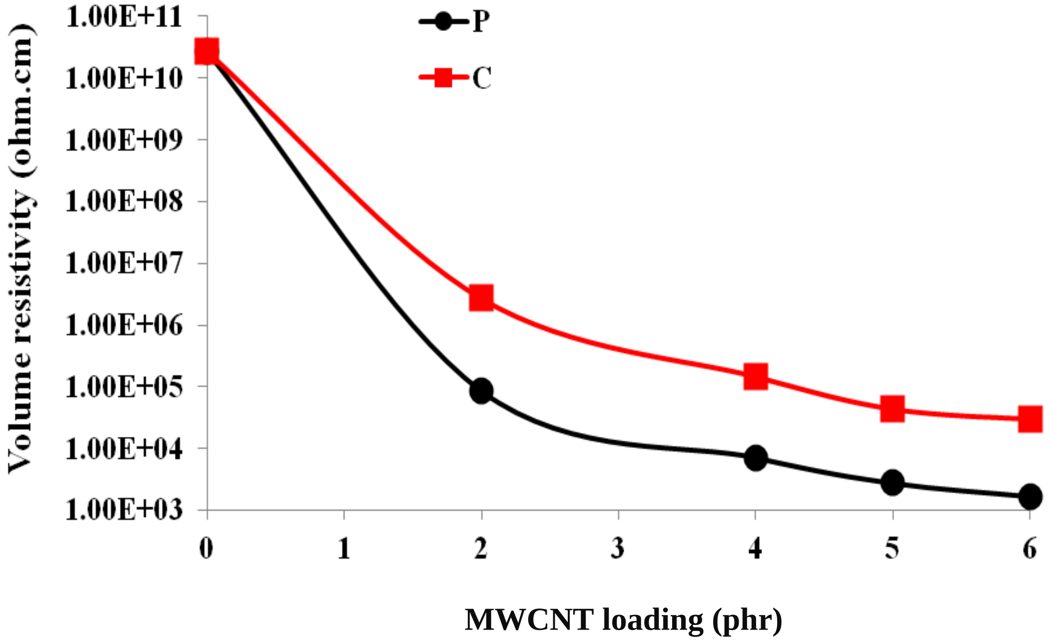

Figure 5.19 Volume resistivity of the MWCNT-filled NR/NBR vulcanizates containing the masterbatch prepared from different methods.

Figure 5.20 shows the thermal conductivity as a function of MWCNT content of all blends. As can be seen, the thermal conductivity of the C blends gradually increases with increasing MWCNT loading, while that of the P blends clearly improves when the amount of MWCNT is increased up to 4 phr. Thermal conductivities of the P and C blends having 4 phr of MWCNT are, respectively, increased by 2.1 and 1.2 times when compared with that of the unfilled one. In other words, thermal conductivity of the P blend having 4 phr of MWCNT is 1.7 times higher than that of the corresponding C blend. However, further addition of MWCNT in the P blend results in a rapid reduction of the thermal conductivity. This indicates that the greatest formation of continuous conductive network is achieved when MWCNT content in the P blend reaches 4 phr. A decrease in interconnecting networks when MWCNT loading is higher than 4 phr may be due to the formation of small MWCNT agglomerates.

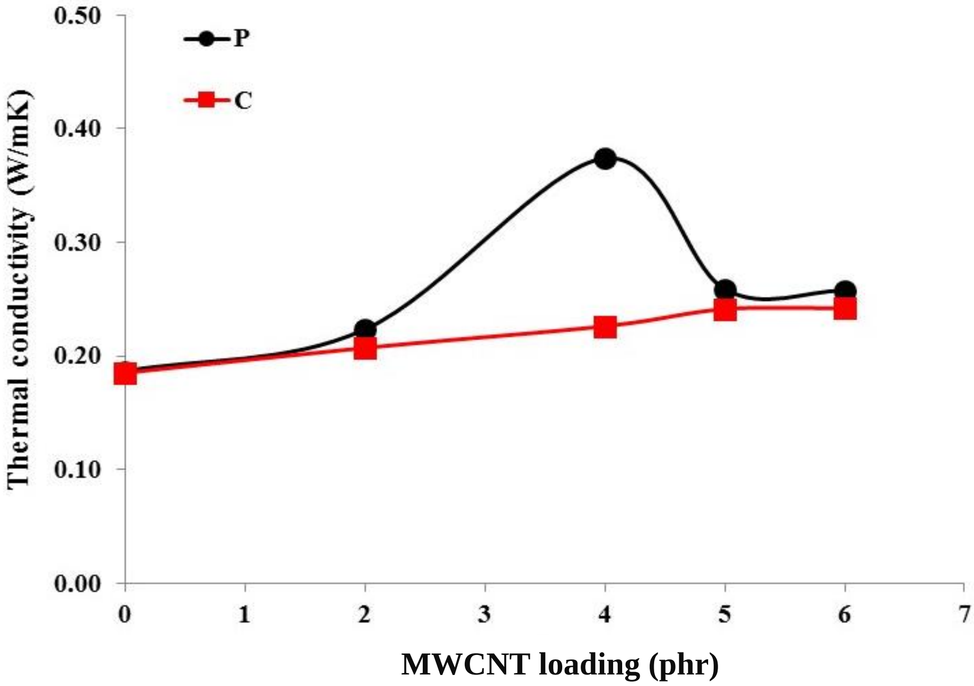

Figure 5.20 Thermal conductivity of the MWCNT-filled NR/NBR vulcanizates containing the masterbatch prepared different methods.

5.1.1.7 Dielectric properties

Figures 5.21 and 5.22 demonstrate the dielectric properties of NR/NBR composites containing the masterbatch prepared by different methods. For this property, the real part of permittivity (ε´) of the P and C blends is measured at various frequencies. It is found that permittivity of the unfilled P and C blends, and the C2 blend is low and it is almost independent of the frequency. When MWCNT is incorporated into the rubber blends, except for the C2, this behaviour is changed. At low frequencies, the permittivity of the P and C blends, except for the C2, significantly increases with increasing MWCNT loading. However, a relaxation process takes place at high frequency resulting in a sharp drop of the permittivity. Previously, the high frequency transitions have been related to a gap process between adjacent particles of the carbon black networks [105]. This gap process refers to the tunnelling or hopping of charge carriers over nanoscopic gaps [16, 18]. Thus, it is thought that a similar phenomenon may occur for the MWCNT networks. Additionally, it is observed that the relaxation transition of both the P and C blends shifts towards higher frequency when the amount of MWCNT is increased. A similar result was also previously observed in the SBR/BR composites filled with MWCNT [16, 18]. In addition, it has been reported that the relaxation transition behaviour would be observed when MWCNT content in the rubber matrix is above the percolation threshold [16, 18]. Moreover, the permittivity is independent of frequency when MWCNT content in the rubber matrices is below the percolation threshold [16]. In this study, the sharp change of the permittivity resulting from relaxation process can be observed when the amount of MWCNT is changed from 0 phr to 2 phr for the P blend and, from 2 phr to 4 phr for the C blend. Therefore, it can be stated that the percolation threshold of the P blend occurs at lower MWCNT loading than that for the C blend. This is due to the better dispersion of MWCNT leading to formation of the interconnecting network at lower MWCNT content. Furthermore, it is found that the permittivity of the P and C blends at low frequencies is rather high of about >10^3 when only 2 phr MWCNT is added for the P blend and, when the MWCNT content is more than 2 phr for the C blend. This results may result from a combined effect of the disordered percolation structure and small gaps of the conducting MWCNT networks capable to form capacitances on different length scales [16]. Interestingly, the permittivity at low frequency of the C blend is lower than that of the corresponding P blend. This is also attributed to the better dispersion of MWCNT in the P blend resulting in the reduction of gap distance between the tips of MWCNTs and thus the increase of conducting network [16].

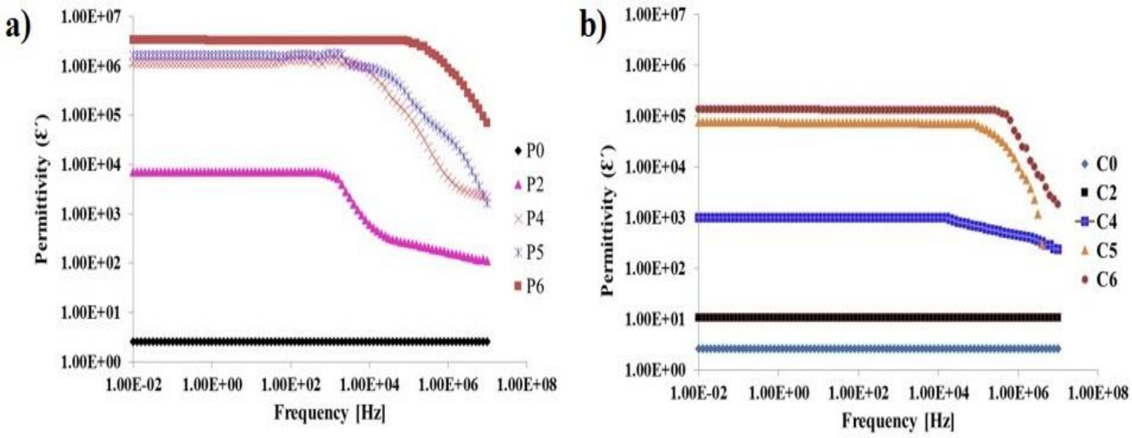

Figure 5.21 Permittivity of the P and C blends at various MWCNT loading; a) P and b) C blends.

5.1.2 The effect of milling direction on the properties of 50/50 NR/NBR blends filled with MWCNT

In this part, the MWCNT/NR masterbatches prepared by predispersing and conventional methods were used to prepare 50/50 NR/NBR blends with various MWCNT loadings. Then, the effect of milling direction, machine direction (MD) and transverse direction (TD), on the mechanical, dynamic mechanical and electrical properties of the blends is elucidated.

5.1.2.1 Morphology

SEM micrographs showing dispersion and alignment of MWCNT within the P and C blends in MD and TD are depicted in Figures 5.22-5.25. It is found that, at low MWCNT loadings (≤4 phr), the MWCNTs are well dispersed and aligned in the P blend. In addition, in the case of low MWCNT loadings (≤ 4 phr) for the P blend, it can be seen in Figure 5.22 that the broken tube ends of MWCNTs protruded from the fractured surfaces of the MD samples, indicating the longitudinal alignment of MWCNTs, while the fractured surfaces of the TD samples displayed MWCNTs aligned parallel to their surfaces, as shown in Figures 5.22-5.23. Thus, this result indicates that most of the MWCNTs are aligned along MD and good dispersion is observed. However, at higher loadings (> 4 phr) for the P blend, the agglomeration of MWCNTs can be observed. The higher the MWCNT loading, the greater the MWCNT agglomerates. Despite the attempts to improve the MWCNT dispersion by sonication of the MWCNT mixture prior to mixing and the application of subsequent intense shearing during mixing, MWCNT agglomeration is still unavoidable. For the C blend, the MWCNT agglomerates can be found at every MWCNT loading. The results indicate that shear force created by two-roll mill cannot break MWCNT agglomerates leading to poor dispersion of MWCNT. Unlike the P blend, the alignment of MWCNT in both MD and TD directions for the C blends as displayed in Figures 5.24 and 5.25 is not clear because of the formation of MWCNT agglomerates. Herein, the SEM micrographs at low magnification (x10,000) of both P4 and C4 shown in Figure 5.26 are additional taken to cover a wider area of the specimen and examine the appearance of MWCNT dispersion on the surface. It is found that small entangled MWCNTs are well dispersed and distributed throughout the P4 specimen as depicted in Figure 5.26 (a). On the contrary, the MWCNT can be found only at some area of the C4 and it appears as large agglomerates as illustrated in Figure 5.26 (b). Also, the area in Figure 5.26 (b) indicated by an arrow is magnified in order to confirm that the bright lump is MWCNT agglomerate, not other chemicals used in the vulcanizate.

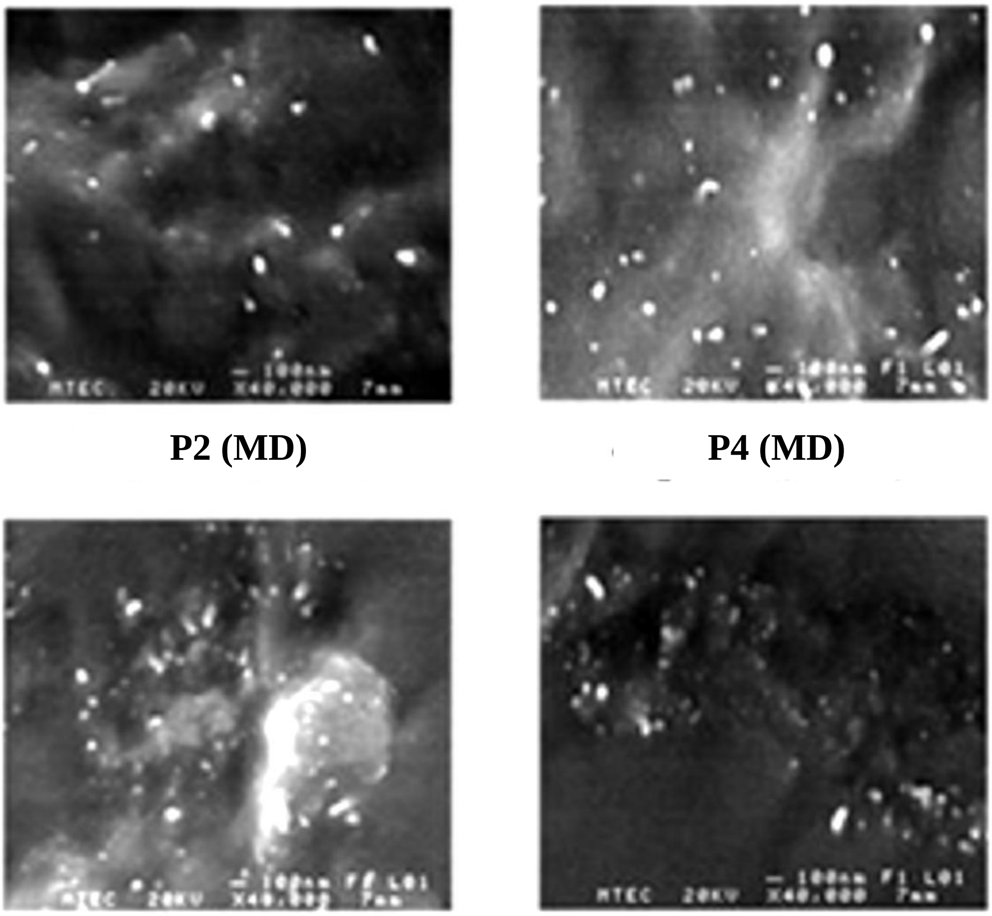

P2 (MD) **P4 (MD)**

P5 (MD) **P6 (MD)**

Figure 5.22 SEM micrographs of the NR/NBR vulcanizates containing the masterbatch prepared by predispersing method in MD.

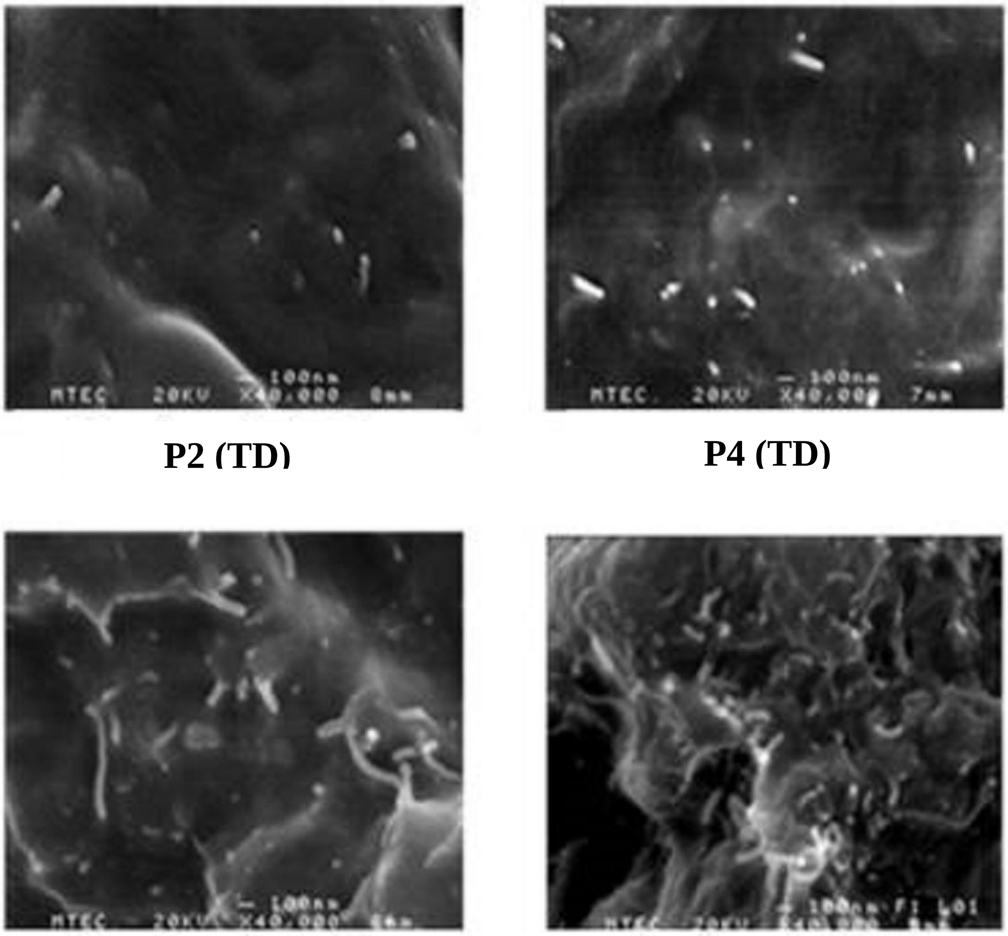

P2 (TD) **P4 (TD)**

P5 (TD) **P6 (TD)**

Figure 5.23 SEM micrographs of the NR/NBR vulcanizates containing the masterbatch prepared by predispersing method in TD.

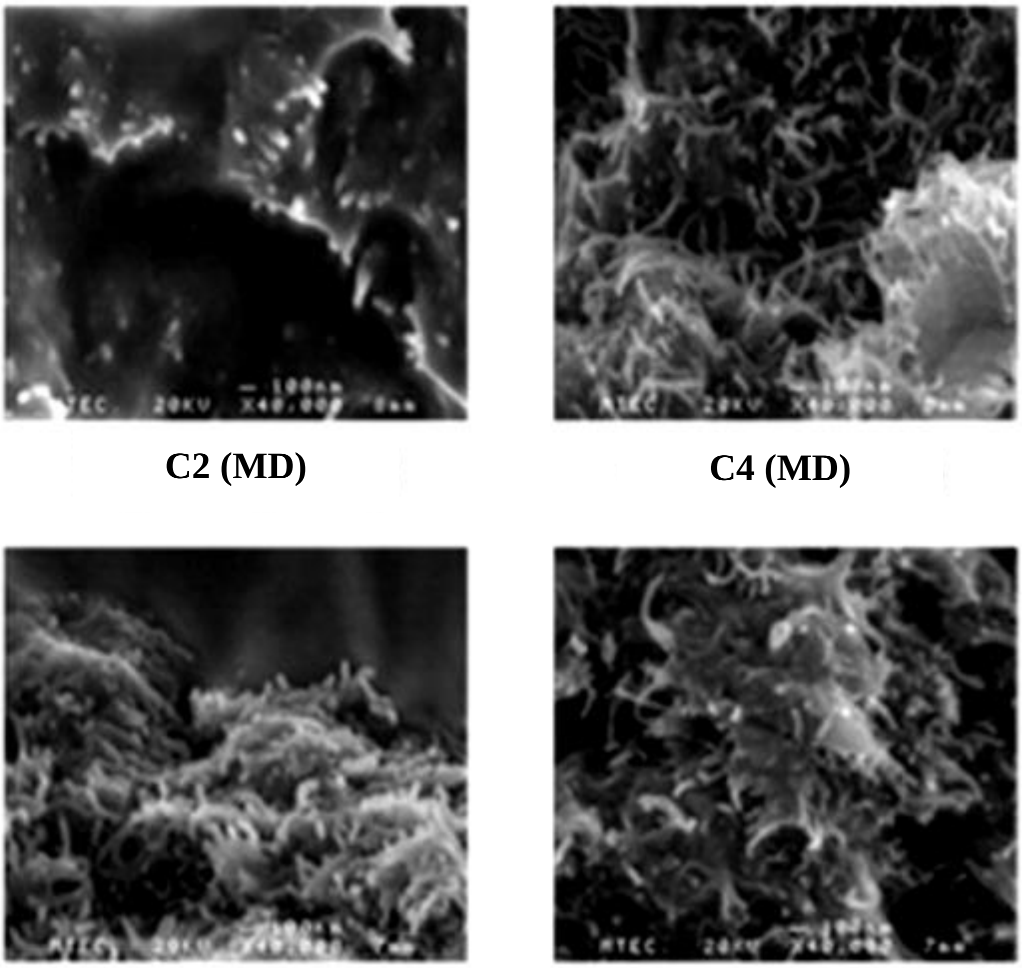

C2 (MD) **C4 (MD)**

C5 (MD) **C6 (MD)**

Figure 5.24 SEM micrographs of the NR/NBR vulcanizates containing the masterbatch prepared by conventional method in MD.

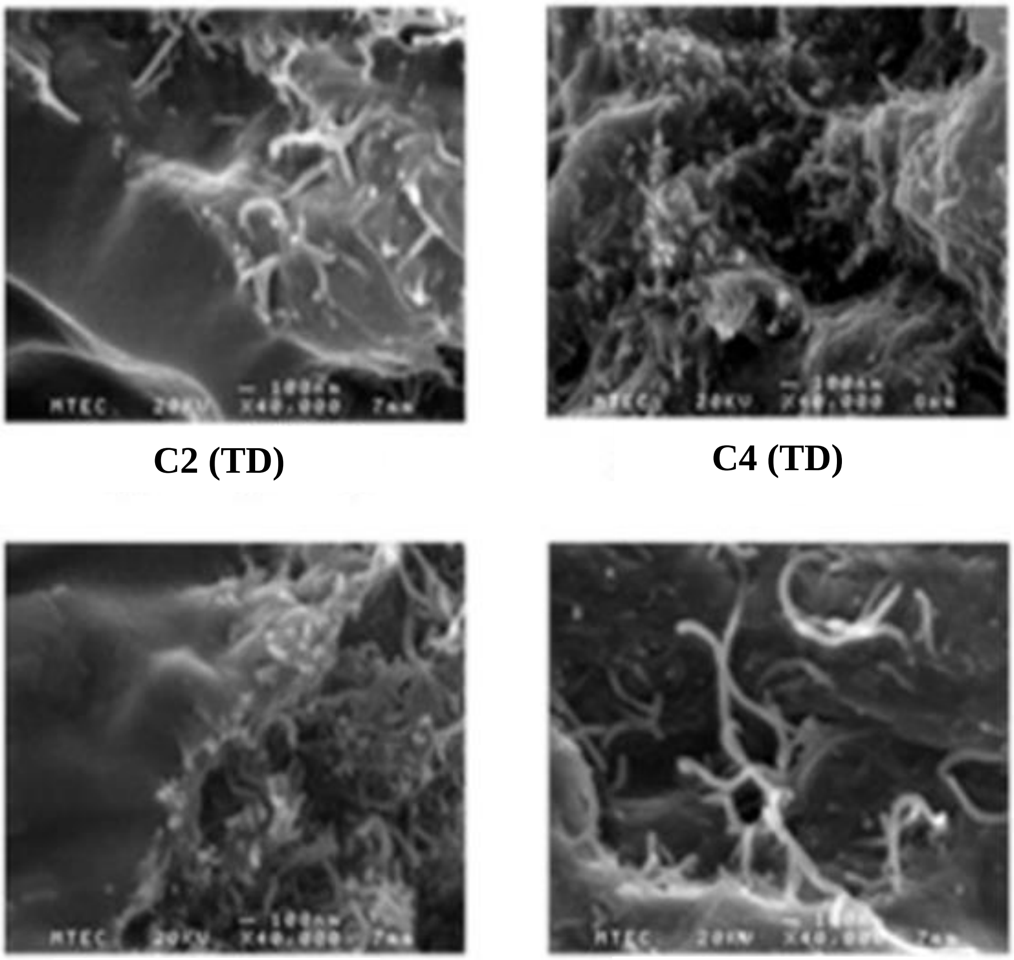

C2 (TD)

C4 (TD)

C5 (TD)

C6 (TD)

Figure 5.25 SEM micrographs of the NR/NBR vulcanizates containing the masterbatch prepared by conventional method in TD.

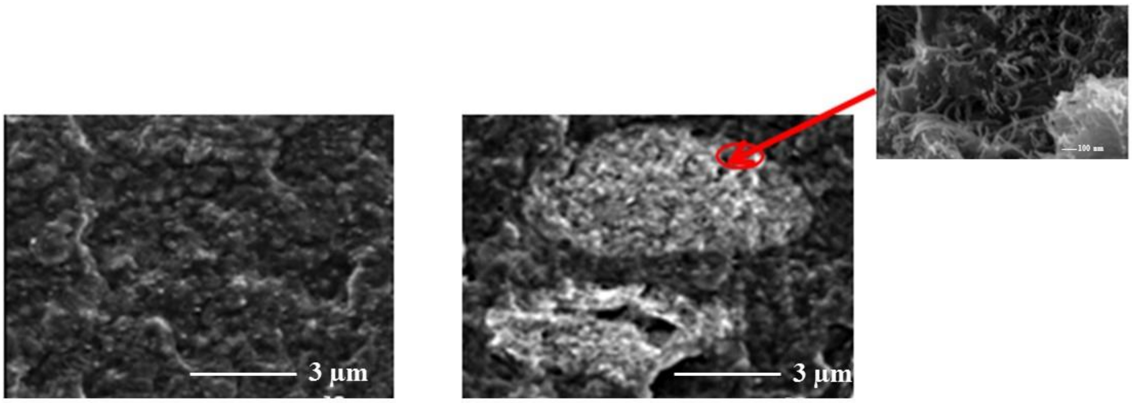

(A) (B)

Figure 5.26 SEM micrographs of 4 phr MWCNT-filled NR/NBR blends containing MWCNT/NR masterbatch prepared from (a) predispersing and (b) conventional methods.

5.1.2.2 Raman spectroscopy

Raman spectroscopy is used to determine the alignment of MWCNT in the P and C blends. Figures 5.27 and 5.28 show two characteristic peaks at 1,340 and 1,570 cm^{-1}, referred to as the D band and the G band, respectively [20]. The D band corresponding to the disorder mode is derived from disordered graphite structures. On the other hand, the G band corresponding to the tangential mode is attributed to the mode with neighbouring carbon atoms vibrating out of phase parallel to the surface of the cylinder [96]. In this study, the quantitative evidence to support the alignment of MWCNT is defined in terms of the dichroic ratio (R) obtained from Raman spectroscopy results [96-97]. R is the ratio of the intensities of the G band of MWCNT at 1,570 cm^{-1} obtained from the sample arranged in parallel and perpendicular to the polarized light [96-97]. If R value approaches 1, it can be said that no alignment occurs. On the other hand, if R is higher than 1, it means that the majority of MWCNTs is aligned along the MD or parallel (0°) to the polarized light direction [96-97]. The dichroic ratio calculated using equation 4.15 is also plotted against MWCNT loading and presented in Figure 5.29. As can be seen, R of both the P and C blends is higher than 1 at all loadings, indicating that most MWCNTs align parallel to polarized light. In other words, it could be said that the majority of MWCNTs align along MD. However, the level of MWCNT alignment for the P and C blends is different for each MWCNT loading. It can be observed that R of the P blend tends to increase with increasing MWCNT loading up to 4 phr and then decreases afterwards. The rise of R at low MWCNT loadings for the P blend is attributed to the increase of aligned MWCNTs in MD or the direction parallel to the polarized light. On the other hand, the reduction of R at high MWCNT loading may be explained by the increase of MWCNT agglomerates, which is confirmed by SEM results. This leads to the limitation to increase the number of aligned MWCNTs in the machine direction. Unlike the P blend, R of the C blends is not significantly change with MWCNT loading due to poor dispersion of MWCNT. A comparable R value for the P and C blend when MWCNT is more than 4 phr of MWCNT could be explained by the formation of agglomerates at high MWCNT loading for both methods.

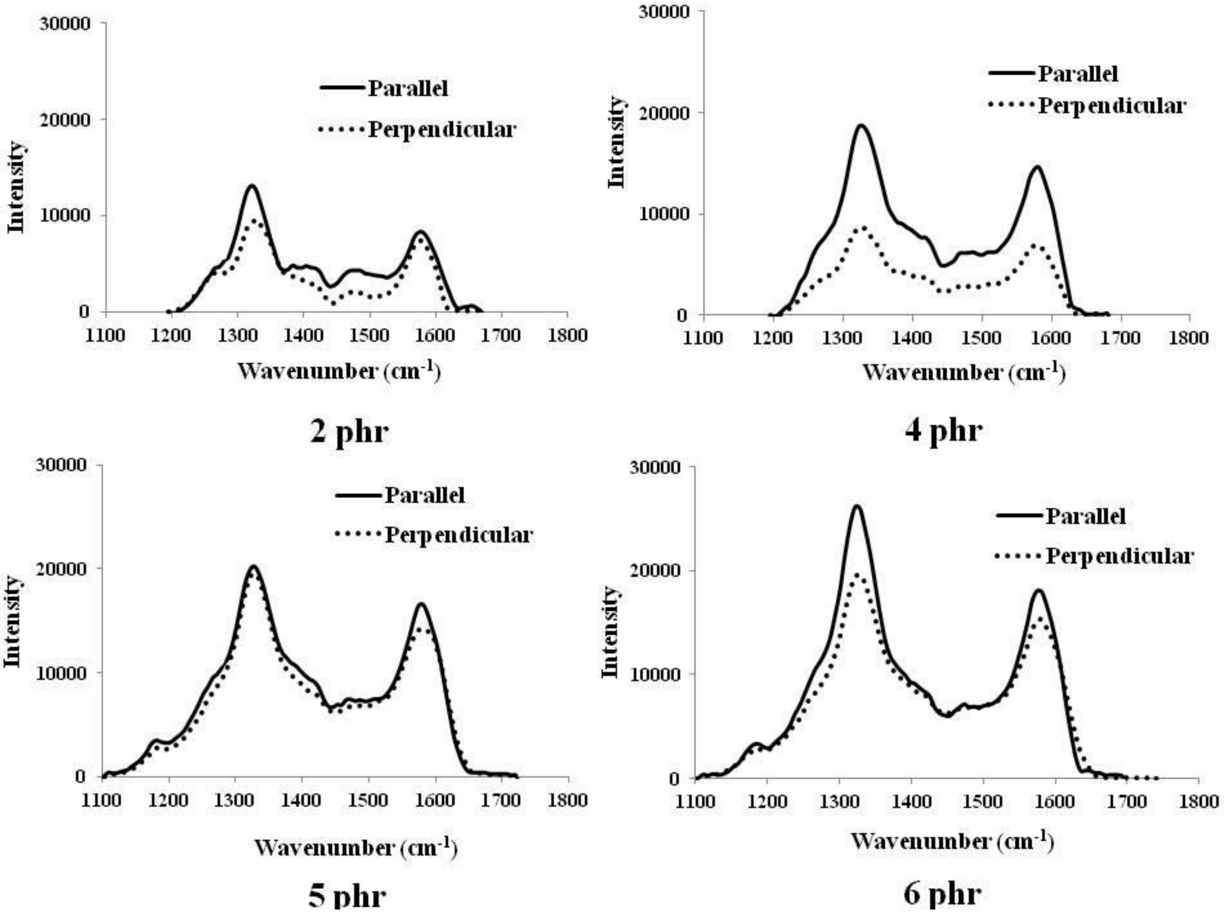

2 phr

4 phr

5 phr

6 phr

Figure 5.27 Raman spectra of the P blends in parallel and perpendicular to polarized light.

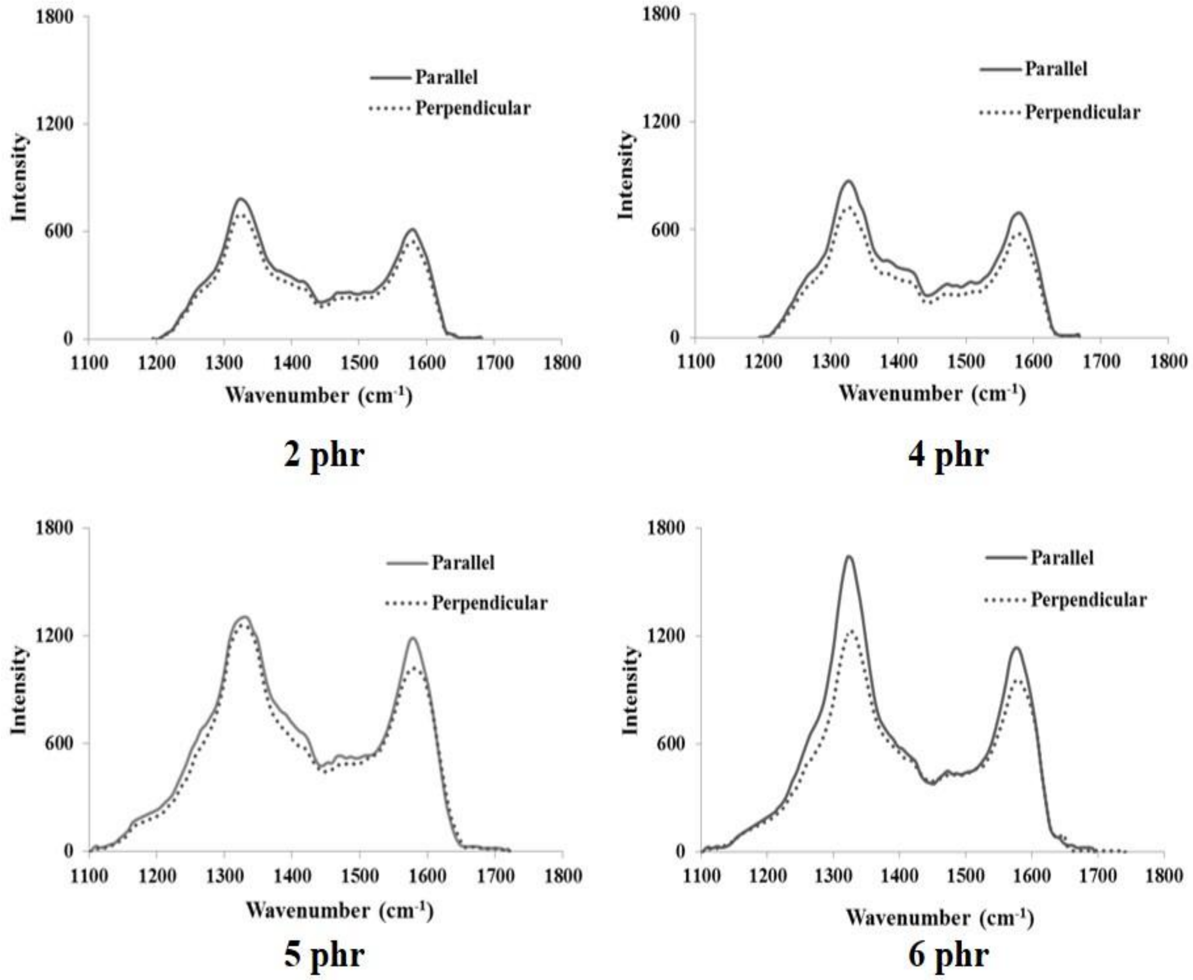
2 phr

4 phr

5 phr

6 phr

Figure 5.28 Raman spectra of the C blends in parallel and perpendicular to polarized light.

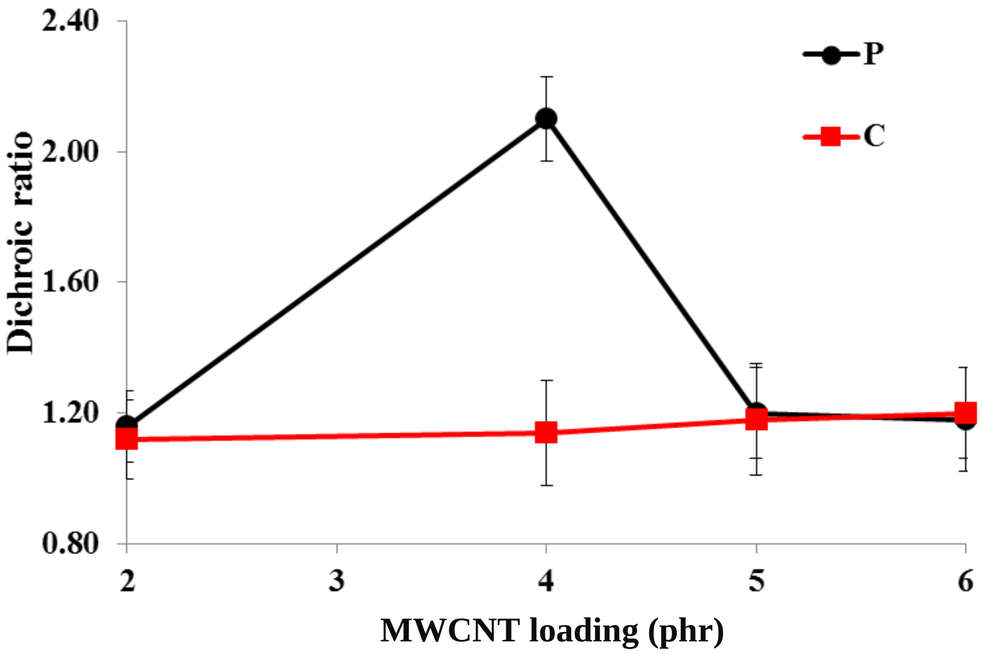

Figure 5.29 Plot of dichroic ratio versus MWCNT loading of the P and C blends.

5.1.2.3 Mechanical properties

The effect of MWCNT alignment on mechanical properties of the P and C blends is illustrated in Figures 5.30-5.33. It can be seen in Figure 5.30 that, at a given MWCNT loading, tensile strength of both P and C blends in the MD is greater than that in the TD. A similar result was also observed in NBR composites filled with nylon fiber, as reported by other researchers [106-107]. The greater tensile strength in the MD of the MWCNT-filled rubber composites could be explained by the basis of fiber orientation. Generally, the tensile strength of the composite depends on the alignment of fibers. When fibers are aligned longitudinally, breakage and pulling out of the fibers take place before rupture [106-107]. It is found that the tensile strength of the P blend in both directions increases with increasing MWCNT loading until it reaches a maximum at 4 phr. The reduction of its tensile strength at higher loadings is thought to arise from poor MWCNT dispersion. At high MWCNT loadings, a greater degree of entanglement could be expected. Entanglements of the long tubes make the dispersion become more difficult, and the agglomeration of MWCNTs at high loadings is also unavoidable. Unlike the P blend, the tensile strength of the C blend in both directions decreases with increasing MWCNT loading. The explanation is also given by poor dispersion of the MWCNT in the blends. Additionally, it is found that the P blend exhibits higher tensile strength than the corresponding C blend. This is attributed to the combination of a higher number of aligned MWCNTs in MD and better MWCNT dispersion for the P blend. These results agree well with the SEM images and dichroic ratio values shown previously in Figures 5.22-5.25 and 5.29. Furthermore, elongation at break of the P and C blends displayed in Figure 5.31 decreases continuously with increasing MWCNT loading, regardless of the alignment direction. The dilution effect could be used to explain the results. Unlike tensile strength, the results of the P blends reveal that the MWCNT alignment only slightly influences the elongation at break of the blends. Additionally, it is found that the elongation at break of the C blend is lower than that of the corresponding P blends. This is because the formation of large agglomerates acts as defects in the tensile samples. The effect of MWCNT alignment on modulus and tear strength of both P and C blends is depicted in Figures 5.32 and 5.33, respectively. As can be seen, the modulus and tear strength of both P and C blends in MD and TD increase continuously with increasing MWCNT loading. This is attributed to the combination of dilution and reinforcing effects of MWCNTs. However, their modulus and tear strength in the MD are higher than those in the TD. Again, these results confirm the alignment of MWCNTs in the MD. Thus, the higher stress is needed to deform the composites having most MWCNTs aligned parallel to the applied force. Also, the MWCNTs aligned parallel to the applied force are able to obstruct the progress of the fracture front, leading to higher tear strength [106]. Moreover, the P blends exhibit higher modulus and tear strength than those of the corresponding C blends. This is thought to be due to the better MWCNT dispersion, as previously mentioned, leading to the higher amount of MWCNT alignment and filler-rubber interaction in the rubber matrices.

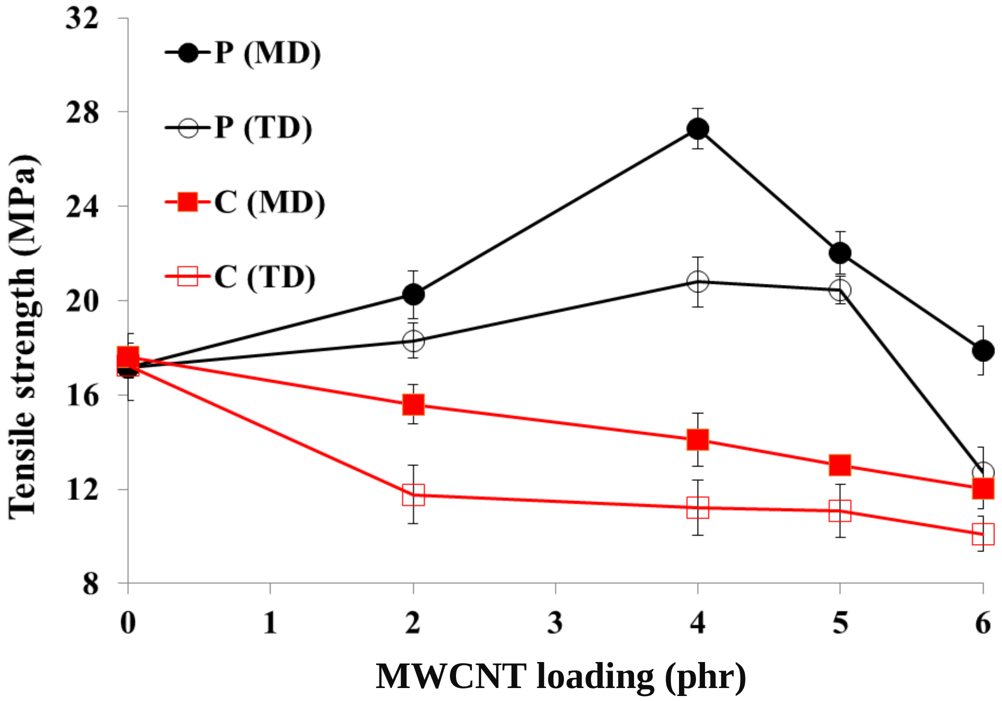

Figure 5.30 Tensile strength of the P and C vulcanizates in MD and TD as a function of MWCNT loading.

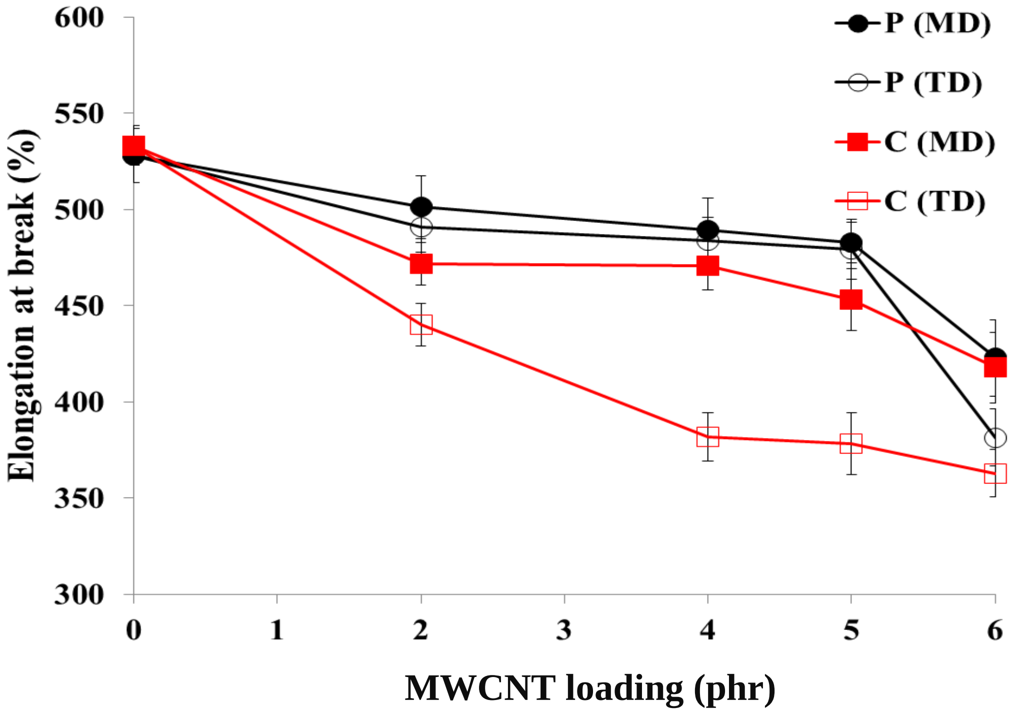

Figure. 5.31 Elongation at break of the P and C vulcanizates in MD and TD at various MWCNT loadings.

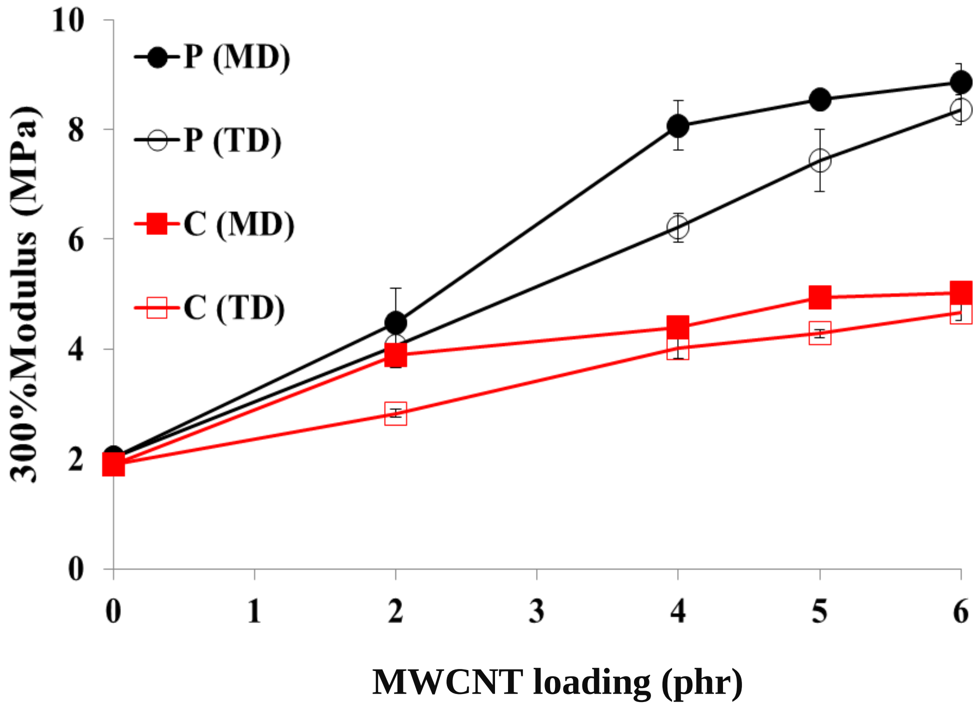

Figure 5.32 Modulus of the P and C vulcanizates in MD and TD at various MWCNT loadings.

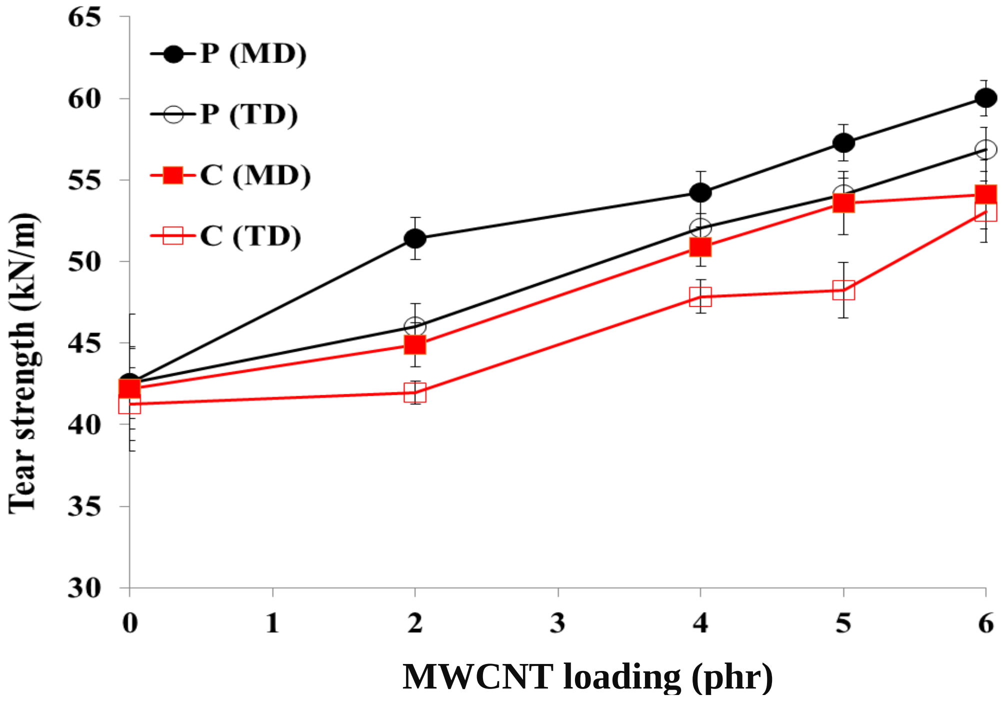

Figure 5.33 Tear strength of the P and C vulcanizates in MD and TD as a function of MWCNT loading.

5.1.2.4 Dynamic mechanical properties

The plots of tan δ (damping factor) versus temperature of the P and C blends in different directions are displayed in Figures 5.34 and 5.35, respectively. It is found that MWCNT loading and alignment direction slightly influence on the T_gs of both phases for the P and C blends. However, the tan δ_{max} of both phases for both P and C blends tends to reduce with increasing MWCNT loading, regardless of the alignment direction. The dilution effect could be used to explain this finding. It is also observed that the tan δ_{max} in the MD of both phases for the P and C blends is lower than that of their TD counterpart. This result may be explained by the higher reinforcement efficiency for MWCNT aligned in longitudinal direction. Moreover, tan δ_{max} of both blends in MD and TD is compared in Figures 5.36 and 5.37, respectively. As can be seen, the tan δ_{max} of both phases for the P blend is lower than that of the corresponding C blend for both milling directions. The better dispersion and alignment of MWCNT are accounted this finding. These results also correspond well with the mechanical properties and dichroic ratio results of the blends.

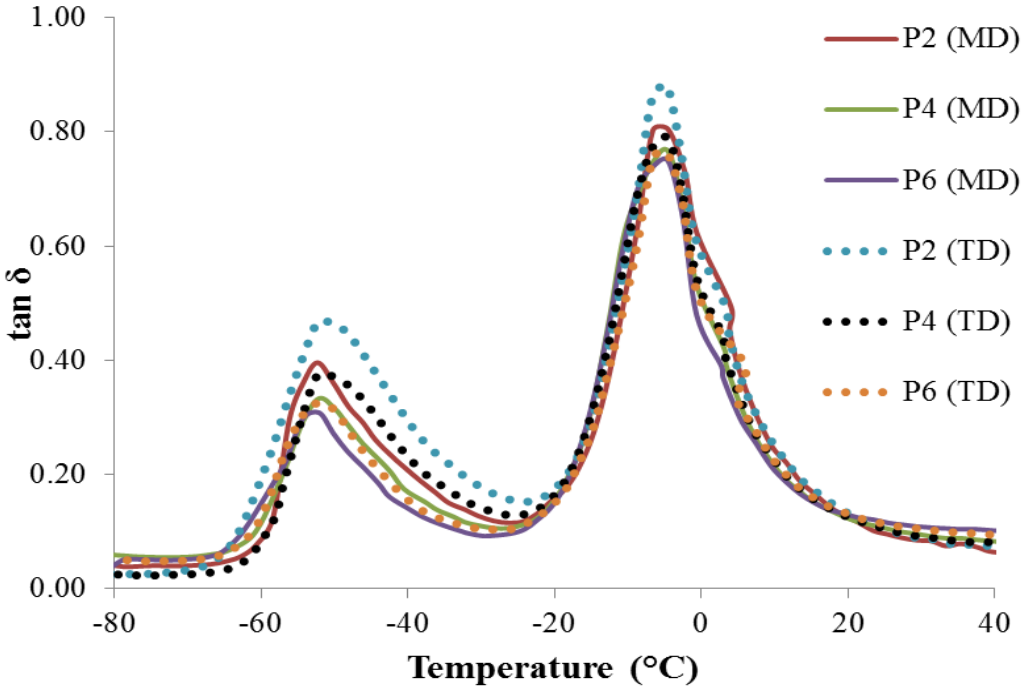

Figure 5.34 Loss tangent (tan δ) of the P vulcanizates in MD and TD as a function of temperature.

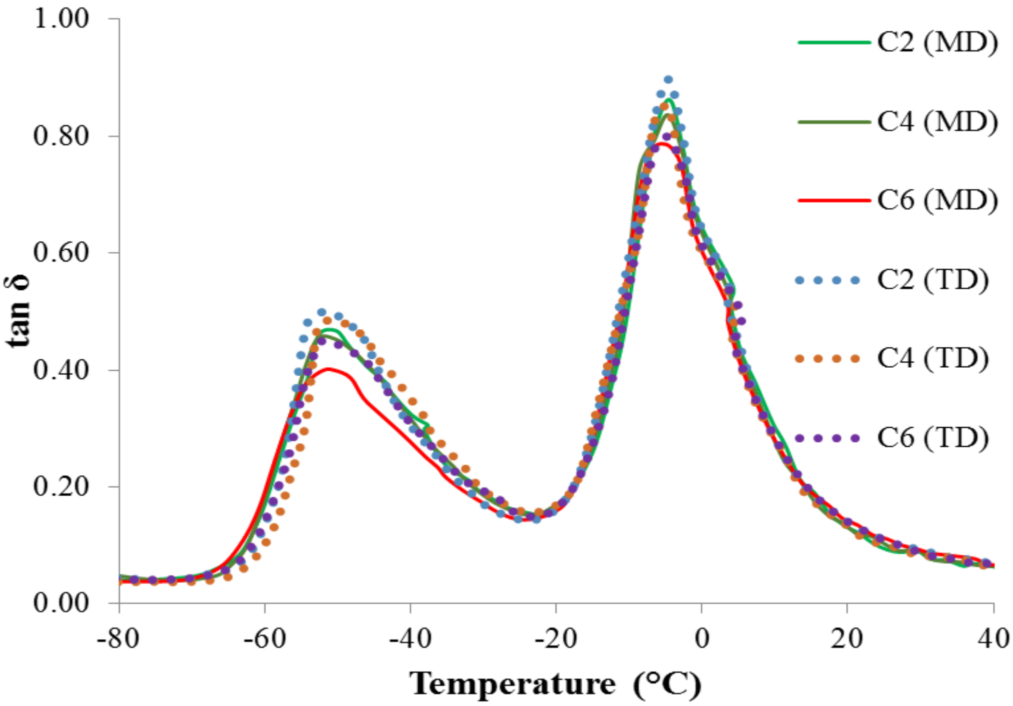

Figure 5.35 Loss tangent (tan δ) of the C vulcanizates in MD and TD as a function of temperature.

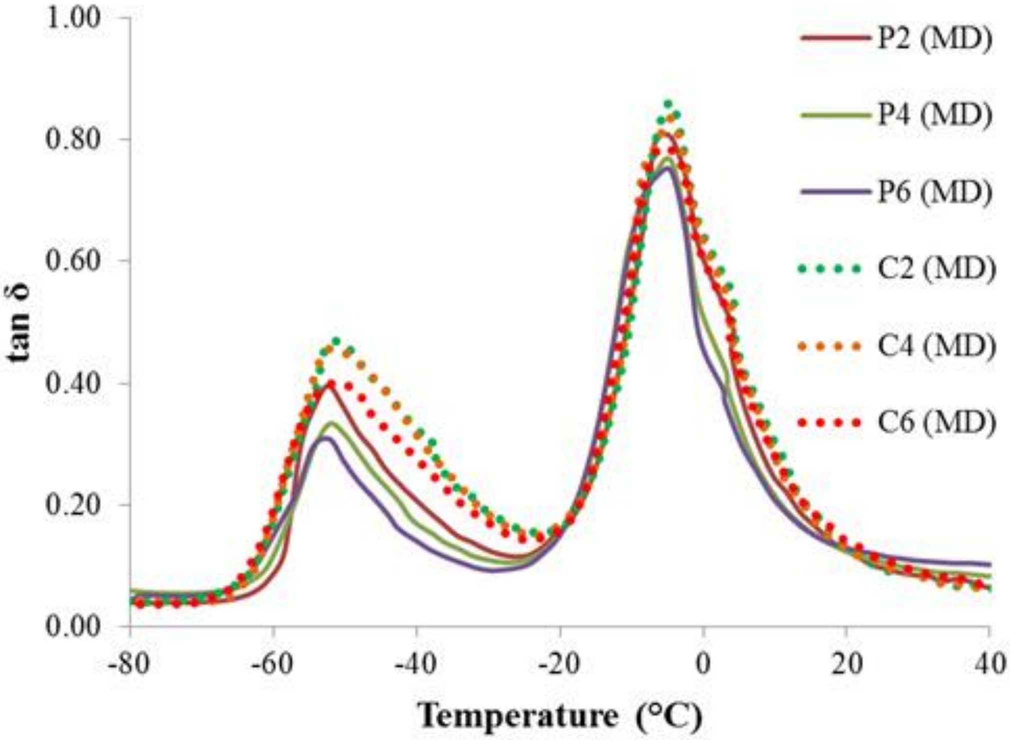

Figure 5.36 Loss tangent (tan δ) of the P and C vulcanizates in MD as a function of temperature.

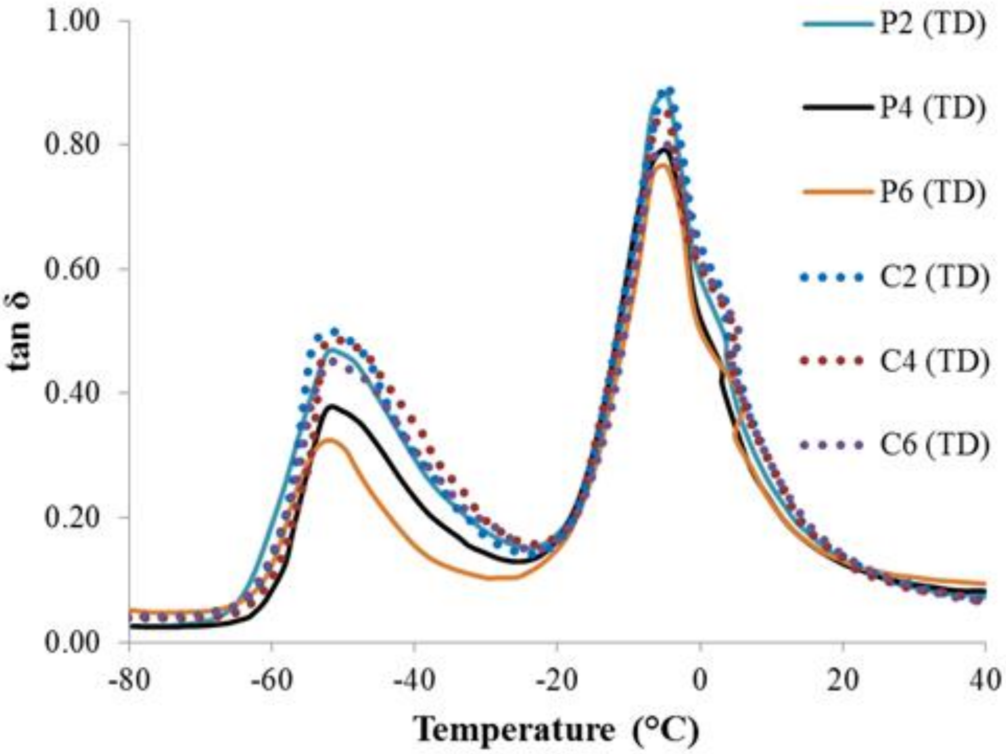

Figure 5.37 Loss tangent (tan δ) of the P and C vulcanizates in TD as a function of temperature.

Figure 5.38 depicts the average storage modulus results at 30°C for both P and C blends. It appears that their storage modulus in MD and TD increases when amount of MWCNT loading is increased. This is attributed to the dilution effect. In addition, in all cases, it is found that the storage modulus of the MD samples is higher than that of the corresponding TD samples. This result may be explained by the higher reinforcement efficiency for MWCNT aligned in longitudinal direction. These results also correspond well with the modulus and tear strength of the blends.

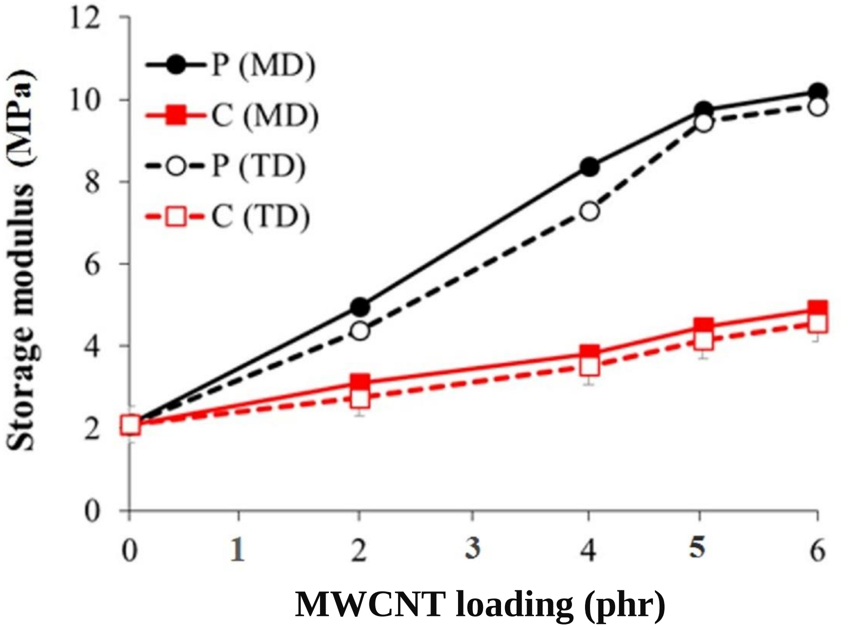

Figure 5.38 Storage modulus at 30°C of the P and C vulcanizates in MD and TD at various MWCNT loadings.

5.1.2.5 Electrical properties

The dependence of electrical conductivity on MWCNT loading and MWCNT alignment is illustrated in Figure 5.39. It can be seen that the unfilled P and C blends have electrical conductivity of about 4.81×10^{-11} S/m and 5.16×10^{-12} S/m, respectively. The addition of a small quantity of MWCNTs results in changing the electrical conductivity by orders of magnitude. For example, when the MWCNT loading increases from 2 phr to 4 phr, the electrical conductivities of the P blends along the MD and TD increase from 2.35×10^{-9} to 4.24×10^{-4} S/m and 5.88×10^{-10} S/m to 2.74×10^{-6} S/m, respectively. In other words, the electrical conductivities of the P blend increase by about 7 (MD) and 5 (TD) orders of magnitude with respect to that of the unfilled rubber. For the C blend, when the MWCNT loading is increased from 2 phr to 4 phr, its electrical conductivity along the MD and TD increases from 2.75×10^{-10} to 1.40×10^{-6} S/m and 5.24×10^{-11} S/m to 3.34×10^{-7} S/m, respectively. Therefore, the electrical conductivity of the C blend increases by about 5 (MD) and 4 (TD) orders of magnitude relative to that of its unfilled blend. The increase of electrical conductivity with increasing MWCNT loading in all cases is mainly caused by the dilution effect. Nevertheless, a slight increase in electrical conductivity is observed when MWCNT content is more than 4 phr. This is possibly because the amount of MWCNT-to-MWCNT junctions which favours the formation of conductive networks is nearly at a maximum when MWCNT loading reaches 4 phr, and it does not markedly increase when MWCNT is higher than 4 phr due to the formation of MWCNT agglomerates. In addition, the electrical conductivity of both P and C blends in the MD is superior to that of the corresponding TD samples. For instance, the electrical conductivity of MD samples of the P and C blends containing 4 phr MWCNTs is higher than that of the TD sample about 3 and 1 orders of magnitude, respectively. The possible explanation is given by a greater number of aligned MWCNTs in MD sample relative to the TD sample resulting in increasing the formation of conductive networks. Therefore, electrons can flow through the formed MWCNT networks in the MD samples more than the TD samples.

The dependence of electrical conductivity of the P blends on dichroic ratio can be observed in Figure. 5.40 when MWCNT loading is ≤ 4 phr. It is interesting that when the dichroic ratio reduces at high MWCNT loading (MWCNT > 4 phr), the level of electrical conductivity still remains at similar level to that of the blend containing 4 phr MWCNT. Moreover, it is apparent that the formation of MWCNT agglomerates when MWCNT is more than 4 phr does not cause a reduction of the electrical conductivity. It is possible that, although the increase of MWCNT content causes the increase of MWCNT agglomerates, it does not reduce the amount of MWCNT-to-MWCNT junctions which favours the formation of conductive networks. Moreover, it has been reported that the formed agglomerates may function as junctions between the conductive MWCNT networks instead of obstructing the conductivity [13]. It should be also noted that the relationship between electrical conductivity and dichroic ratio of the C blend is not discussed herein because its dichroic ratio is not significantly change with increasing MWCNT content.

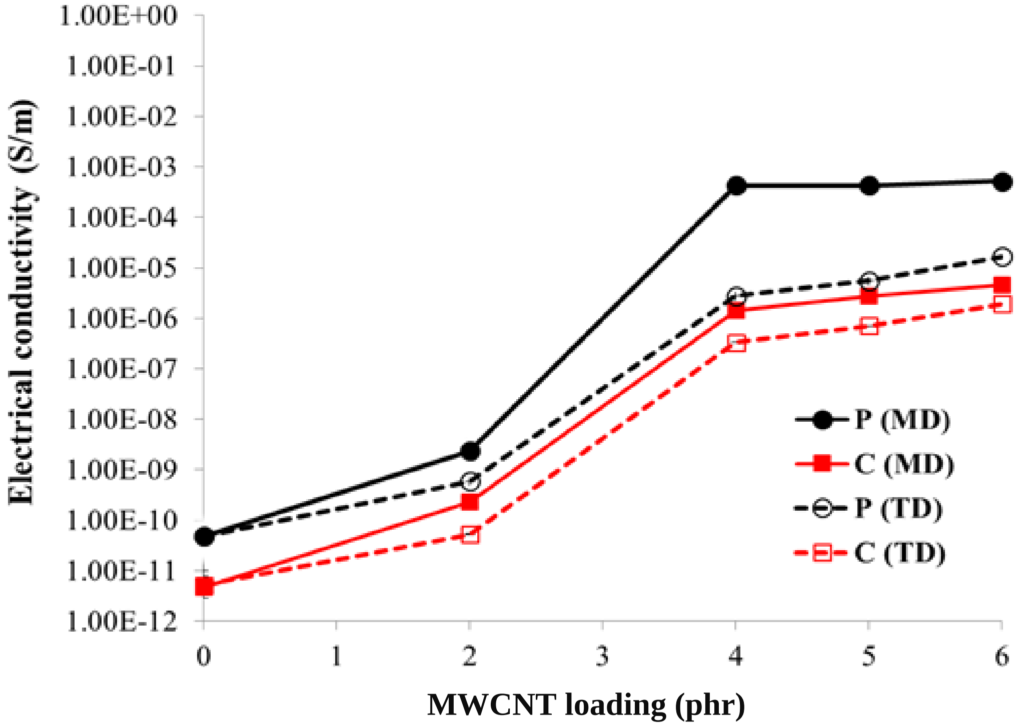

Figure 5.39 Electrical conductivity of the P and C vulcanizates in MD and TD at various MWCNT loadings.

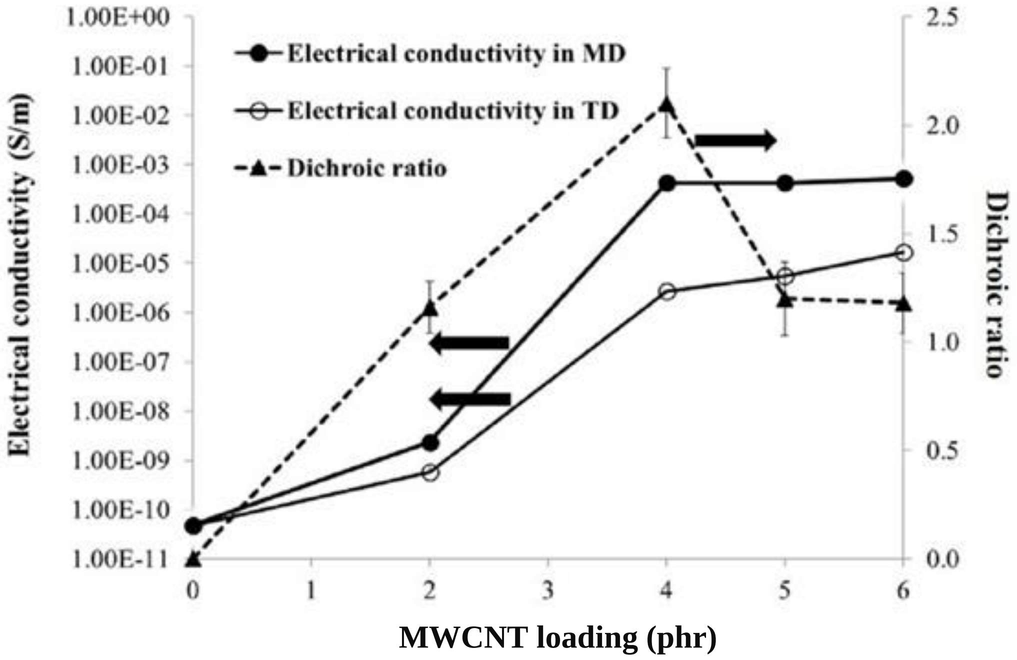

Figure 5.40 Electrical conductivity and dichroic ratio of the P vulcanizats as a function of MWCNT loading.

5.1.3 The effect of stretching and temperature on the electrical conductivity of 4 phr MWCNT-filled NR/NBR blend containing MWCNT/NR masterbatch prepared from predispersing method

In this section, the 50/50 NR/NBR blends containing the masterbatch prepared by using predispersing method and having 4 phr MWCNT is selected for studying the electrical conductivity with different extension ratios and temperatures. Figure 5.41 represents the relationship between the electrical conductivity and the extension ratio for both MD and TD samples. As can be seen, the electrical conductivity of the blend slightly decreases when extension ratio is in between 1.0-1.1. Thereafter, the electrical conductivity rapidly decreases from $4.14\text{x}10^{-4}$ S/m to $1.14\text{x}10^{-4}$ S/m when extension ratio is increased from 1.1 to 1.6. In other words, the electrical conductivity of the MD sample decreases 3.6 times when the extension ratio is increased from 1.1 to 1.6. The electrical conductivity slightly reduces when the extension ratio is further increased from 1.6 to 2.2. The sharp decrease in the electrical conductivity may be explained by disconnections of MWCNT networks when the MD sample is strained and the disconnection of MWCNT networks begins when the extension ratio is more than 1.1. On the contrary, the electrical conductivity of the TD sample increases continuously when the extension ratio is in the range of 1.1-1.6. However, when extension ratio is higher than 1.6, the electrical conductivity of the blend slightly enhances. It is likely that the rapid increase of the electrical conductivity of the blend in TD is caused by the rearrangement of MWCNT networks under tension, thus leading to the enhancement of interconnecting MWCNT networks. However, the change in the electrical conductivity of the MD sample is higher than that of the TD sample, regardless of the increase or decrease in the electrical conductivity value. Therefore, it is expected that electrical conductivity of the MD sample would be more sensitive than that of the TD sample when the temperature is changed. Thus, the MD sample is chosen for studying the effect of temperature on the electrical conductivity of the blend.

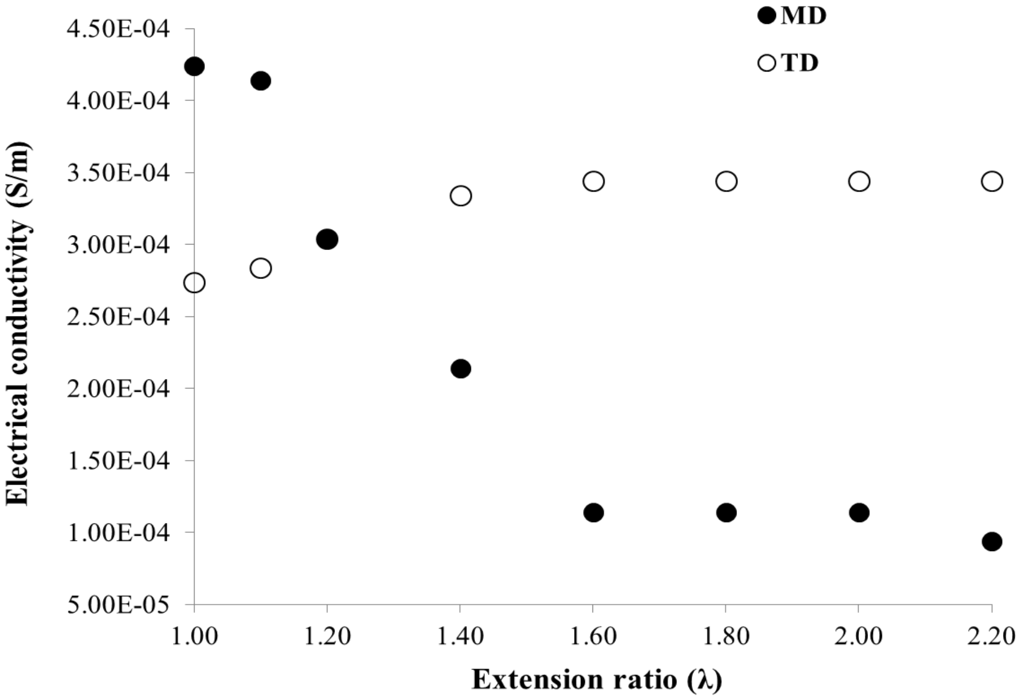

Figure 5.41 Electrical conductivity of the P blend containing 4 phr MWCNT in MD and TD at various extension ratios.

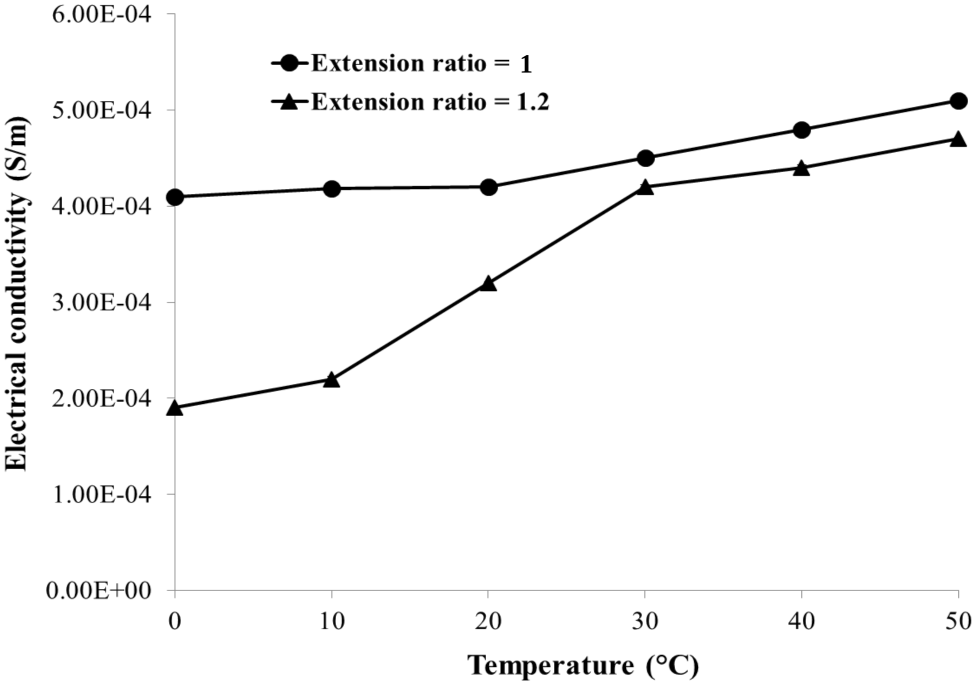

Figure 5.42 Electrical conductivity of the P blend containing 4 phr MWCNT in MD at various temperatures.

The electrical conductivity of the stretched and unstretched MD samples, is plotted as a function of temperature and compared in Figure 5.42. It can be observed that the electrical conductivity of the stretched sample markedly increases with increasing temperature. The electrical conductivity of the stretched sample increases about 2 times when the temperature is increased from 0°C to 30°C. It is possible that the rotation of rubber chains occurring when the temperature is increased results in the decrease of distance between the tips of MWCNTs. Also, an increase in the electrical conductivity of MWCNT when temperature is increased can be another factor for the increase in the electrical conductivity [16]. The latter factor can be confirmed by the enhancement of the electrical conductivity of the unstretched sample (extension ratio = 0) with increasing temperature. Additionally, it is apparent that when the temperature is increased from 20 °C to 50 °C, the electrical conductivity of unstretched and stretched rubbers increases about 1.2 and 1.5 times, respectively.

5.2 Comparison of the properties of NR/NBR blends prepared from MWCNT/NR masterbatch and MWCNT/NBR masterbatch

In this part, the properties of the NR/NBR blends prepared from the MWCNT/NR masterbatch (mNR) and those prepared from MWCNT/NBR masterbatch (mNBR) are compared. The blend ratios are also varied at 100/0, 70/30, 50/50, 30/70 and 0/100 % w/w while the amount of the MWCNT in all NR/NBR blends is kept constant at 4 phr. The MWCNT/NR and MWCNT/NBR masterbatches used in this part are prepared by using the predispersing method.

5.2.1 Cure characteristics of NR/NBR compounds

Cure curves of the mNR and mNBR blends with various blend ratios are shown in Figure 5.43. It can be seen that the reversion behaviour, a continuous decrease of torque with time after complete cure, can be observed in NR rich blends for both mNR and mNBR blends. Additionally, it is found that the reversion of both mNR and mNBR blends tends to decrease when NBR content in the blend is increased. The reversion is reported to be due to the decomposition of polysulfidic linkages under applied oscillating shear normally occurring in sulphur vulcanization of

NR [108]. Therefore, a decrease reversion could be explained by the dilution effect. Scorch time and cure time of the mNR and mNBR blends as a function of blend ratio are also compared in Figure 5.44. It is found that the scorch time and cure time of both mNR and mNBR blends slightly increase when NBR content in the blend is increased. This is because NBR has less double bonds than NR resulting in slower cure than NR. However, at the blend ratio of 70/30 and 50/50, the scorch time and cure time of the mNR compounds are lower than those of the corresponding mNBR compounds. This may be due to a greater distribution of MWCNT resulting in better formation of a continuous MWCNT network, leading to better thermal conductivity [16]. In addition, Figure 5.45 reveals that the mNR compound containing 50 %wt NBR obviously exhibits the highest minimum torque, maximum torque and torque difference. Again, this may be due to better distribution of MWCNT leading to the enhancement of thermal conductivity. Additionally, the increased curative concentration in the mobilized rubber portion of the mNR blend having 50/50 NR/NBR can lead to its higher crosslink density and thus the higher torque difference. However, it is apparent that the minimum torque, maximum torque and torque difference of the mNR compounds at the other blend ratios are not significantly different and similar to those of the corresponding mNBR blends. The slight increase in the minimum torque of the mNR and mNBR blends, except for the 50/50 mNR blend, with increasing NBR content could be explained by the higher viscosity of NBR.

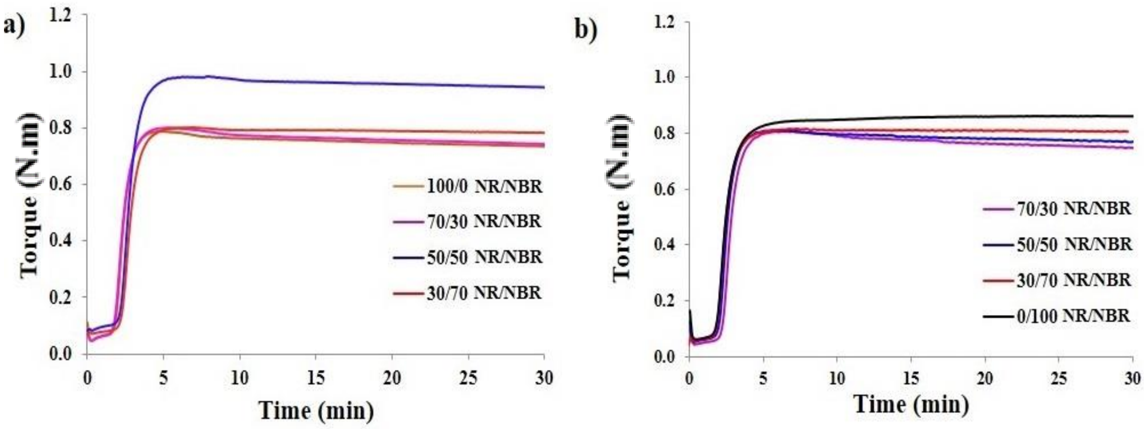

Figure 5.43 Cure characteristics of a) mNR and b) mNBR compounds with various blend ratios.

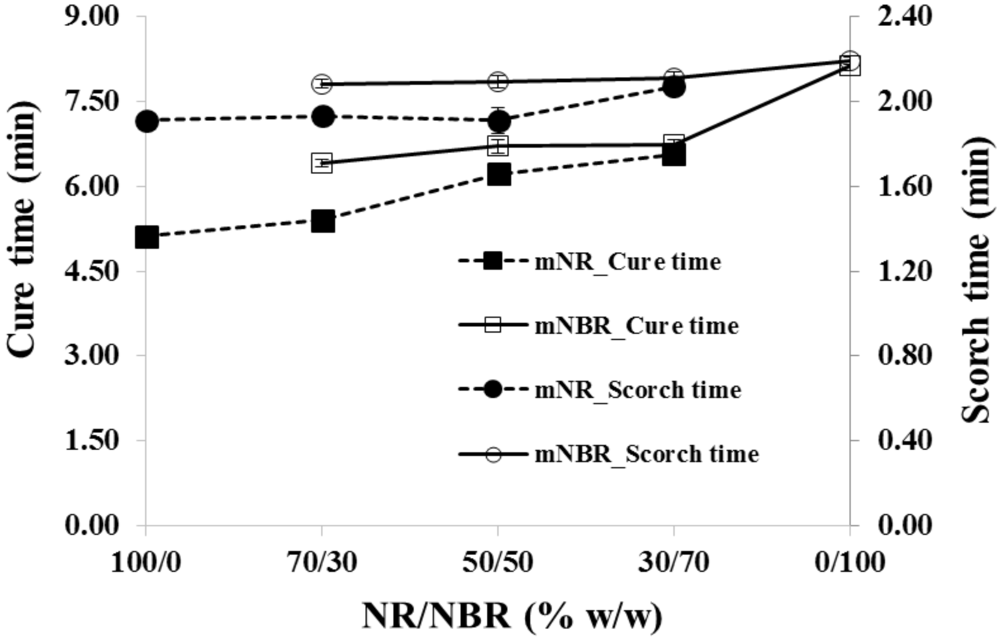

Figure 5.44 Scorch time and cure time of the mNR and mNBR compounds with various blend ratios.

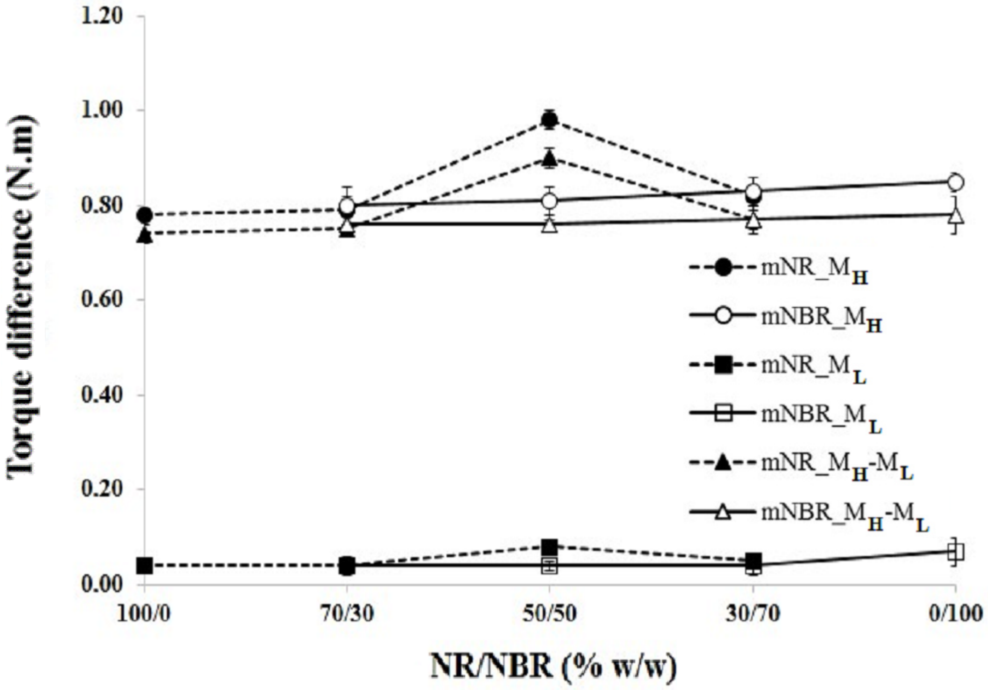

Figure 5.45 Torque difference (M_H-M_L), maximum (M_H) and minimum torques (M_L) of the mNR and mNBR blends with various blend ratios.

5.2.2 Dichroic ratio of NR/NBR blends

From Figure 5.46, it reveals that dichroic ratio (R) of both mNR and mNBR blends is higher than 1 at all blend ratios. This indicates that the majority of MWCNTs align along MD. However, the level of MWCNT alignment for the mNR and mNBR blends is different for each blend ratio. It can be seen that R of both mNR and mNBR blends tends to decrease with increasing NBR content. The reduction of R for both mNR and mNBR blends is attributed to an increase of NBR content. This may be explained by the difference of MWCNTs alignment between the 100/0 mNR and the 0/100 mNBR blends. As can be seen in Figure 5.46, the alignment level of MWCNTs in the 100/0 mNR blend is higher than that in the 100/0 mNBR blend about 1.6 times. This reason may be due to higher elongational capability of NR leading to improvement of MWCNT alignment. Although R of the mNR and mNBR blends gives a similar trend, R of mNR blends is higher than that of the corresponding mNBR blends. It may be explained by greater alignment of MWCNTs in NR phase for NR/NBR blend when the majority of MWCNT content is in the NR phase.

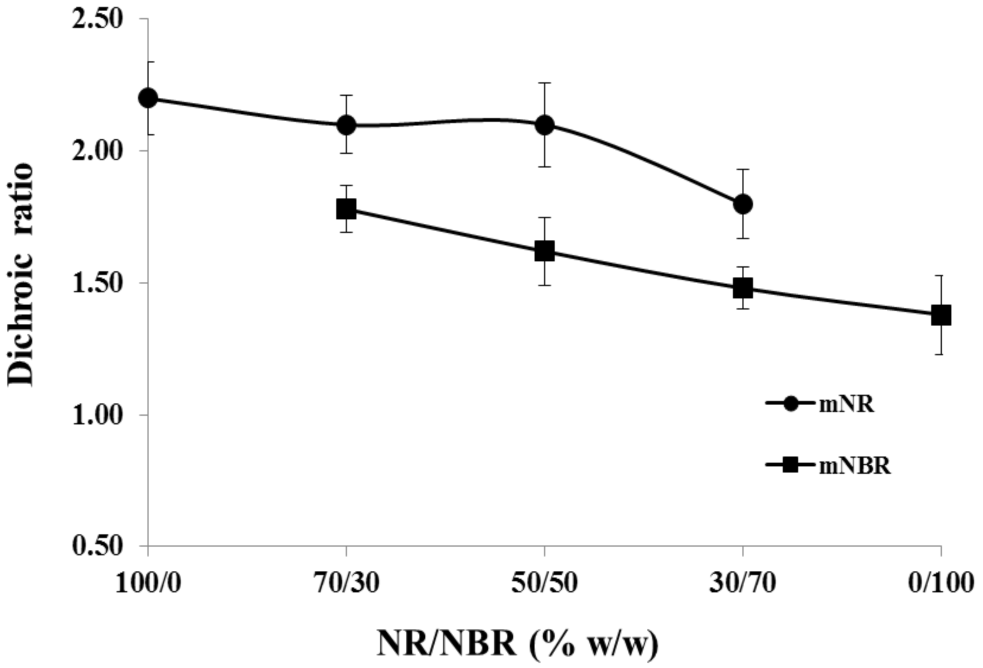

Figure 5.46 Plot of Dichroic ratio (R) versus blend ratio of the mNR and mNBR blends.

5.2.3 Dynamic mechanical properties

The 4 phr MWCNT-filled NR/NBR vulcanized sheets prepared by using MWCNT/NR and MWCNT/NBR masterbatches are punched in MD and TD directions. Then, their dynamic mechanical properties expressed in term of damping factor (tan δ) are determined and depicted in Figures 5.47 and 5.48. It can be seen that both 100/0 mNR blend and 0/100 mNBR blend show single peak. Additionally, 100/0 mNR blend and 0/100 mNBR blend show T_g at about -56 ºC and -14 ºC corresponding to NR and NBR phases, respectively. When NR is blended with NBR, two peaks of tan δ belong to NR and NBR phases can be observed. Since the polarity of NR and NBR is much different, the preference of MWCNT in each rubber phase which can affect their T_g and tan δ_{max} can also be different. Tan δ_{max} values of the NR and NBR phases in MD for both mNR and mNBR blends can be used to estimate the preference of MWCNT in each rubber phase by using equation 4.14 and the result is given in Table 5.3 [51-54]. From Table 5.3, the amount of MWCNT located in the NR phase of mNR blends at 70/30, 50/50 and 30/70 blend ratios is respectively about 2.4, 1.2 and 3.3 times higher than that in the corresponding NBR phase. These results indicate that the 50/50 NR/NBR blend gives the highest balance of MWCNT distribution between the NR and NBR phases compared among the mNR blends. The migration of MWCNT from the NR phase to the NBR phase for the 50/50 mNR blend is about 46% of the total MWCNT loading. On the other hand, it is apparent that the 30/70 NR/NBR shows the poorest MWCNT distribution in the two rubber phases compared among the mNR blends. As can be seen, only about 23% of the total MWCNT loading migrate from the NR phase to the NBR phase. For the mNBR blends, it appears that the amount of MWCNT in the NBR phase is clearly higher than that in the NR phase at all blend ratios. The amount of MWCNT in the NBR phase of the mNBR blends at 70/30, 50/50 and 30/70 blend ratios is respectively about 3.5, 3.2 and 2.8 times higher than that of the corresponding NR phase. In other words, the migration of MWCNT from the NBR phase to the NR phase of 70/30, 50/50 and 30/70 mNBR blends is respectively about 22%, 24% and 25.5% of the total MWCNT loading. It can be seen that the amount of MWCNT in 70/30 and 50/50 mNBR blends transferring from the NBR phase to the NR phase is less than the amount of MWCNT transferring from the NR phase to the NBR phase for the corresponding mNR blends. As a result, MWCNT distribution in the 70/30 and 50/50 mNBR blends is poorer than the corresponding mNR blends. Additionally, Figures 5.47 and 5.48 show that T_g and tan δ_{max} of NR and NBR phases for both mNR and mNBR blend slightly changes when the blend ratio is changed. As can be seen, T_g of NR phase slightly increases with increasing NBR content in the mNR blend, whereas that of the NBR phase slightly decreases. In addition, tan δ_{max} of NR phase for the mNR blends tends to decrease with increasing NBR content while that of their NBR phase increases. The increase in T_g and lowering in tan δ_{max} of the NR phase with increasing NBR content is caused the greater restricted motion of NR molecular chains by due to the increment of MWCNT concentration in the NR phase as can be seen in Table 5.3. Likewise, the decrease in T_g and increase in tan δ_{max} of the NBR phase with increasing NBR content is resulted from in the lower restricted motion of NBR molecular chains caused by the reduction of MWCNT concentration in the NBR phase. Similar observation is also found for the mNBR blends as can be seen in Figure 5.48. Furthermore, it is observed that the tan δ_{max} of both NR and NBR phases in the mNR and mNBR blends is lower than that of its corresponding phase in the single rubber system. The explanation is given to the lower energy dissipation of NR and NBR molecular chains in the blends relative to its corresponding phase in the single rubber system as a result of the dilution effect. The similar trend of tan δ_{max} is also found for the mNBR blends. In order to study MWCNT reinforcement efficiency in the NR and NBR, tan δ_{max} of the 100/0 and 0/100 NR/NBR vulcanizates containing 4 phr MWCNT and, unfilled 100/0 NR/NBR (gum NR) and unfilled 0/100 NR/NBR (gum NBR) is determined and shown in Table 5.4. It appears that the addition of MWCNT into these vulcanizates affects their tan δ_{max} value. As can be seen, tan δ_{max} of the 100/0 and 0/100 NR/NBR vulcanizates containing 4 phr MWCNT is lower than that of their unfilled counterpart. Additionally, tan δ_{max} of the NR sample drops more than that of the NBR sample when 4 phr MWCNT is added. This result indicates that the interaction between MWCNT and NR is higher than that between MWCNT and NBR due to their similar polarity. Therefore, reinforcement efficiency of MWCNT in NR phase should be higher than that in the corresponding NBR phase of the NR/NBR blend. It has been also reported previously that the interaction between CB and NR is higher than that between CB and NBR [109]. This is because of the similar polarity between CB and NR.

Results also show that type of masterbatch used for preparing the blends affects tan δ_{max} of each phase in the blends as depicted in Figures 5.47 and 5.48. When MWCNT/NR masterbatch is used for preparing the mNR blends, tan δ_{max} of their NR phase is lower than that of NR phase in the corresponding blend prepared from MWCNT/NBR masterbatch. In contrast, when MWCNT/NBR masterbatch is used for preparing the mNBR blend, tan δ_{max} of their NBR phase is lower than that of NBR phase in the corresponding blend prepared from MWCNT/NR masterbatch. This result coincides with the higher amount of MWCNTs in the rubber phase used for preparing the MWCNT/rubber masterbatch as can be seen in Table 5.3. Also, it can be seen that the tan δ_{max} in MD of both phases for the mNR and mNBR blends is lower than that of their TD counterpart. This is because the majority of MWCNTs aligns in MD as previously discussed in section 5.2.2. Additionally, NR phase of the mNR blends shows the larger difference in the tan δ_{max} between MD and TD than its NBR counterpart. This is because the NR phase of the mNR blends contains higher amount of the MWCNTs than its NBR counterpart as depicted in Table 5.3. In addition, the MWCNT in NR phase exhibits the higher alignment degree and reinforcement efficiency than that in the NBR counterpart.

Table 5.3 Tan δ_{max} of NR and NBR phases and amount of MWCNT in NR and NBR phases for the mNR and mNBR blends.

Blend	NR/NBR	Tan δ_{max} of each phase		Amount of MWCNT in each phase (phr)	
		NR	NBR	NR	NBR
mNR	100/0	1.21	N/A	4.00	N/A
	70/30	0.44	0.40	2.81	1.19
	50/50	0.37	0.77	2.15	1.85
	30/70	0.18	0.99	3.08	0.92
mNBR	70/30	0.68	0.29	0.88	3.12
	50/50	0.43	0.56	0.96	3.04
	30/70	0.20	1.02	1.06	2.94
	0/100	N/A	1.32	N/A	4.00

Table 5.4 Tan δ_{max} of 100/0 NR/NBR (or NR) and 0/100 NR/NBR (or NBR) in MD, with and without MWCNT

NR/NBR (%w/w)	Tan δ_{max}		Reduction in Tan δ_{max}
	Unfilled sample	4 phr MWCNT-filled sample	
100/0	2.40	1.21	1.19
0/100	1.70	1.32	0.38

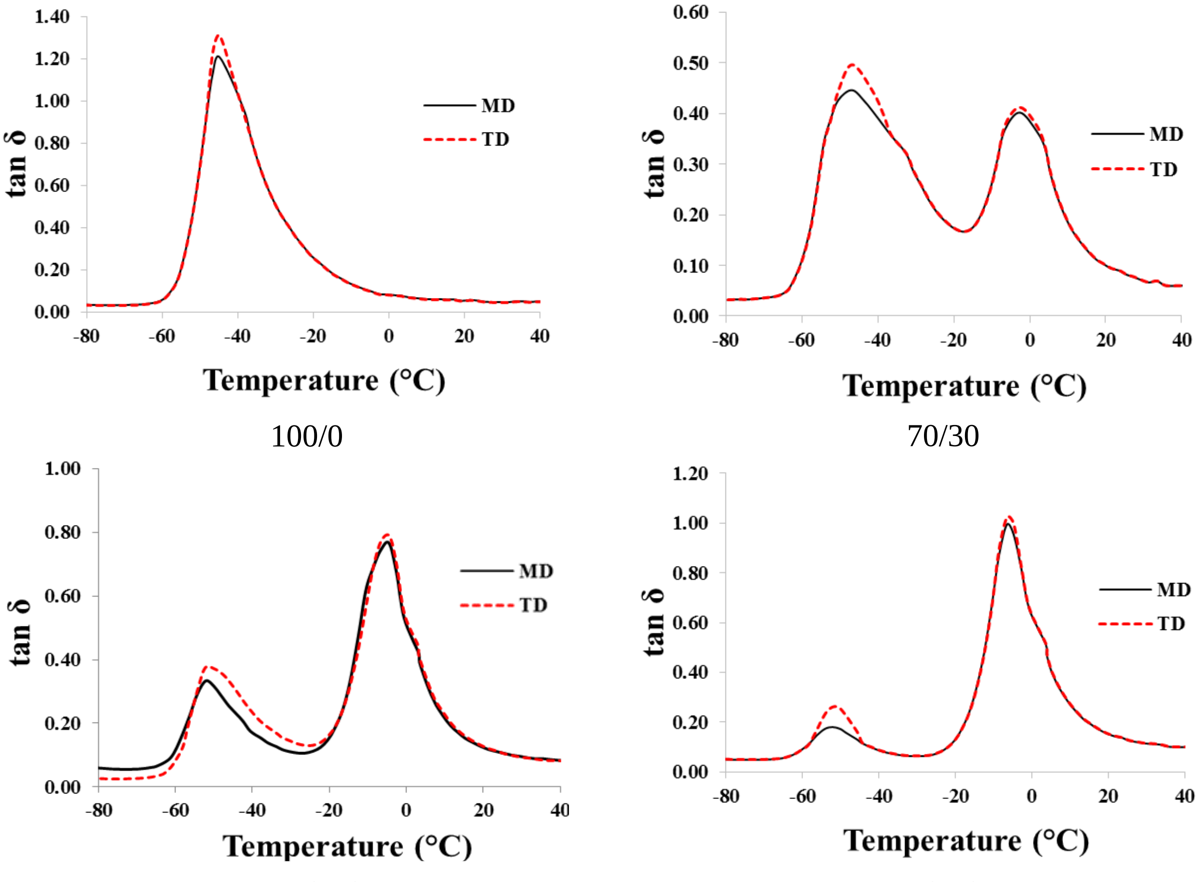

100/0

70/30

50/50

30/70

Figure 5.47 Loss tangent (tan δ) as a function of the temperature for the mNR blends in MD and TD at various blend ratios.

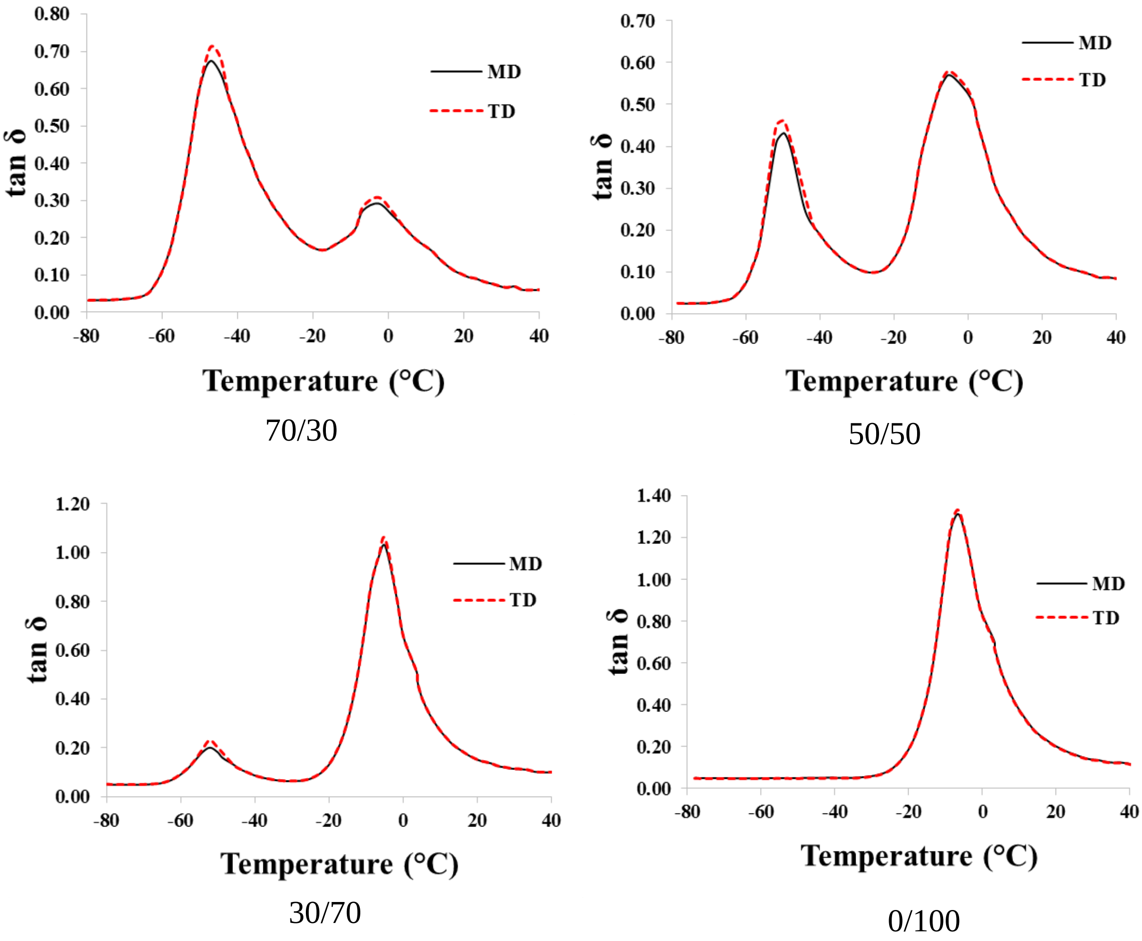

70/30

50/50

30/70

0/100

Figure 5.48 Loss tangent (tan δ) as a function of the temperature for the mNBR blends in MD and TD at various blend ratios.

Figure 5.49 shows the average storage modulus results at 30°C for the mNR and mNBR blends at various blend ratios. It reveals that the storage modulus in MD and TD of both blends increases when NBR content is increased. This is due to the dilution effect resulting from the higher modulus of the NBR relative to NR. In addition, it is found that the storage modulus of both blends in MD is higher than its corresponding TD sample at all blend ratios. As shown previously by the dichroic ratio results (Figure 5.46), the majority of MWCNTs align parallel to the applied force. Therefore, it is more difficult to deform the MD samples than the corresponding TD samples. Additionally, the largest difference in the storage modulus between the MD and TD can be observed for the 50/50 mNR blend. Several reasons are responsible for the obtained result. Firstly, the dichroic ratio of the 50/50 mNR is at maximum value and comparable with that of the other mNR blends having NR as the continuous phase. This means that degree of MWCNT alignment for the 50/50 mNR is at maximum value and similar to that of the other mNR blends. Secondly, it can be seen from Table 5.3 that MWCNT concentration in the NR continuous phase of the 50/50 mNR is higher than the other mNR blends having NR as the continuous phase. Thus, the higher reinforcement by MWCNT in the MD sample of the 50/50 mNR is achieved. As a result, its storage modulus in MD is much higher than that in TD. Unlike the 50/50 mNR, the 30/70 mNR blend has NBR as its continuous phase. Therefore, the higher MWCNT concentration in the NR phase of 30/70 mNR blend does not lead to its higher storage modulus in MD. For the 0/100 mNBR blend, it exhibits the smallest difference in the storage modulus between the MD and TD because it has the smallest difference in MWCNT alignment between MD and TD as shown by its lowest dichroic ratio. The result also shows that the storage modulus in MD of the mNR blend is higher than that of the corresponding mNBR blend. The possible explanation is partly given by the higher MWCNT alignment for the mNR blend as verified by its higher dichroic ratio (Figure 5.46). In addition, the higher reinforcement efficiency of the MWCNT in the mNR blend discussed previously in this section is another reason for the obtained result.

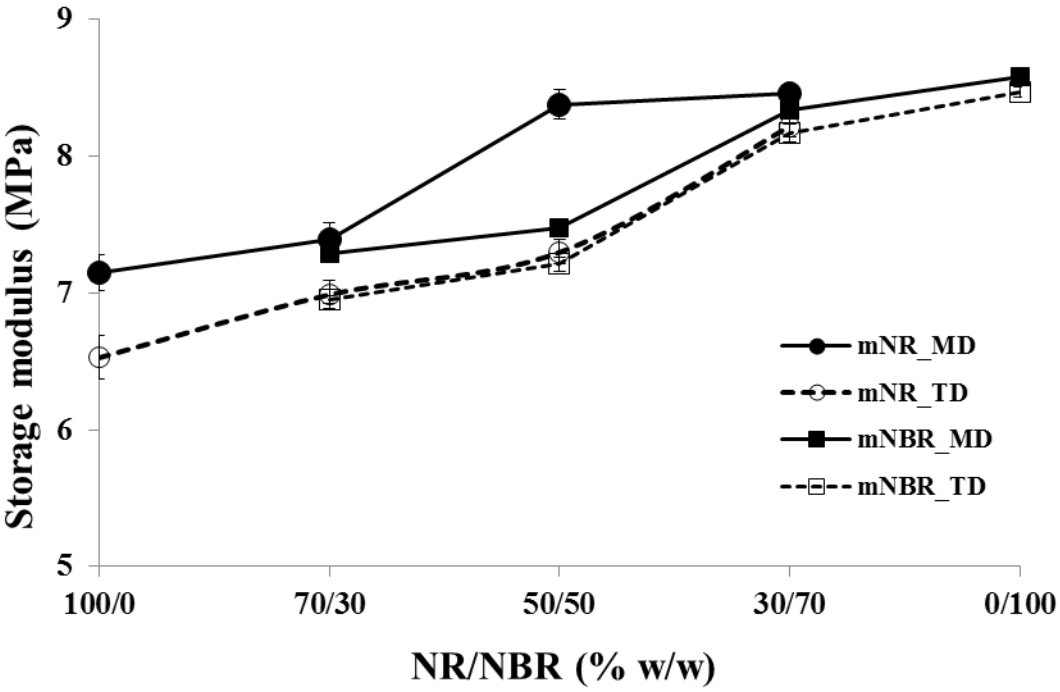

Figure 5.49 Storage modulus at 30°C of the mNR and mNBR blends in MD and TD at various blend ratios.

Heat build-up and dynamic compression set of the mNR and mNBR blends at various blend ratios are presented in Figures 5.50 and 5.51, respectively. As can be seen, both heat build-up and dynamic compression set of both blends tend to increase when NBR content in the blend is increased. This is because NBR containing sterically hindered molecular structure requires high energy for molecular mobility, thus leading to high energy dissipation. Therefore, higher hysteresis loss during applied dynamic force would be more pronounced in NBR rich blends. Additionally, the mNBR blends give higher heat build-up and dynamic compression set than the corresponding mNR blends. The higher energy loss during the dynamic test found in the mNBR blends is due to lower reinforcement efficiency of the MWCNTs which are mainly present in NBR phase. However, there is only slight difference in dynamic compression set of the mNR and mNBR at 30/70 blend ratio. This may be because the NBR is the major component for both mNR and mNBR blends. Therefore, their dynamic compression set is mainly controlled by the NBR phase having rather low reinforcement by the presence of MWCNT.

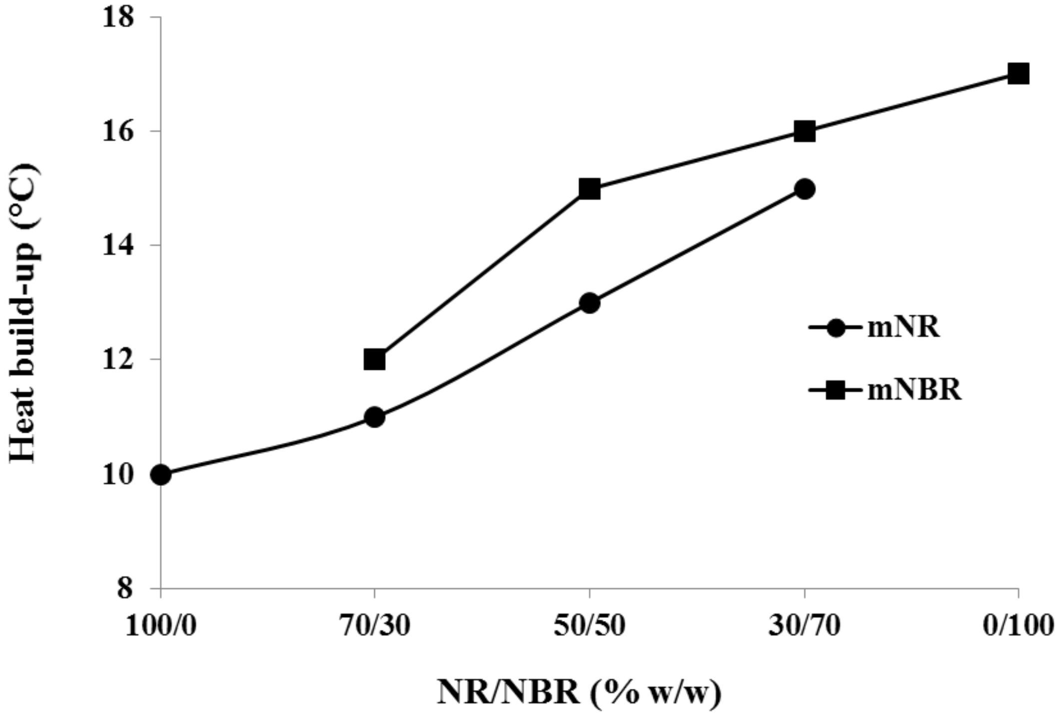

Figure 5.50 Heat build-up of the mNR and mNBR blends at various blend ratios.

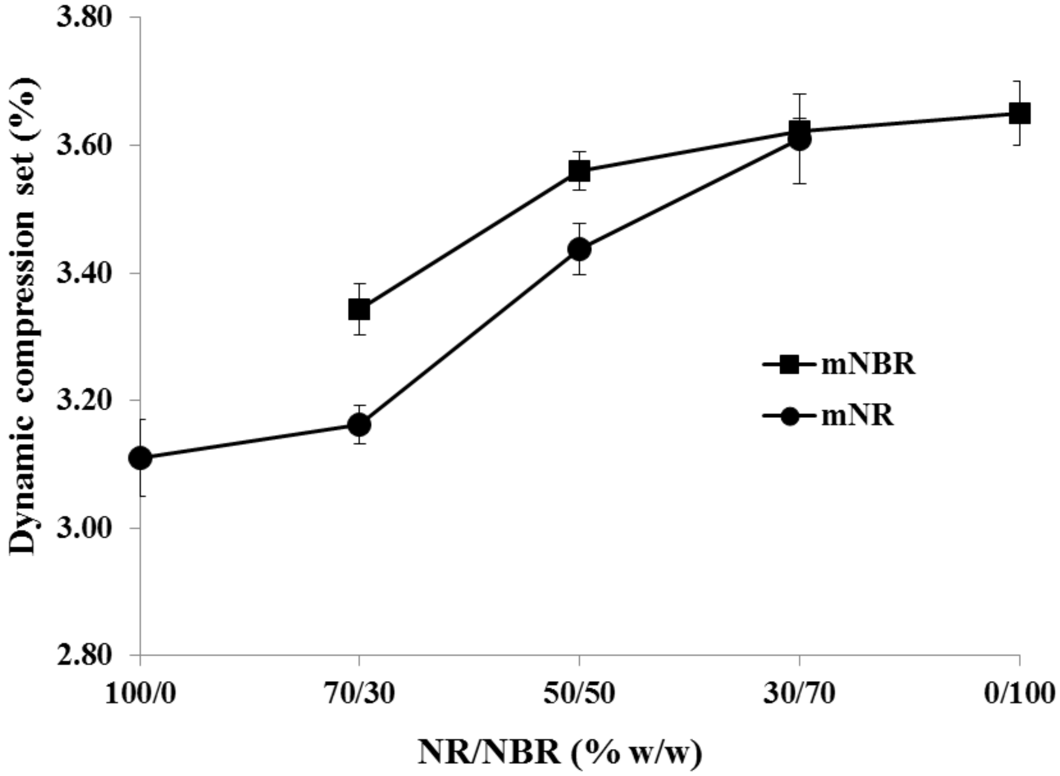

Figure 5.51 Dynamic compression set of the mNR and mNBR blends at various blend ratios.

5.2.4 Morphology

Phase morphology of the mNR and mNBR blends at various blend ratios was examined by using SEM in back-scattered electron imaging mode and it is illustrated in Figure 5.52. In the SEM micrographs, the grey phase and the dark phase correspond to NR phase and NBR phase, respectively. It should also be noted that bright spots in the rubber phases of all blends are the individual entangled MWCNTs. It is found that the morphology of both mNR and mNBR blends changes when NBR content is increased. For the 70/30 mNR blend, NBR can be seen as the small dispersed phase having nearly spherical structure in the continuous NR phase. When the amount of the NBR in the mNR blend is increased to 50 wt%, the size of the dispersed NBR phase in the NR continuous phase is larger than that in the 70/30 mNR blend. It is thought that the smaller particle size of the dispersed NBR phase in the 70/30 mNR blend compared with that in the 50/50 mNR blend arises from the lower viscosity of NBR phase in the 70/30 mNR resulted from its lower MWCNT content as shown in the section 5.2.3. Therefore, the NBR phase of the 70/30 mNR blend is easier to be deformed and broken up than that of the 50/50 mNR blend. Furthermore, phase inversion in the mNR blend is observed at 30/70 blend ratio. This means that NR is the dispersed phase and NBR becomes the continuous phase. For the mNBR blends, it can be seen that the NBR is also the dispersed phase in the continuous NR phase at both 70/30 and 50/50 blend ratios. In addition, the size and shape of the NBR dispersed phase of 70/30 mNBR blend are not significantly different from those in the 50/50 mNBR blend. However, a higher number of the dispersed NBR phases can be observed for the 50/50 mNBR blend because it has higher NBR content. Also, phase inversion of the mNBR blend is observed at 30/70 blend ratio. Additionally, it appears that the particle size of the dispersed NBR phase in the 70/30 and 50/50 mNBR blends is much larger than that in the corresponding mNR blends. This is because there is higher MWCNT content in the dispersed NBR phase for the mNBR blends relative to that for the mNR blends (see Table 5.3). This results in the higher viscosity of the dispersed NBR phase for the mNBR blends relative to that for the mNR blends. Therefore, it is more difficult to deform and break up the NBR phases of the 70/30 and 50/50 for mNBR blend than those for the corresponding mNR blend.

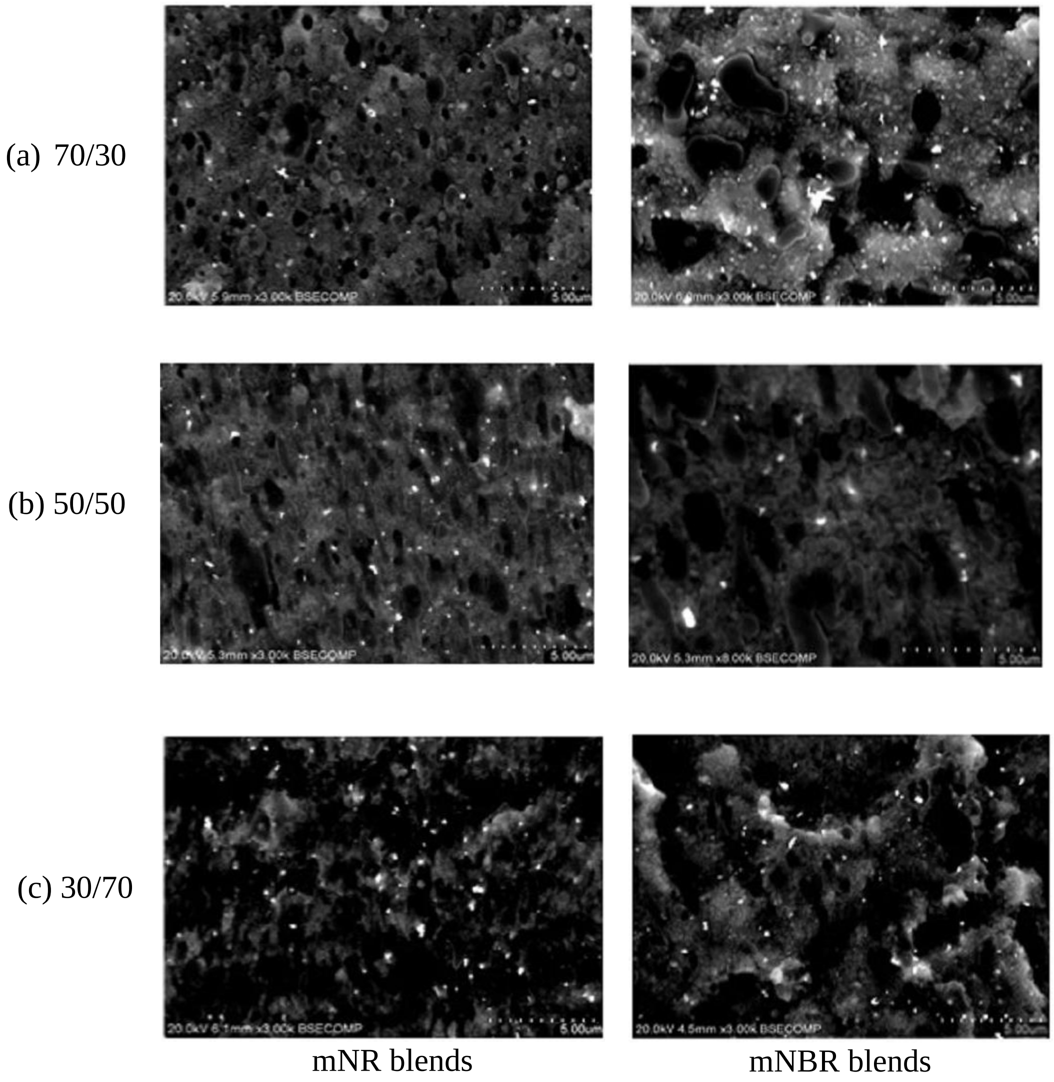

Figure 5.52 Scanning electron micrographs of the mNR and mNBR blends at different blend ratios.

5.2.5 Mechanical properties

Hardness, modulus, elongation at break, tensile strength and tear strength of the mNR and mNBR blends at various blend ratios are presented in Figures 5.53-5.57. Additionally, the effect of milling direction on the tensile properties and tear strength of the mNR and mNBR blends in MD and TD are compared. It is found that hardness and 100% modulus of all blends tend to increase slightly with increasing NBR content in the blends as depicted in Figures 5.53 and 5.54, respectively. On the other hand, Figure 5.55 depicts that elongation at break of both mNR and mNBR blends does not significantly change when NBR content is not more than 50 wt% because the natural rubber is a continuous phase. Then, it obviously decreases when NBR content is higher than 50 wt%. This is because the nitrile rubber becomes a continuous phase and it has higher modulus and lower elongation at break than the natural rubber. Therefore, the dilution effect could be used to describe this finding. It is also observed that hardness and modulus of the mNR blends are superior to those of the corresponding mNBR blends. Explanation is given by the better MWCNT distribution and higher reinforcement efficiency of MWCNT in the mNR blends as previously discussed in section 5.2.3. In addition, it can be seen that modulus and tensile strength of both mNR and mNBR blends in the MD is greater than those in the corresponding TD sample while elongation at break displays inverse trend. This is because the majority of MWCNTs align in MD. It is interesting to observe the difference in tensile strength trend as shown in Figure 5.56 when the different masterbatches were utilized. It is found that tensile strength of the mNR blends in MD increases slightly with increasing NBR content in the blends up to 50 %wt. Then, it tends to decrease sharply when NBR content in the blend is further increased. A reduction of tensile strength could be explained by the low strength of the nitrile rubber for NBR rich blends and the reduction in alignment degree of MWCNTs in MD when NBR content is increased. On the other hand, tensile strength of the mNR blends in TD is not significantly different when the blend ratio is changed from 70/30 to 50/50. However, its tensile strength also decreases markedly at 30/70 blend ratio in which the nitrile rubber is the continuous phase. For the mNBR blends, their tensile strength in both MD and TD continuously decreases with increasing NBR content due to the dilution effect. In addition, it is found that the mNR blends in MD exhibit higher tensile strength than the corresponding mNBR blends. This is also because the mNR blends contains higher amount of MWCNTs aligned parallel to the applied force which are able to bear the load than that for the corresponding mNBR blends. The higher dichroic ratio value of the mNR blends relative to that of their corresponding mNBR blends shown Figure 5.46 can be used to support this explanation. Also the smaller dispersed NBR phase of the mNR blends compared with that of the corresponding mNBR blends, especially at 70/30 and 50/50 blend ratios, can be used to explain the obtained results. The smaller dispersed NBR phase of the mNR blends indicating the more compatibility between two rubber phases can also be the reason for their higher tensile strength in TD when compared with the corresponding mNBR blends. Moreover, tear strength of the mNR and mNBR blends in both MD and TD continuously decreases when NBR content in the blends is increased as presented in Figure 5.57. This is attributed to the dilution effect. It is well known that tear strength of NR is much higher than that of NBR. This is because the crystallization can occur near the tear tip upon stretching the NR sample [110]. It is also found that tear strength of the mNR and mNBR blends in MD is slightly higher than that of their corresponding TD samples. This is because MWCNTs in MD aligned perpendicular to the crack front can obstruct the crack propagation, thus resulting in the higher tear strength [106]. At a specific blend ratio, it can also be seen that all mNR samples exhibit higher tear strength than the mNBR samples. This may be due to the combination of greater alignment and reinforcing efficiency of most MWCNTs in the mNR blends.

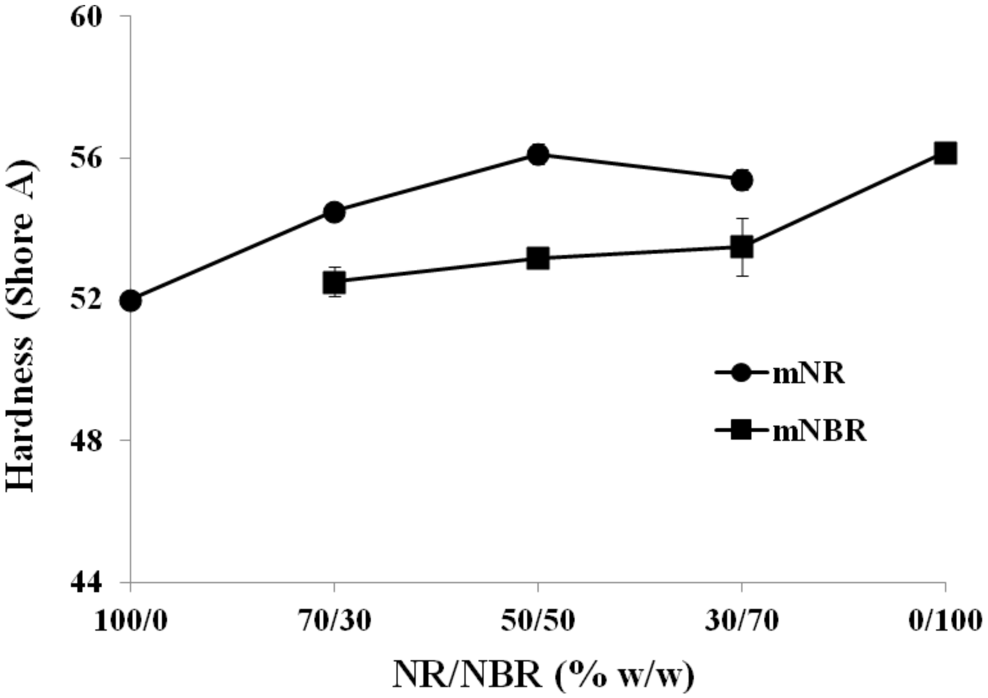

Figure 5.53 Hardness of the mNR and mNBR blends at various blend ratios.

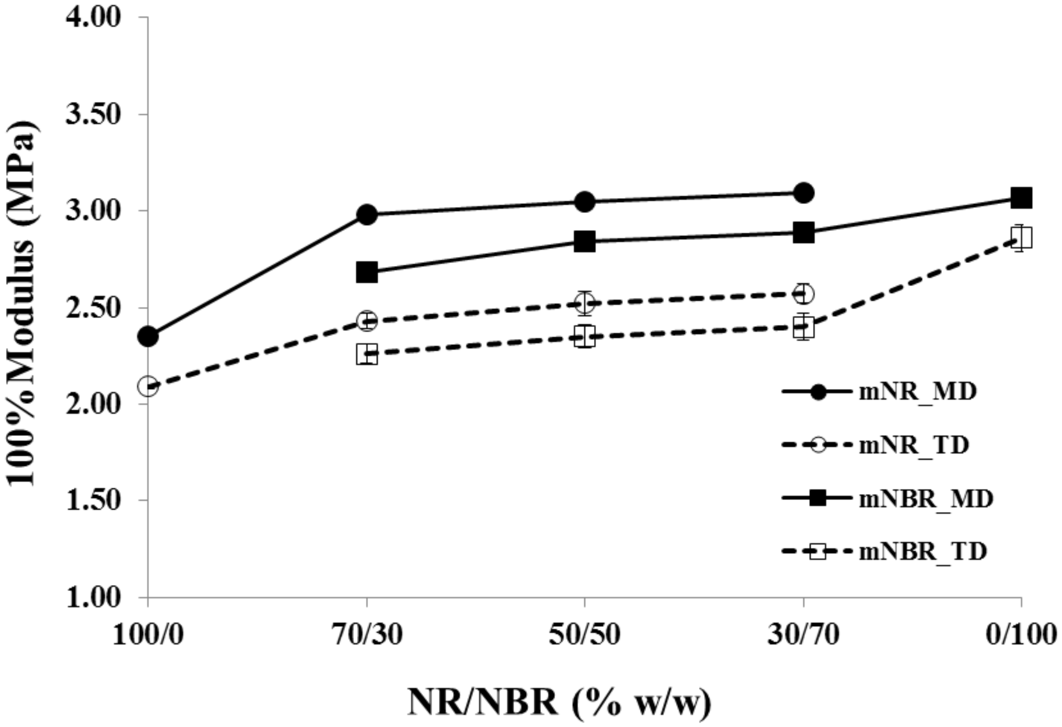

Figure 5.54 100% Modulus of the mNR and mNBR blends in MD and TD at various blend ratios.

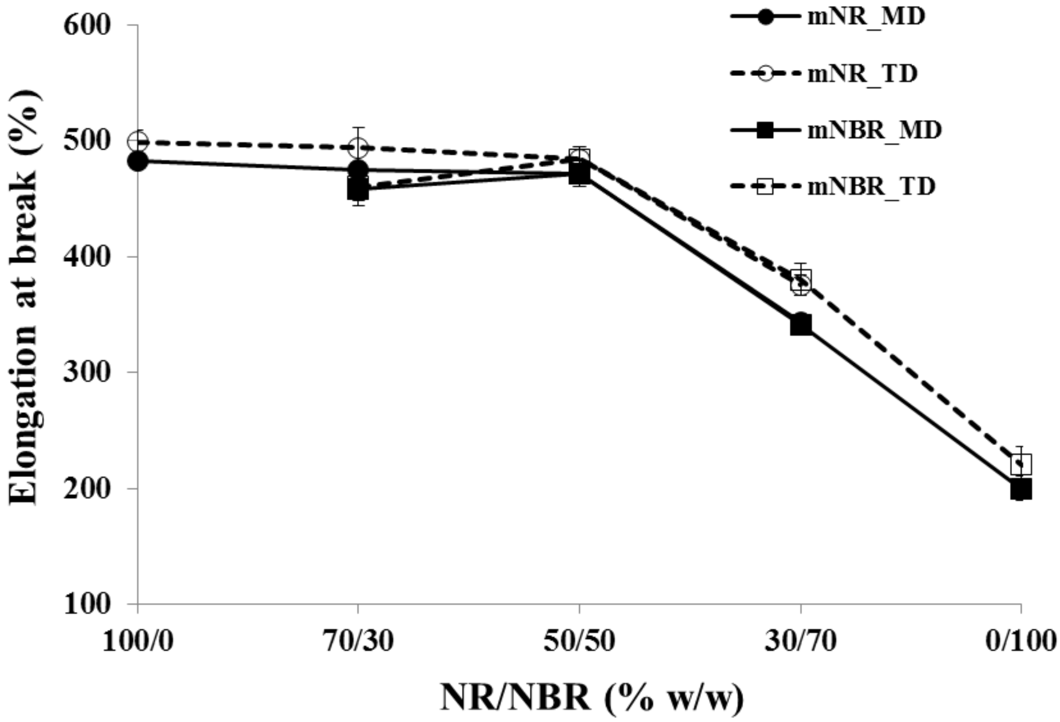

Figure 5.55 Elongation at break of the mNR and mNBR blends in MD and TD at various blend ratios.

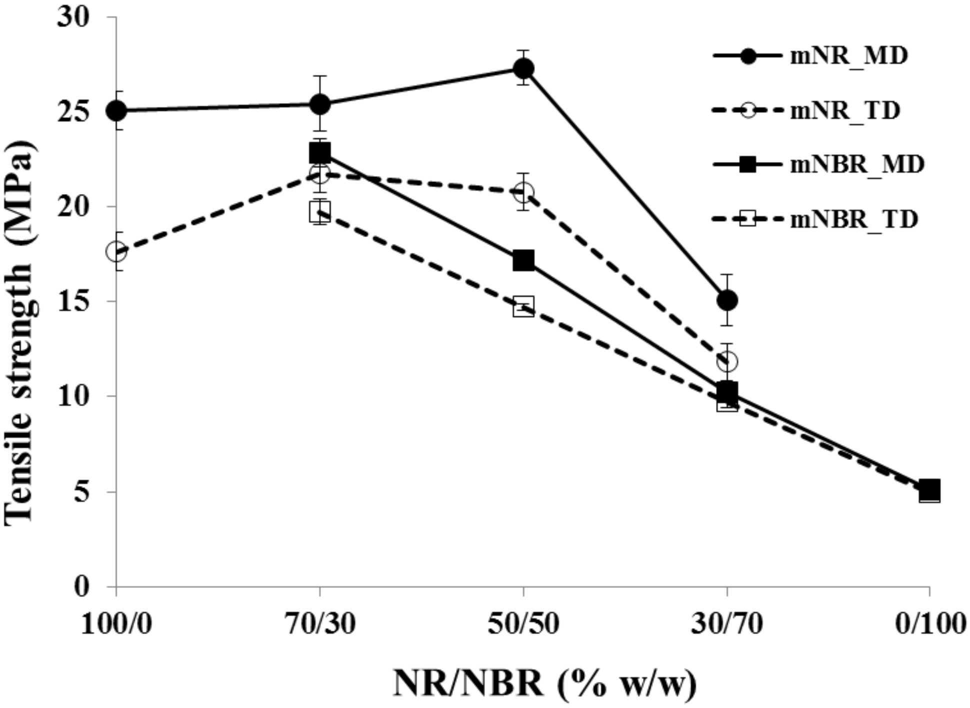

Figure 5.56 Tensile strength of the mNR and mNBR blends in MD and TD at various blend ratios.

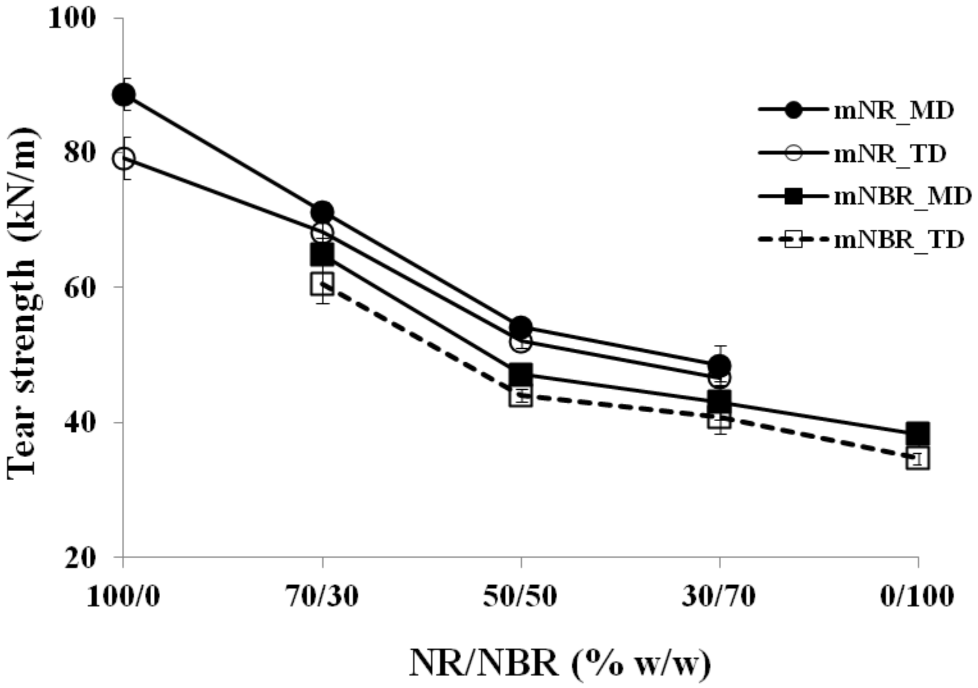

Figure 5.57 Tear strength of the mNR and mNBR blends in MD and TD at various blend ratios.

Figure 5.58 shows abrasion loss of the mNR and mNBR blends at different blend ratios. It is found that the abrasion resistance of both mNR and mNBR blends increases when NBR content in the blend is increased. The better abrasion resistance of the nitrile rubber relative to the natural rubber could be used to explain this result. Additionally, the greater abrasion resistance of NR/NBR blends is achieved when the MWCNT/NR masterbatch is used. This result can be explained by higher reinforcing efficiency of MWCNT in the mNR blends as previously discussed in section 5.2.3.

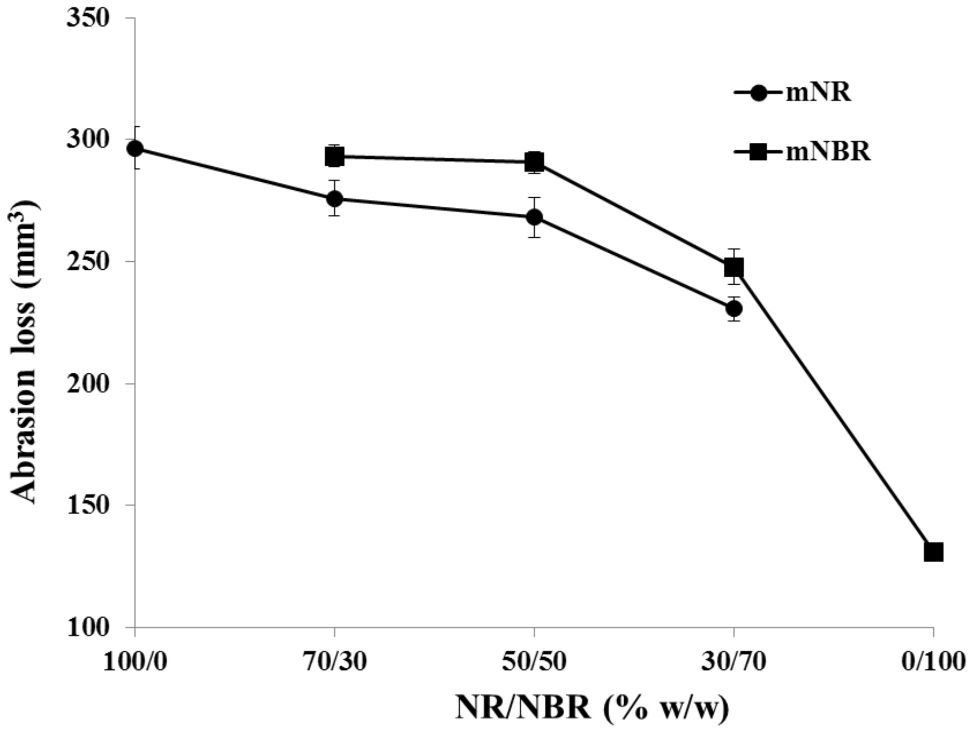

Figure 5.58 Abrasion loss of the mNR and mNBR blends as a function of blend ratio.

5.2.6 Electrical and thermal conductivities

Table 5.5 compares electrical conductivity of the mNR and mNBR blends in both MD and TD at various blend ratios. It can be seen that the electrical conductivity of MWCNT-filled 100/0 NR/NBR the lowest and it is lower than that of the MWCNT-filled 0/100 NR/NBR about 1 order of magnitude. In addition, the electrical conductivities of both mNR and mNBR blends at 30/70, 50/50 and 70/30 blend ratios, in both MD and TD, are in between those of 100/0 NR/NBR and 0/100 NR/NBR. Also, their electrical conductivities tend to increase when NBR content in the blend is increased due to the dilution effect. Moreover, the electrical conductivities of both mNR and mNBR blends in the MD are superior to those of their TD counterpart. For instance, the electrical conductivities of the 30/70 mNR and 30/70 mNBR blends in MD are higher than that of their TD counterpart about 1.20 and 1.18 times, respectively. It has been shown previously by the dichroic ratio results that most of the MWCNTs in the MD samples align parallel to the applied force. It has been shown previously in Figure 5.46 that the dichroic ratio of all blends is more than one indicating a greater number of MWCNTs aligned in MD than TD. Thus, a number of aligned MWCNTs facilitating the formation of conductive networks in the MD samples are higher than those in the TD samples. As a consequence, electrons flowing through the formed MWCNT networks in the MD samples are higher relative to the TD samples. Furthermore, it appears that the MD samples of the mNR blends exhibit higher electrical conductivity than their corresponding mNBR blends. The possible explanation is also given by a greater number of MWCNTs aligned parallel to the applied electrical current in the MD samples of mNR blend relative to the corresponding mNBR blend.

Figure 5.59 displays the thermal conductivity as a function of blend ratio of the mNR and mNBR blends. It can be seen that the thermal conductivity of the mNBR blends continuously increases with increasing NBR content in the blend. The dilution effect could be used to explain the obtained result because it has been reported that the nitrile rubber gives higher thermal conductivity than the natural rubber [111]. For the mNR blend, it shows an increase in the thermal conductivity with increasing NBR content in the blend up to 50 %wt and then its thermal conductivity sharply drops when NBR content is further increased. The highest thermal conductivity of 50/50 mNR blend is due to a balance of MWCNT distribution in each rubber phase as given in Table 5.3 leading to the greatest formation of continuous conductive network and hence facilitating the thermal conductivity. On the other hand, a decrease in thermal conductivity of the mNR blends may be due to poor distribution of MWCNT between two rubber phases leading to the reduction of interconnecting networks when NBR content is higher than 50 %wt. The thermal conductivities of the mNR and mNBR blends at 50/50 blend ratio are 1.22 and 1.08 times, respectively higher than that of the 100/0 NR/NBR blend. Additionally, the thermal conductivities of the mNR blends at 70/30 and 50/50 blend ratios are higher than those of their corresponding mNBR blends. As can be seen, the thermal conductivity of the 50/50 mNR blend is 1.13 times higher than that of the corresponding mNBR blend. As mentioned previously, the better MWCNT distribution between two rubber phases in the mNR blends is responsible for the obtained result. On the other hand, it appears that the thermal conductivity of the 30/70 mNBR blend is slightly higher than that of the corresponding mNR blend. It should be noted that the NBR phase behaves as a continuous phase for both mNR and mNBR blends at 30/70 blend ratio. However, MWCNT content in the NBR phase of the 30/70 mNBR blend is higher than that of the 30/70 mNR blend as presented previously in Table 5.3. Therefore, it can be stated that the higher MWCNT content in the continuous NBR phase of the 30/70 mNBR blends brings about the higher thermal conductivity.

Table 5.5 Electrical conductivity of the mNR and mNBR blends at various blend ratios.

Blend	NR/NBR	Electrical conductivity (S/m)	
		MD	TD
mNR	100/0	6.10×10^{-5}	4.27×10^{-5}
	70/30	4.00×10^{-4}	3.32×10^{-4}
	50/50	4.24×10-4	3.22×10^{-4}
	30/70	5.05×10^{-4}	4.13×10^{-4}
mNBR	70/30	3.43×10^{-4}	2.92×10^{-4}
	50/50	3.44×10^{-4}	3.01×10^{-4}
	30/70	4.55×10^{-4}	3.81×10^{-4}
	0/100	8.47×10^{-4}	8.11×10^{-4}

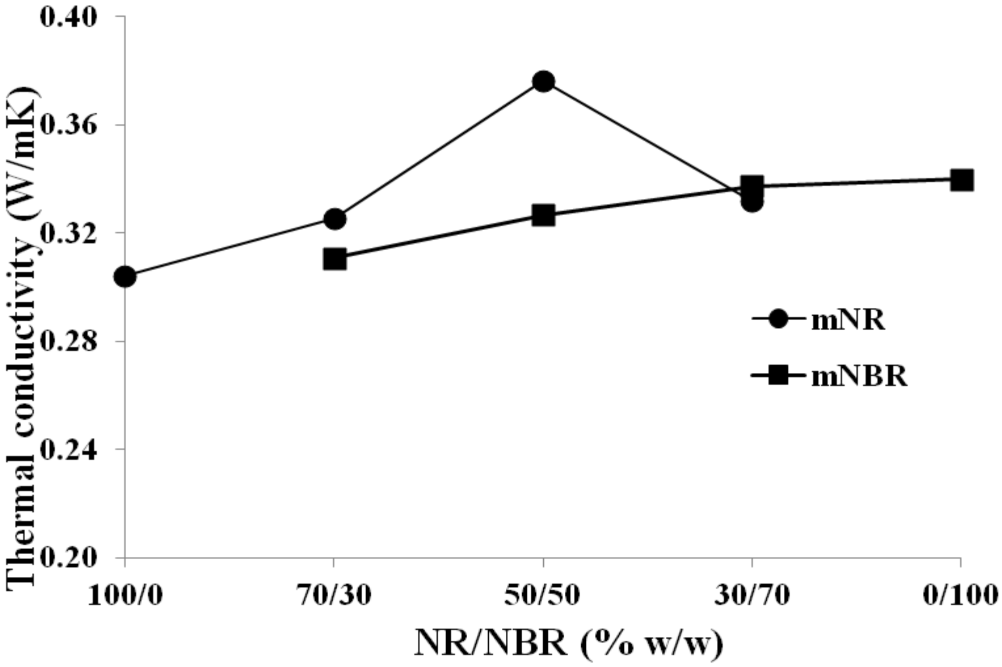

Figure 5.59 Thermal conductivity of the mNR and mNBR blends at various blend ratios.

5.2.7 Oil resistance

Figures 5.60 and 5.61 present swelling ratio, a reciprocal of swelling resistance, of the mNR and mNBR blends in gasohol and hydraulic oils, respectively. It can be seen that swelling resistance of both mNR and mNBR blends in the gasohol and hydraulic oils improves when NBR content in the blends is increased. It can be seen that the 100/0 mNR sample shows that highest swelling ratio in both gasohol and hydraulic oils. This is because the solubility parameter of the natural rubber is closer to that of these oils than the nitrile rubber having higher polarity. As a result, an increase of NBR content in the blends also leads to the reduction of the swelling ratio in the gasohol and hydraulic oils for both mNR and mNBR blends. At a specific blend ratio, the swelling ratio of both blends in the gasohol is higher than that of their corresponding samples in the hydraulic because the solubility parameter of the nitrile rubber blended with natural rubber is closer to that of the gasohol than the hydraulic oil. Additionally, it is clear that the swelling resistance of the mNR blends at 70/30 and 50/50 blend ratios in both oils are greater than that of the corresponding mNBR blends. The explanation is given by the higher reinforcement efficiency of MWCNT in the mNR blends as explained previously in the dynamic mechanical properties (section 5.2.3). However, there is only slight difference in swelling ratio of the mNR and mNBR at 30/70 blend ratio in both gasohol and hydraulic oils because the NBR phase is the continuous phase for both blends as revealed by the SEM micrographs. It should be also noted that the reinforcement efficiency of MWCNT in the NBR continuous phase is rather low as discussed previously. Therefore, it can be stated that NBR phase is mainly responsible for the swelling ratio of both blends at 30/70 blend ratio.

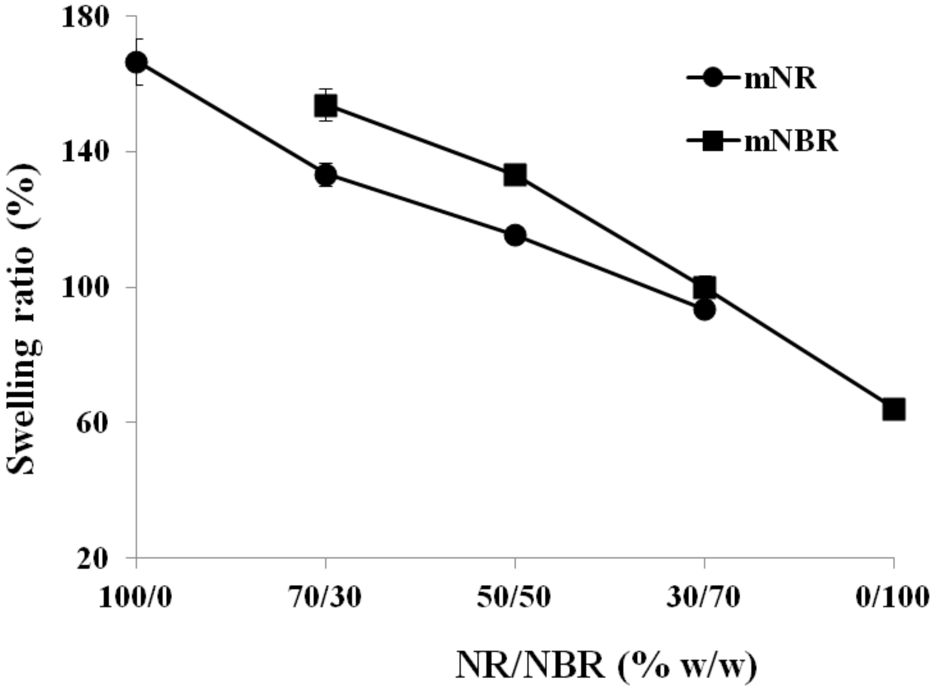

Figure 5.60 Swelling ratio of the mNR and mNBR blends in gasohol oil at various blend ratios.

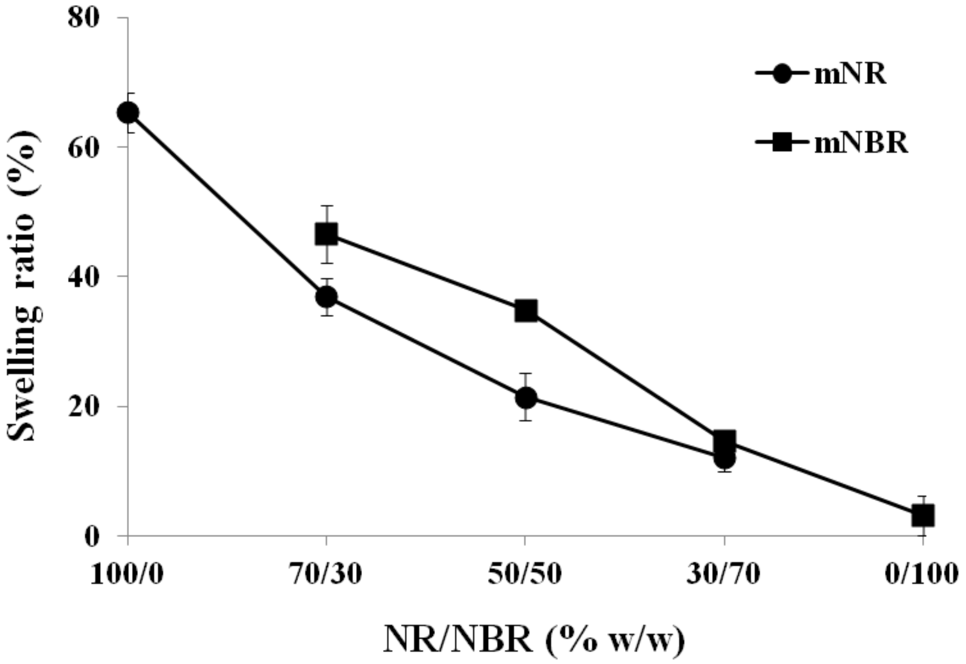

Figure 5.61 Swelling ratio of the mNR and mNBR blends in hydraulic oil at various blend ratios.

5.3 Properties of 50/50 NR/NBR vulcanizates filled with hydroxyl modified multi-wall carbon nanotube functionalized with silane coupling agent (Si-69)

In this part, hydroxyl modified multi-wall carbon nanotube functionalized with silane coupling agent (SiOH-MWCNT) is prepared by modifying the hydroxyl modified multi-wall carbon nanotube (OH-MWCNT) with Si-69. The optimum Si-69 concentration needed for grafting Si-69 onto the OH-MWCNT surface is determined. Then, the unmodified and modified OH-MWCNTs are characterized using Fourier transform infrared (FTIR) analysis. FTIR spectra of OH-MWCNT treated with various Si-69 concentrations are shown in Figure 5.62 and the FTIR characteristic peaks are summarized in Table 5.6. It can be seen that the FTIR spectrum of OH-MWCNT without Si-69 (0 % Si-69) shows a broad absorption peak of –OH functionality at 3442 cm^{-1}. The small peaks at 1680 cm^{-1} and 1576 cm^{-1} are associated with the C=O stretching of the carboxylic (–COOH) group and C=C stretching of the MWCNT, respectively [112, 113]. The peak at 1346 cm^{-1} is due to O–H bending deformation in –COOH [113]. In addition, the peak at 850 cm^{-1} is typical signal of MWCNT [113]. When Si-69 is added, the characteristic peaks of each spectrum are changed as can be seen also in Figure 5.62. The peaks appearing at 800 cm^{-1} and 2919 cm^{-1} are associated with CH_2–S group of Si-69 and C–H stretching vibration of Si-69, respectively [95]. Furthermore, the grafting of the Si-69 molecules onto OH-MWCNT surface is confirmed by the presence of the established Si–O–C bonds at 1100 cm^{-1} and 1153 cm^{-1} [95]. Thus, the SiOH-MWCNT is successfully prepared. It also appears that the intensities of the characteristic signals at 1100 and 1153 cm^{-1} increase with increasing Si-69 concentration. This could be explained by increasing the amount of Si-69 grafted on the OH-MWCNT surface. The mechanism of silanization reaction between OH-MWCNT and Si-69 has been previously proposed and it is shown in Figure 5.63 [95]. In this study, grafting index of SiOH-MWCNT calculated using equation 4.20 is used to indicate the amount of Si-69 grafted onto the OH-MWCNT surface. It is found that the grafting index of SiOH-MWCNT increases with increasing Si-69 concentration, though it does not significantly increase when Si-69 concentration is changed from 4 to 6 %w/v as displayed in Table 5.7. Therefore, 4 %w/v Si-69 is selected for preparing the SiOH-MWCNT. Thereafter, the SiOH-MWCNT/NR masterbatch is prepared using dispersing method and mixed with the NBR to prepare the 50/50 NR/NBR vulcanizate containing 4 phr SiOH-MWCNT. Various properties such as mechanical, thermal and electrical properties of the 50/50 NR/NBR blend filled with SiOH-MWCNT are determined. Additionally, its properties are compared with those of the blends containing unmodified-MWCNT (MWCNT) and hydroxyl modified multi-wall carbon nanotube (OH-MWCNT) prepared by using the same conditions.

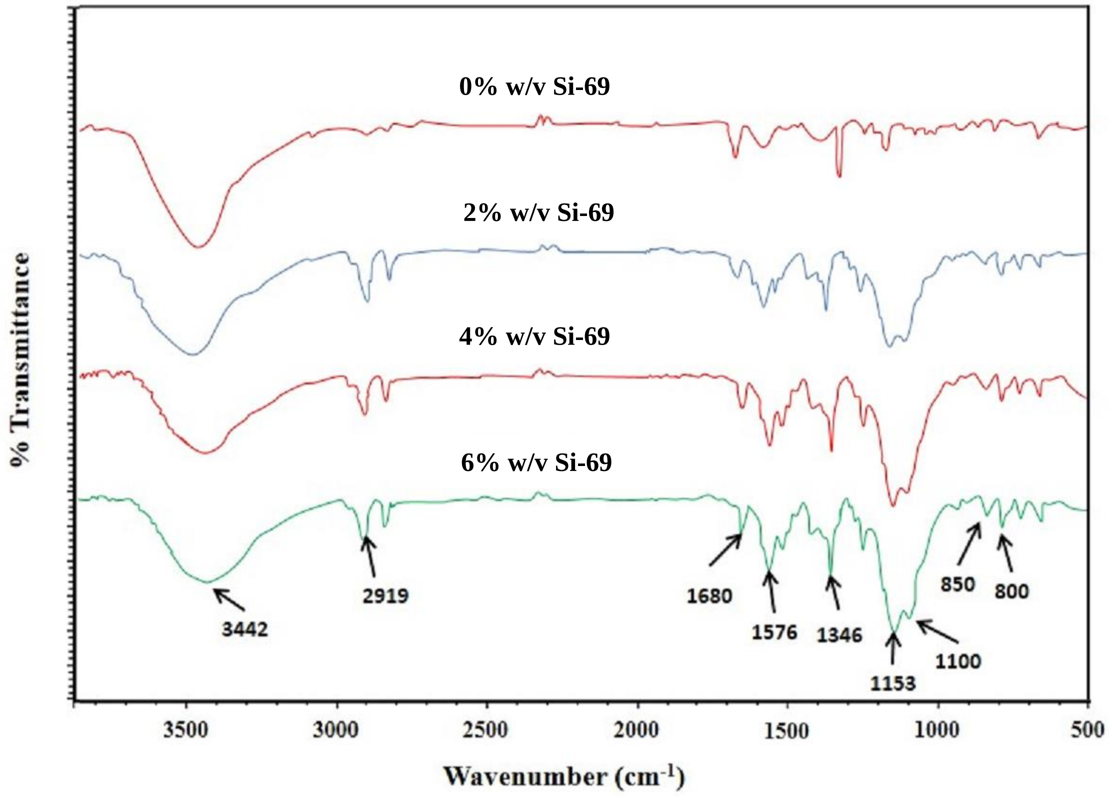

Figure 5.62 FTIR spectra of OH-MWCNT treated with Si-69 at various concentrations for preparing SiOH-MWCNT.

Table 5.6 Positions and assignments of bands observed in FTIR spectra of OH-MWCNT treated with Si-69 at various concentrations for preparing SiOH-MWCNT.

Wavenumber (cm^{-1})	Assignment
800	CH_2-S group
850	Typical signals of MWCNT
1100	Si–O–C stretching vibration
1153	Si–O–C stretching vibration
1346	Carboxyl group (-COOH)
1576	Typical signals of MWCNT (−C=C)
1680	Quinone and carboxylate groups exist in these oxidized MWCNT
2919	C–H stretching vibration
3442	O–H stretching vibration

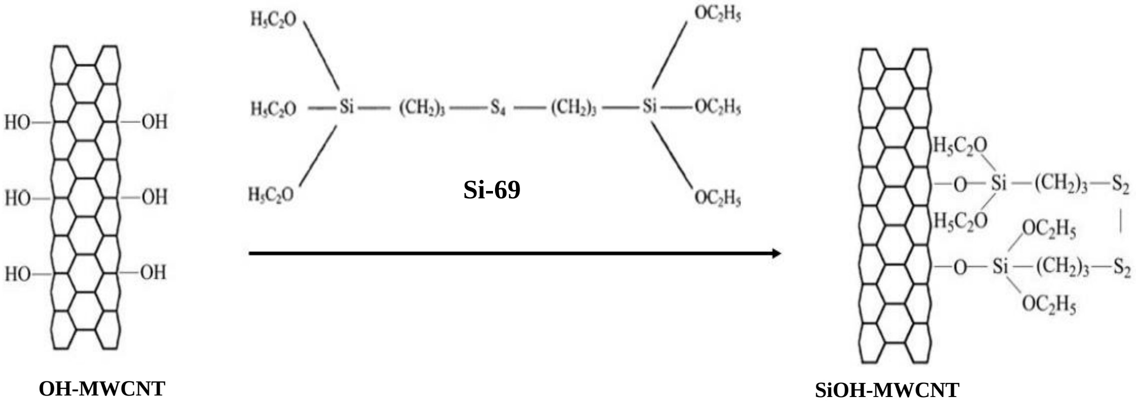

Figure 5.63 The proposed mechanism of OH-MWCNT functionalized with Si-69 [95].

Table 5.7 Grafting index of SiOH-MWCNT at various Si-69 concentrations.

Si-69 concentration (%w/v)	Grafting index
2	1.63±0.05
4	2.10±0.01
6	2.12±0.03

5.3.2 Mechanical properties and dichroic ratio

It can be seen in Figure 5.64 that hardness of the blend containing SiOH-MWCNT is the highest followed by that of the blends containing OH-MWCNT and MWCNT, respectively. This may be because SiOH-MWCNT gives the highest interaction with rubber. Additionally, Figure 5.65 shows that the blend containing SiOH-MWCNT exhibit the higher torque difference than the other blends. These results indicate that the blend containing SiOH-MWCNT has the highest crosslink density. This is thought to be because the unreacted Si-69 may not be totally washed off and thus it can involve in the S-vulcanization reaction leading to the higher crosslink density of the blend containing SiOH-MWCNT relative to other blends. Therefore, its higher crosslink density compared to the other blends can also be another reason for its highest hardness. In addition, 300% modulus and tensile strength of the 50/50 NR/NBR vulcanizates containing MWCNT, OH-MWCNT and OH-

MWCNT 4 phr are depicted in Figures 5.66-5.67, respectively. The effect of milling direction on their tensile properties and tear strength is also compared. It is observed that modulus and tensile strength of all blends in MD are higher than those of TD. These results indicate that most of the MWCNTs aligns in MD so they can assist the rubbers to bear the load. The alignment of the majority of MWCNTs in MD is confirmed by the dichroic ratio results illustrated in Figure 5.68. Moreover, modulus and tensile strength of the blend containing SiOH-MWCNT in both MD and TD are the highest followed by those of the blends containing OH-MWCNT and MWCNT, respectively. For example, tensile strength of the blends containing SiOH-MWCNT and OH-MWCNT in MD is, respectively, 1.2 and 1.04 times higher than that of the corresponding blend containing MWCNT. In addition, tensile strength of the blend containing SiOH-MWCNT in MD and TD is respectively 1.12 and 1.14 times higher than that of the corresponding sample containing OH-MWCNT. The highest modulus and tensile strength of the blend containing SiOH-MWCNT could be explained by the improvement of rubber-filler interaction between the SiOH-MWCNT and rubber matrices. This brings about higher stress transfer ability in the NR/NBR blend. The possible mechanism of interaction between SiOH-MWCNT and NR is shown in Figure 5.69 [95]. As can be seen, the chemical interaction can take place between the double bond of NR and sulfur in Si-69. Another explanation is given to the higher crosslink density of blend containing SiOH-MWCNT compared to the others as discussed previously. In addition, a slightly higher tensile strength of the blend containing OH-MWCNT relative to that of the blend containing MWCNT is caused by the higher reinforcing efficiency of OH-MWCNT in the NBR phase. This is because hydroxyl group of OH-MWCNT can interact with acrylonitrile group of NBR [114]. It can be seen in Figure 5.70 that elongation at break of each blend in both MD and TD is similar and elongation at break of all blends is also similar. Furthermore, it can be seen in Figure 5.71 that tear strength of all blends in MD is higher than that of the corresponding samples in TD. This is because MWCNTs in the MD aligned perpendicular to the crack front can obstruct the crack propagation, thus resulting in the higher tear strength [106]. However, the blend containing SiOH-MWCNT gives the highest tear strength followed by the blends containing OH-MWCNT and MWCNT. This can also be attributed to the higher rubber-filler interaction and higher crosslink density of blend containing SiOH-MWCNT compared to the others as discussed earlier.

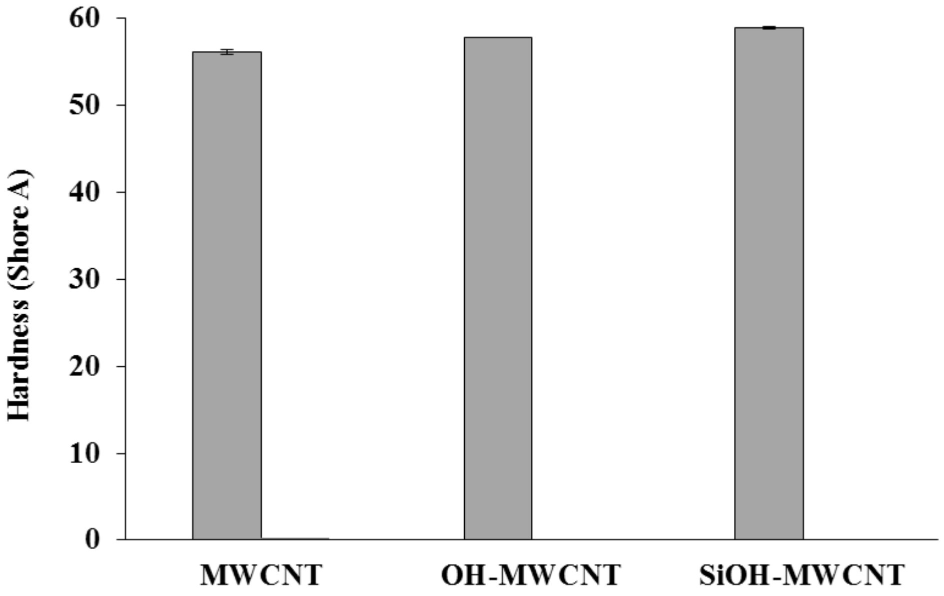

Figure 5.64 Hardness of the 50/50 NR/NBR blends containing MWCNT, OH-MWCNT and SiOH-MWCNT.

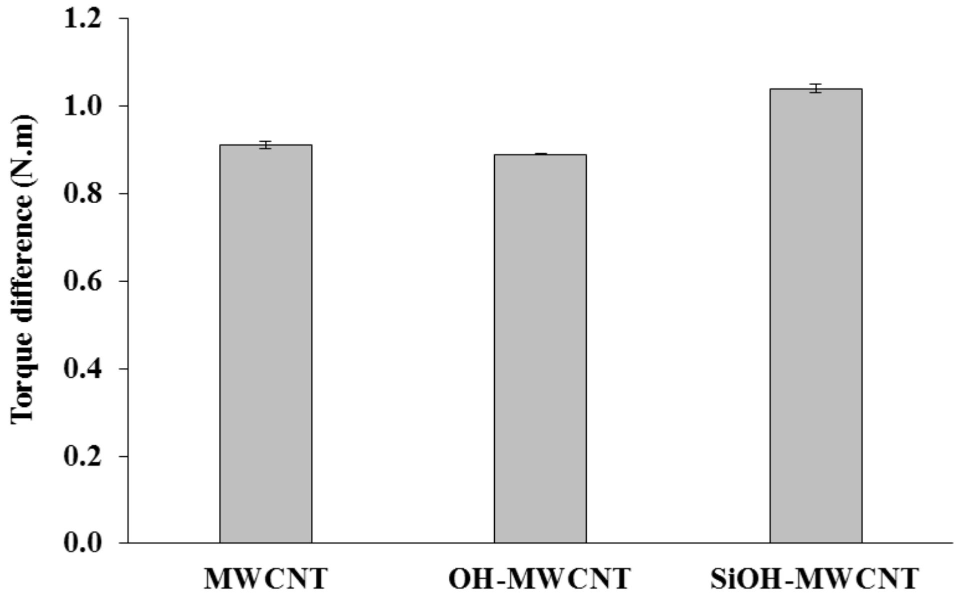

Figure 5.65 Torque difference of the 50/50 NR/NBR blends containing MWCNT, OH-MWCNT and SiOH-MWCNT.

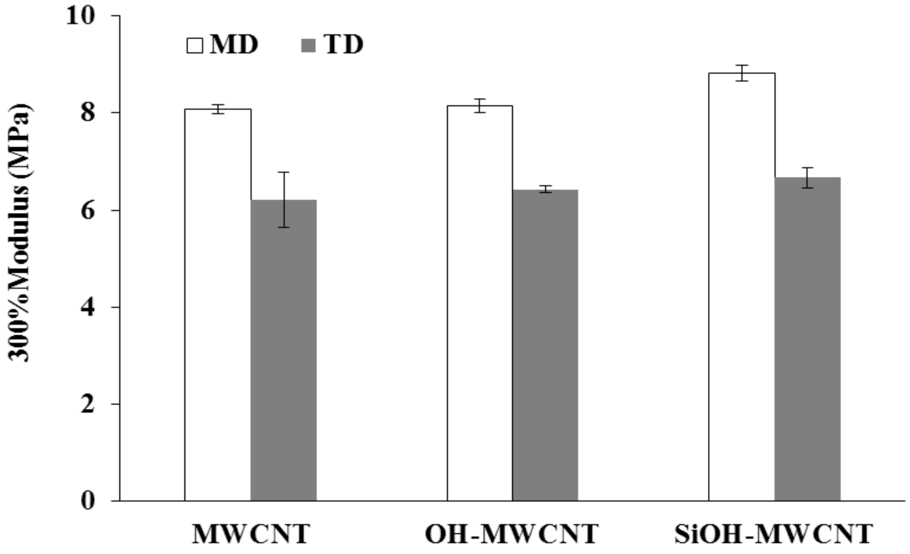

Figure 5.66 300%Modulus of the 50/50 NR/NBR blends containing MWCNT, OH-MWCNT and SiOH-MWCNT.

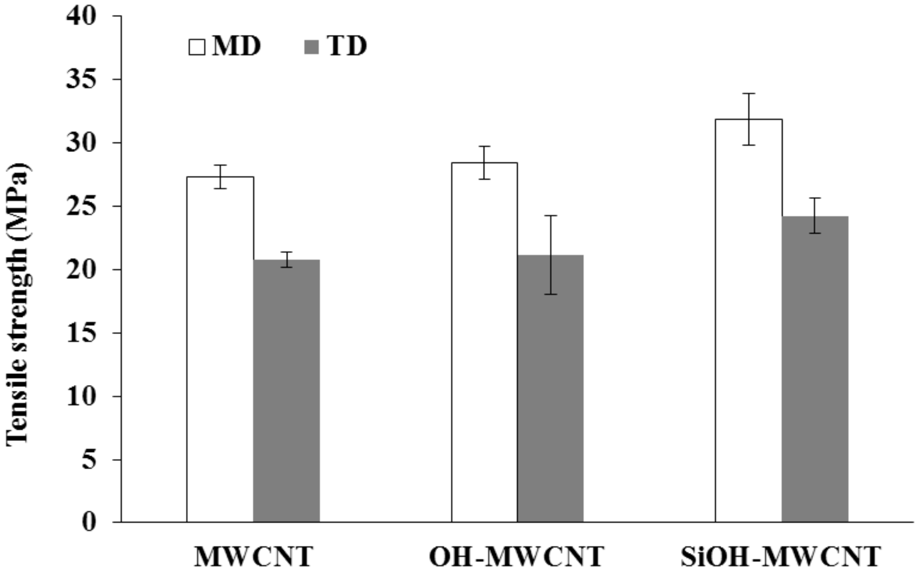

Figure 5.67 Tensile strength of the 50/50 NR/NBR blends containing MWCNT, OH-MWCNT and SiOH-MWCNT.

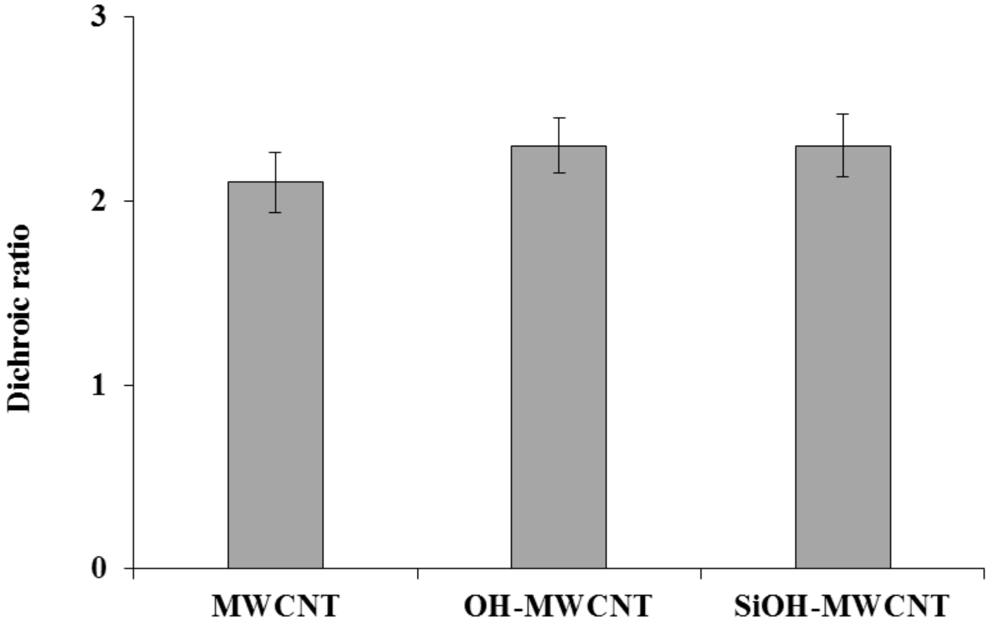

Figure 5.68 Dichroic ratio of the 50/50 NR/NBR blends containing MWCNT, OH-MWCNT and SiOH-MWCNT.

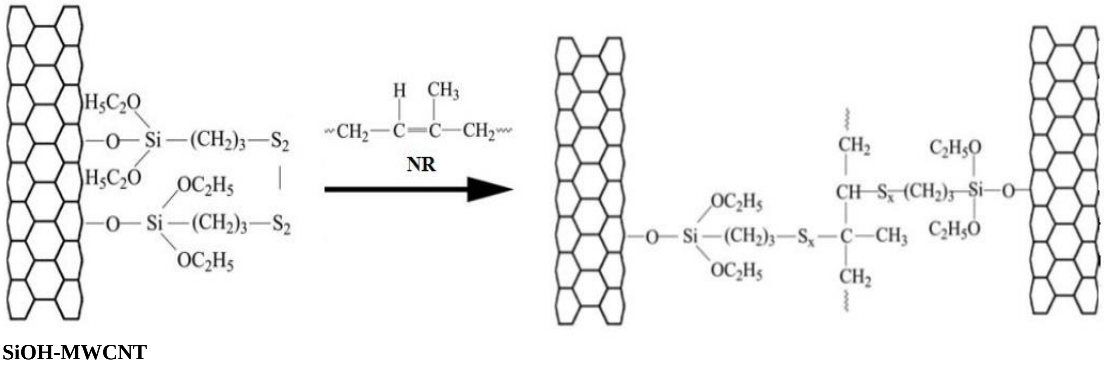

Figure 5.69 Probable mechanism of interaction between NR and the SiOH-MWCNT surface [95].

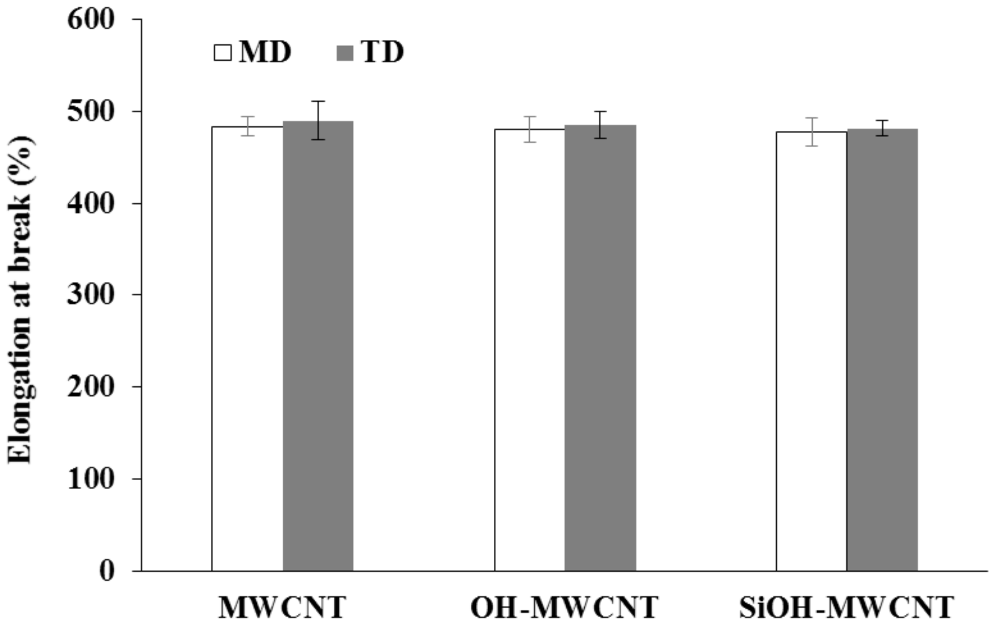

Figure 5.70 Elongation at break of the 50/50 NR/NBR blends containing MWCNT, OH-MWCNT and SiOH-MWCNT.

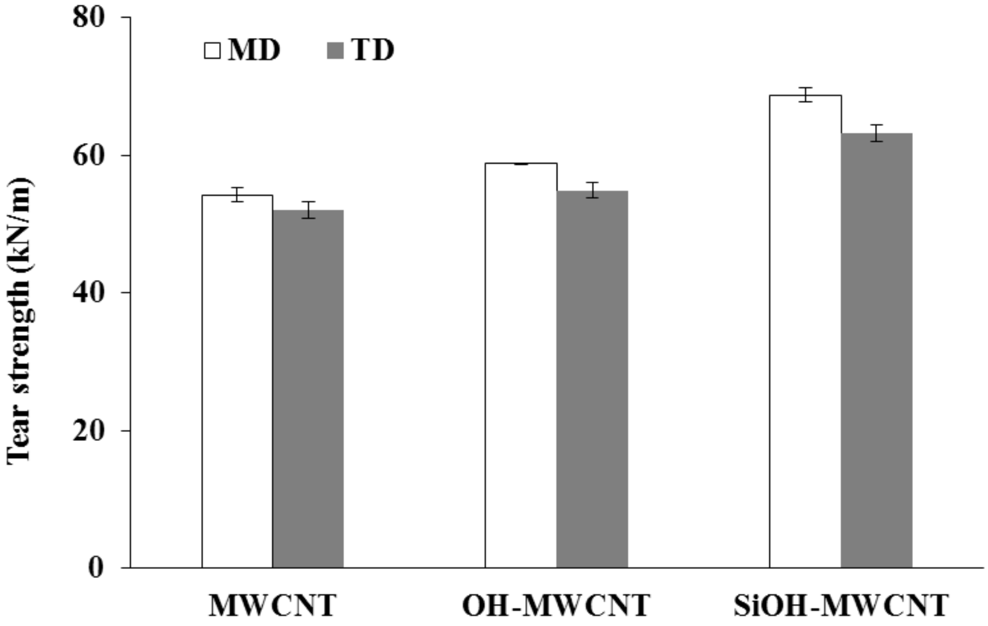

Figure 5.71 Tear strength of the 50/50 NR/NBR blends containing MWCNT, OH-MWCNT and SiOH-MWCNT.

Figure 5.72 displays abrasion loss of the 50/50 NR/NBR blends containing MWCNT, OH-MWCNT and SiOH-MWCNT. It is also found that the blend containing SiOH-MWCNT exhibits the highest abrasion resistance followed by the blends containing OH-MWCNT and MWCNT, respectively. The highest rubber-filler interaction and crosslink density of the blend containing SiOH-MWCNT could be also used to explain the obtained results. Additionally, the improvement of reinforcing efficiency of MWCNT in NBR phase may lead to the better abrasion resistance of the blend having OH-MWCNT relative to the blend having MWCNT. This is because there is interaction between hydroxyl group of OH-MWCNT and acrylonitrile group of NBR.

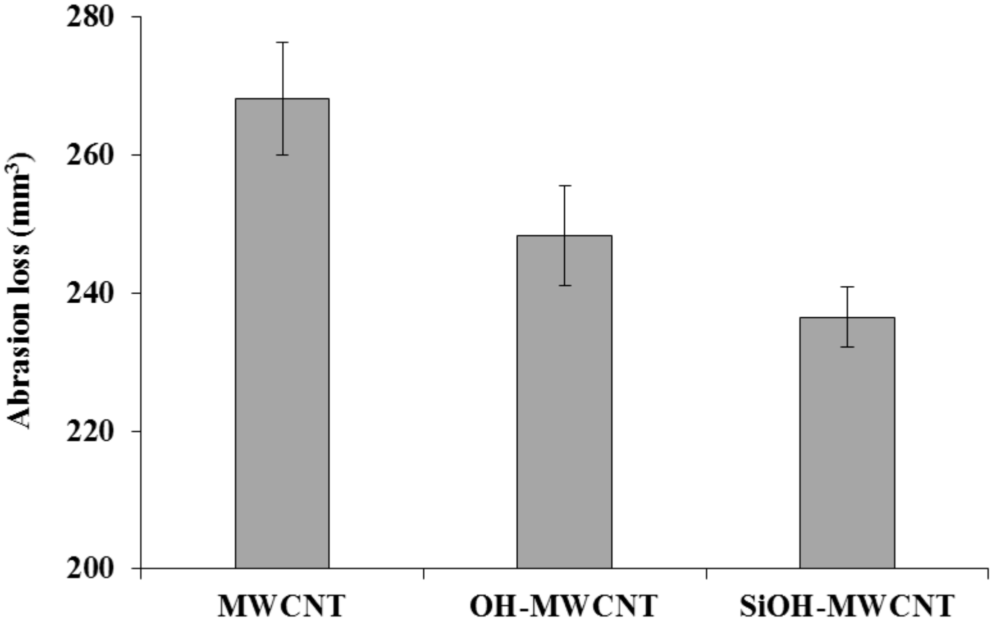

Figure 5.72 Abrasion loss of the 50/50 NR/NBR blends containing MWCNT, OH-MWCNT and SiOH-MWCNT.

5.3.3 Dynamic mechanical properties

As can be seen in the previous part, two peaks of tan δ belong to NR and NBR phases can be observed for the 50/50 NR/NBR blend. Therefore, Figure 5.73 shows tan δ_{max} of both NR and NBR phases in MD and TD of the 50/50 NR/NBR blends containing MWCNT, OH-MWCNT and SiOH-MWCNT. It is found that the blend containing SiOH-MWCNT exhibits the lowest tan δ_{max} value in both NR and NBR phases, regardless of the alignment direction. This could be explained by its highest filler-rubber interaction in both phases. Also, the highest crosslink density of the blend containing SiOH-MWCNT can be another reason for this finding as previously discussed in section 5.3.2. In addition, tan δ_{max} of the NBR phase for the blend containing OH-MWCNT is slightly lower than that for the blend containing MWCNT whereas that of their NR phases is rather similar. The lower tan δ_{max} value of the NBR phase for the blend having OH-MWCNT may be due to the improvement of rubber-filler interaction in the NBR phase. It is also observed that tan δ_{max} in the MD of both phases in all cases is lower than that in the TD. This is because the amount of

MWCNTs aligned in MD is more than that in TD as previously discussed in section 5.3.2.

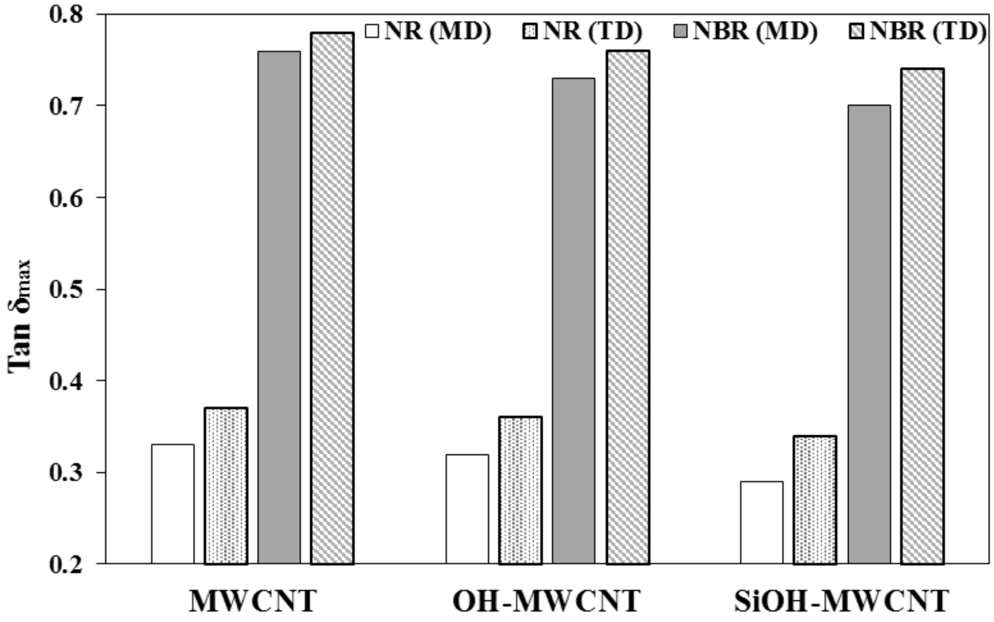

Figure 5.73 Tan δ_{max} in MD and TD of the 50/50 NR/NBR blends containing MWCNT, OH-MWCNT and SiOH-MWCNT.

Figure 5.74 shows the average storage modulus values at 30 °C of all blends. It appears that the storage modulus in MD of all blends is higher than that of their TD counterpart. This is attributed to the higher reinforcement efficiency of MWCNT aligned in the longitudinal direction. These results also agree well with their modulus. Moreover, it is found that the blend containing SiOH-MWCNT exhibits the highest storage modulus followed by that of the blends containing OH-MWCNT and MWCNT, respectively. This is again because there is the highest rubber-filler interaction the blend containing SiOH-MWCNT. Also, the highest crosslink density for the blend containing SiOH-MWCNT as verified by its highest torque difference (Figure 5.65) can be another possible explanation for the obtained result. Additionally, the hydroxyl group of OH-MWCNT can possibly interact with acrylonitrile group of the NBR leading to the slight higher storage modulus in both MD and TD of the blend containing OH-MWCNT relative to that of the blend containing MWCNT.

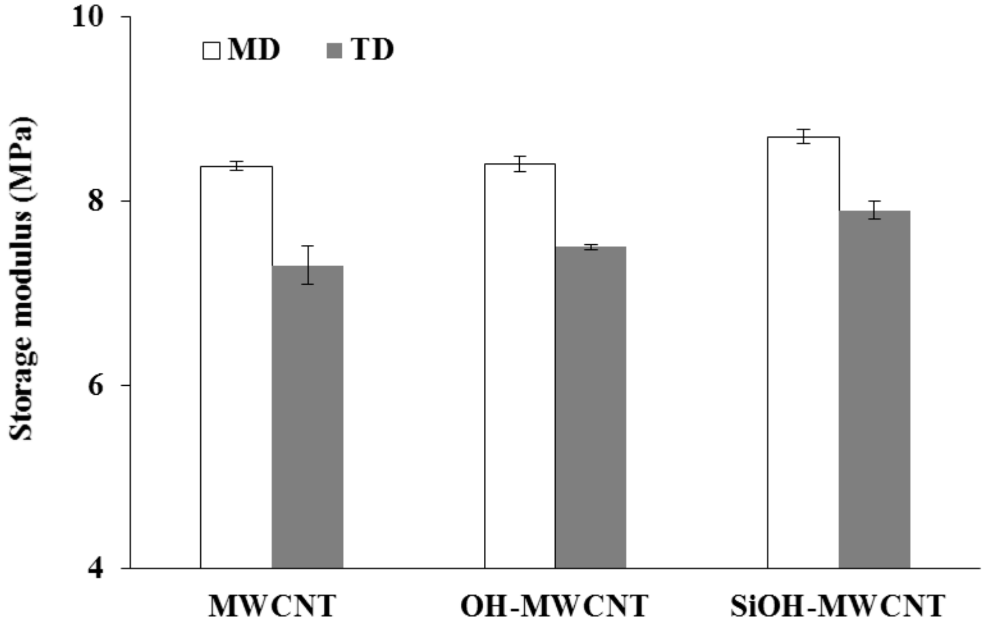

Figure 5.74 Storage modulus at 30 °C in MD and TD of the 50/50 NR/NBR blends containing MWCNT, OH-MWCNT and SiOH-MWCNT.

Heat build-up and dynamic compression set of the blends containing MWCNT, OH-MWCNT and SiOH-MWCNT are presented in Figures 5.75 and 5.76, respectively. It can be seen that the blend containing SiOH-MWCNT exhibits the lowest heat build-up and dynamic compression set followed by the blend containing OH-MWCNT and MWCNT, respectively. This is because SiOH-MWCNT can interact with NR and NBR via covalent bonding [95], thus leading to lowest energy dissipation and lowest hysteresis loss during applied dynamic force. Additionally, the higher crosslink density of the blend containing SiOH-MWCNT compared to the other blends can be another cause for this finding. The lower energy loss during the dynamic test found in the blend containing OH-MWCNT is due to the greater rubber-filler interaction of the MWCNTs presented in the NBR phase.

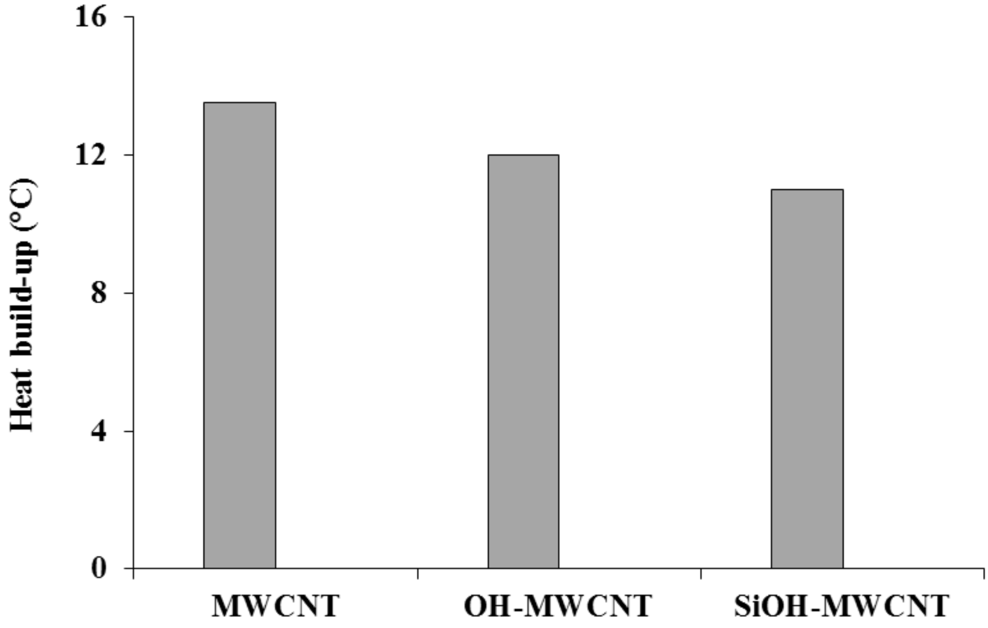

Figure 5.75 Heat build-up of the 50/50 NR/NBR blends containing MWCNT, OH-MWCNT and SiOH-MWCNT.

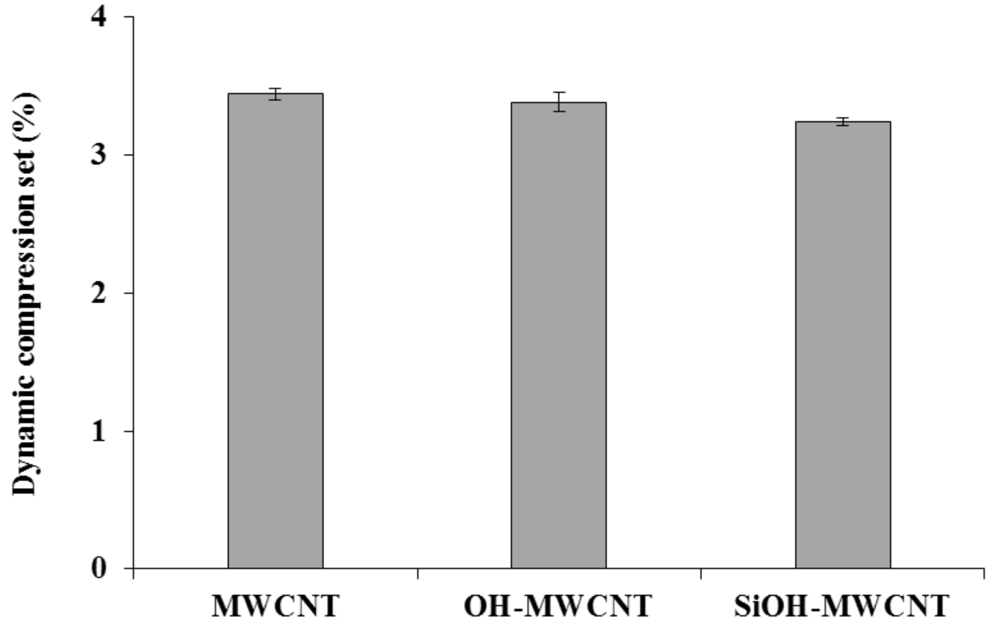

Figure 5.76 Dynamic compression set of the 50/50 NR/NBR blends containing MWCNT, OH-MWCNT and SiOH-MWCNT.

5.3.4 Electrical and thermal conductivities

Figure 5.77 displays electrical conductivity in MD and TD of the blends reinforcing with MWCNT, OH-MWCNT and SiOH-MWCNT. It can be seen that the electrical conductivity of all blends in a specific milling direction is not significantly different. Therefore, it can be stated that the modification of MWCNT surface does not affect the electrical conductivity of the blends. However, the electrical conductivity of all blends in the MD is clearly superior to that of their corresponding TD sample. The possible explanation is given by a greater number of aligned MWCNTs in MD sample relative to the TD sample. This leads to the enhancement of the formation of conductive networks and, thus electrons can flow through the formed MWCNT networks in the MD samples more than the TD samples.

Figure 5.78 depicts the thermal conductivity of all blends. It is found that the thermal conductivity of all blends is not significantly different. As can be seen, their thermal conductivity value is about 0.37 W/mK. This may be because all MWCNTs used in this study is MWCNT having many layers of the rolled-up graphene sheets but the modification occurs only at the outmost layer of their surfaces. Thus, their thermal conductivity may not be affected by surface modification used in this experiment. In addition, it has been reported that the thermal conductivity of the blend is mainly controlled by the degree of MWCNT alignment [16, 115]. However, the degree of MWCNT alignment in all blends is not significantly different as previously presented in Figure 5.68. Therefore, this can be another reason for the similar thermal conductivity of the blends reinforcing with MWCNT, OH-MWCNT and SiOH-MWCNT.

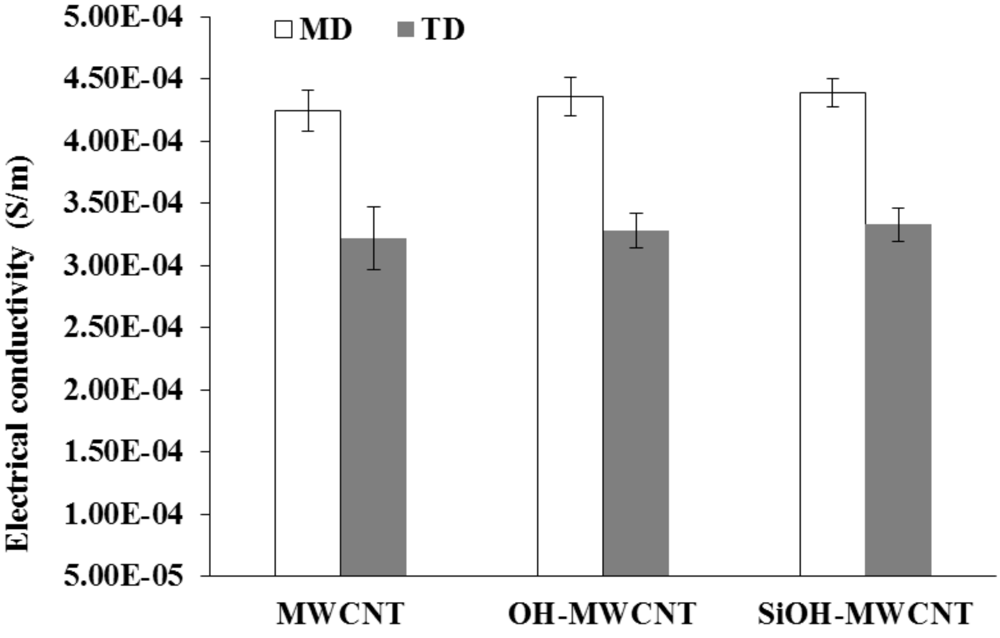

Figure 5.77 Electrical conductivity of the 50/50 NR/NBR blends containing MWCNT, OH-MWCNT and SiOH-MWCNT.

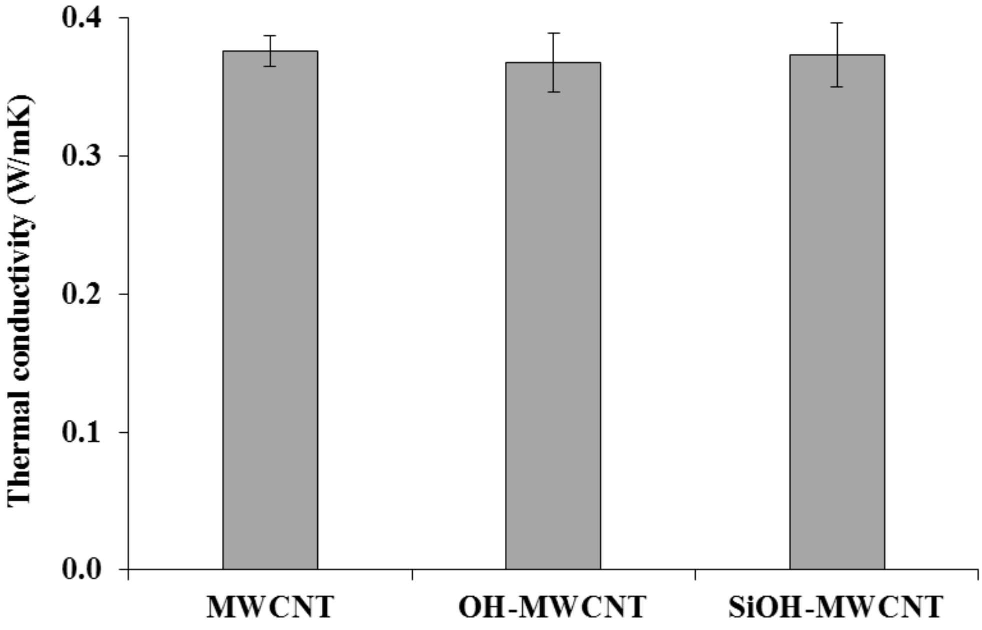

Figure 5.78 Thermal conductivity of the 50/50 NR/NBR blends containing MWCNT, OH-MWCNT and SiOH-MWCNT.

5.3.5 Oil resistance

The swelling ratio in the gasohol and hydraulic oil of the blends having MWCNT, OH-MWCNT and SiOH-MWCNT is depicted in Figures 5.79. It is found that the blend containing SiOH-MWCNT exhibit the lowest swelling ratio in both gasohol and hydraulic oils. This is again due to the greater rubber-filler interaction and higher crosslink density of the blend containing SiOH-MWCNT compared to the other blends. In addition, the swelling ratio of the blend containing OH-MWCNT is slightly lower than that of the blend containing MWCNT. Again, the improvement of rubber-filler interaction in NBR phase could be used to explain this result. Additionally, it is apparent that the swelling ratio of all blends in the gasohol is higher than that of their corresponding samples in the hydraulic oil. This is because the solubility parameter of the 50/50 NR/NBR blend used in this work is closer to that of the gasohol having higher polarity than the hydraulic oil.

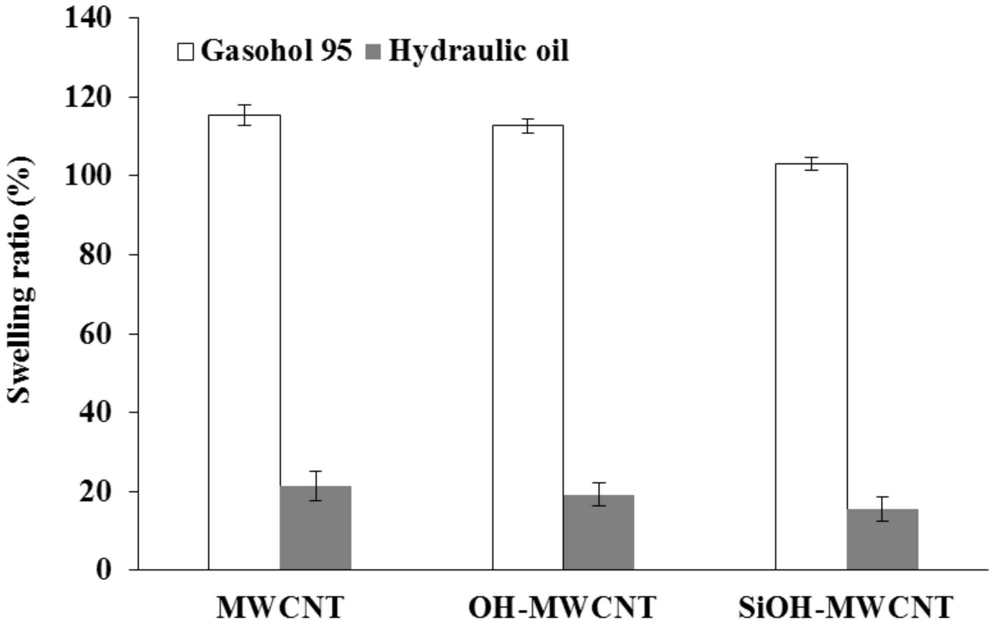

Figure 5.79 Swelling ratio in the gasohol and hydraulic oils of the 50/50 NR/NBR blends containing MWCNT, OH-MWCNT and SiOH-MWCNT.

CHAPTER VI

CONCLUSIONS

From the results of the present study, it can be summarized as follows

1. Well-dispersed MWCNT in 50/50 NR/NBR blend can be prepared by mixing NBR with MWCNT/NR masterbatch prepared from the predispersing method when the amount of MWCNT in the blends is not more than 4 phr.

2. The 50/50 NR/NBR blends prepared by mixing NBR with MWCNT/NR masterbatch prepared from the predispersing method (the P blends) exhibit better mechanical, dynamic, electrical and thermal properties than the corresponding blends prepared from the conventional method (the C blends).

3. Modulus, storage modulus at 30 ºC, tensile strength, tear strength and electrical conductivity of the P and C blends in MD are higher than those of the corresponding TD samples.

4. The difference of the modulus, storage modulus at 30 ºC, tensile strength, tear strength and electrical conductivity of the P blend in MD and TD is greatest when 4 phr MWCNT is loaded, corresponding to the highest dichroic ratio.

5. When MWCNT content in the P blend is more than 4 phr, the increase of MWCNT agglomerates and reduction of dichroic ratio are observed. This leads to the reduction of mechanical properties while the electrical conductivity remains almost constant.

6. Electrical conductivity of 4 phr MWCNT-filled P blend in MD markedly decreases with increasing extension ratio while that of the corresponding TD sample slightly increases. This is because of the greater number of aligned MWCNTs in MD sample relative to the TD sample.

7. Modulus, tensile strength, tear strength, oil resistance, abrasion resistance, thermal and electrical properties of the mNR blends are clearly greater than those of the corresponding mNBR blends. This is due to the combination effect of the

better MWCNT distribution in each phase and higher reinforcement efficiency in the NR phase.

8. 100% modulus, storage modulus at 30 ºC, tensile strength, tear strength and electrical conductivity of both mNR and mNBR blends in MD are higher than those of their corresponding TD samples.

9. 50/50 mNR blend exhibits the better overall properties because of the better balance of MWCNT distribution between the NR and NBR phases.

10. Modulus, tensile strength, tear strength and oil resistance of the 50/50 NR/NBR blend containing SiOH-MWCNT are greater than those of the blends containing OH-MWCNT and MWCNT. The explanation is given to the higher rubber-filler interaction and crosslink density of the blend containing SiOH-MWCNT compared to those of the other blends.

11. Modification of MWCNT surface with Si-69 does not affect the electrical and thermal conductivities of the 50/50 NR/NBR blend.

REFERENCES

1. Chan YP. Cure characteristics and dynamic mechanical properties of acrylic rubber and epoxidized natural rubber blend. J Ind Eng Chem 2001; 7: 212-217.
2. El-Sabbagh SH, Hussain AI, El-Ghaffar MA. Utilisation of maleic anhydride and epoxidised soyabean oil as compatibilisers for NBR/EPDM blends reinforced with modified and unmodified polypropylene fibres. Pigm Resin Technol 2005; 34: 203-217.
3. Ismail MN, El-Sabbagh SH, Yehia AA. Fatigue and mechanical properties of NR/SBR and NR/NBR Blend vulcanizates. J Elastom Plast 1999; 31: 255-270.
4. Saad AL, El-Sabbagh SH. Compatibility studies on some polymer blend systems by electrical and mechanical techniques. J Appl Polym Sci 2001; 79: 60–71.
5. Rajasekar R, Pal K, Heinrich G, Das A, Das CK. Development of nitrile butadiene rubber-nanoclay composites with epoxidized natural rubber as compatibilizer. Mater Design 2009; 30: 3839–3845.
6. Hashim AS, Azahari B, Ikelda Y, Kohjiya S. The Effect of Bis (3-triethoxy silylpropyl) tetrasulfide on silica reinforcement of styrene-butadiene rubber. Rubber Chem Technol 1998; 71: 289-299.
7. Xie XL, Mai YW, Ping X. Dispersion and alignment of carbon nanotubes in polymer matrix: A review. Mater Sci Eng 2005; 49: 89-112.
8. Coleman JN, Khan U, Blau WJ, Gun'ko YK. Small but strong: A review of the mechanical properties of carbon nanotube–polymer composites. Carbon 2006; 44: 1624–1652.
9. Shanmugharaj AM, Bae JH, Lee KY, Noh WH, Lee SH, Ryu SH. Physical and chemical characteristics of multi-walled carbon nanotubes functionalized with aminosilane and its influence on the properties of natural rubber composites. Compos Sci Technol 2007; 67: 1813–1822.

10. Kueseng K, Jacob KI. Natural rubber nanocomposites with SiC nanoparticles and carbon nanotubes. Eur Polym J 2006; 42: 220–227.

11. Lopez-Manchado MA, Biagiotti J, Valentini L, Kenny JM. Dynamic mechanical and raman spectroscopy studies on interaction between single-walled carbon nanotubes and natural rubber. J Appl Polym Sci 2004; 92: 3394–3400.

12. Liu CH, Huang H, Wu Y, Fan SS. Thermal conductivity improvement of silicone elastomer with carbon nanotube loading. J Appl Phys 2004; 84: 4248-4250.

13. Aguilar JO, Bautista-Quijano JR, Avilés F. Influence of carbon nanotube clustering on the electrical conductivity of polymer composite films. Express Polym. Lett 2010; 4: 292-299.

14. Kader MA, Choi D, Lee SK, Nah C. Morphology of conducting filler-reinforced nitrile rubber composites by electrostatic force microscopy. Polym Test 2005; 24: 363–366.

15. Knite M, Tupureina V, Fuith A, Zavickis J, Teteris V. Polyisoprene-multi wall carbon nanotube composites for sensing strain, Mater Sci Eng C 2007; 27: 1125–1128.

16. Das A, Stöckelhuber KW, Jurk R, Saphiannikova M, Fritzsche J, Lorenz H, Klüppel M, Heinrich G. Modified and unmodified multiwalled carbon nanotubes in high performance solution-styrene-butadiene and butadiene rubber blends. Polymer 2008; 49: 5276-528.

17. Lan L, Yinghao Z, Yong Z, Christopher O, Sharon G. Reinforcement of hydrogenated carboxylated nitrile–butadiene rubber by multi-walled carbon nanotubes. Appl Surf Sci 2008; 255: 2162–2166.

18. Lorenz H., Fritzsche J, Das A, Stockelhuber KW, Jurk R, Heinrich G, Kluppel M. Advanced elastomer nano-composites based on CNT-hybrid filler systems. Compos Sci Technol 2009; 69: 2135–2143.

19. Xiao KQ, Zhang LC. The stress transfer efficiency of a single-walled carbon nanotube in epoxy matrix. J Mater Sci 2004; 39: 4481–4486.

20. Hill DE, Lin Y, Rao AM, Allard LF, Sun YP. Functionalization of carbon nanotubes with polystyrene. Macromolecules 2002; 35: 9466–9471.

21. Velasco-Santos C, Martínez-Hernández AL, Lozada-Cassou M, Alvarez-Castillo A, Castaño VM. Chemical functionalization of carbon nanotubes through an Organosilane. Nanotechnology 2002; 13: 495–498.

22. Vast L, Philippin G, Destree A, Moreau N, Fonseca A, Nagy JB. Chemical functionalization by a fluorinated trichlorosilane of multi-walled carbon nanotubes. Nanotechnology 2004; 15: 781–785.

23. Buryachenko VA, Roy A. Effective elastic moduli of nanocomposites with prescribed random orientation of nanofibers. Compos Part B 2005; 36: 405–416.

24. Coleman JN, Cadek M, Ryan KP, Fonseca A, Nagy JB, Blau WJ. Reinforcement of polymers with carbon nanotubes. The role of an ordered polymer interfacial region. Experiment and modeling. Polymer 2006; 47: 8556–8561.

25. Thostenson ET, Chou T.W. Aligned multi-walled carbon nanotube-reinforced composites: processing and mechanical characterization. J Phys D Appl Phys 2002; 35: 77–80.

26. Koyama T, Steinbuchel A. Biopolymers: Polyisoprenoids. Weinheim: WILEY-VCH Verleg GmbH; 2001.

27. Kovuttikulrangsie S, Sakdapipanich J. The molecular weight and molecular weight dristribution of NR from different age and clone Hevea trees. Songklanakarin J Sci Technol 2005; 27: 337-342.

28. Hofmann W. Rubber Technology Handbook, Hanser Publisher, 1989.

29. Poompradub S, Tosaka M, Kohjiya S, Ikeda Y, Toki S, Sics I, Hsiao BS. Mechanical of strain-induced crystallization in filled and unfilled natural rubber vulcanizates. J Appl Phys 2005; 97: 1-9.

30. Chapman AV. 24th International H.F. Mark-Symposium, Vienna, 2007.

31. Black EJ, Mccall EB. Relationships between the structures of natural rubber vulcanizates and their thermal and oxidative aging. Rubber Chem Technol 1970; 43: 651-663.

32. Kader MA, Choi D, Lee SK, Nah C. Morphology of conducting filler-reinforced nitrile rubber composites by electrostatic force microscopy. Polym Test 2005; 24: 363-366.

33. Fuith A, Reinecker M, Sanchez-Ferrer A, Mezzenga R, Mrzel A, Knite M, Aulika I, Dunce M, Schranz W. Dynamic- and thermo- mechanical Analysis of inorganic Nanotubes/Elastomer Composites, Sensors & Transducers J 2011; 12: 71-79

34. Nagdi K. Rubber as an engineering material: Guideline for user. New York: Henser Plublishers; 1993.

35. Roberts AD. Natural Rubber Science and Technology. Oxford: Oxford University Press; 1988.

36. http://global.britannica.com/EBchecked/topic/416122/nitrile-rubber-NBR

37. Sau KP, Chaki TK, Khastgir D. Carbon fibre filled conductive composites based on nitrile rubber NBR), ethylene propylene diene rubber (EPDM) and their blend. Polymer 1998; 39(25): 6461-6471.

38. http://en.wikipedia.org/wiki/Nitrile_rubber

39. Tinker AJ, Jones KP. Blends of Natural Rubber-Novel Techniques for Blending with Specific Polymers. London: Chapman & Hill; 1998.

40. Manson JA, Sperling LH. Polymer Blends and Composites. New York: Plenum Press; 1976.

41. Mangaraj D. Elastomer blends. Rubber Chem Technol 2002; 75: 365-427.

42. Ali Z, Le HH, Ilisch S, Thurn-Albrecht T, Radusch H-J. Morphology development and compatibilization effect in nanoclay filled rubber blends. Polymer 2010, 51: 4580-4588.

43. Sirisinha C, Limcharoen S, Thunyarittikorn J. Oil resistance controlled by phase morphology in natural rubber/nitrile rubber blends. J Appl Polym Sci 2003; 87: 83-89.

44. Botrose SH. Preparation and characteristics of NR/EPDM rubber blends. Polym-Plast Technol Eng 2002; 41: 341-359.

45. Sae-oui P, Sirisinha C, Hatthapanit K. Effect of blend ratio on aging, oil and ozone resistance of silica-filled chloroprene rubber/natural rubber (CR/NR) blends. Exp Polym Lett 2007; 1: 8-14.

46. Varkey JT, Augustine S, Thomas S. Thermal degradation of natural rubber/styrene butadiene rubber latex blends by thermogravimetric method. Polym Plast Technol Eng 2000; 39: 415-435.

47. Le HH, Owald K, Ilisch S, Pham T, Stockelhuber KW, Heinrich G, Radusch H-J. Silica transfer in ternary rubber blends: calculation and experimental determination. macromol Mater Eng 2012; 297: 464–473.

48. Edirisinghe D, Freakley PK. Effect of varied carbon black distribution on the morphology and properties of blends of natural and nitrile rubber. J. Rubb. Res. Inst., Sri Lanka. 2003, 86, 58-79.

49. Collan JE, Hess WM, Scott CE. Elastomer blends. Compatibility and relative response to fillers. Rubber Chem Technol 1971; 44: 814-837.

50. Zerda TW, Song G, Waddell WH. Distribution of elastomers and silica in polymer blends characterized by Raman microimaging technique. Rubber Chem Tech 2003; 76:. 769-778.

51. Meier G, Klu¨ppel M, Geisler H, Schuster RH. Control of the mixing state and the material properties of silica filled elastomer blends by master batch technology. Kautsch Gummi Kunst 2005; 58: 587-594.

52. Sirisinha C, Prayoonchatphan N. Study of carbon black distribution in BR/NBR blends based on damping properties: Influences of carbon black particle size, filler, and rubber polarity. J Appl Polym Sci 2001; 13: 3198–3203.

53. Maiti S, De SK, Bhowmick AK. Quantitative estimation of filler distribution in immiscible rubber blends by mechanical damping studied. Rubber Chem Technol 1992; 65: 293-302.

54. Phewphong P, Saeoui P, Sirisinha C. The use of dynamic mechanical thermal analysis technique for determining an uneven distribution of precipitated silica in CPE/NR blends. Polym Test 2008; 27: 873-880.

55. Fred I-H. Review of vulcanization chemistry. Rubber World 1999; 220: 24-30.

56. Hills DA. Heat transfer and vulcanization of rubber. London: Applied Science Publishers Ltd.; 1971.

57. Gardiner JR. Curative diffusion between dissimilar elastomers and its influence on adhesion. Rubber Chem Technol 1968; 41: 1312-1328.

58. Collan JE, Hess WM, Scott CE. Elastomer blends. Compatibility and relative response to fillers. Rubber Chem Technol 1971; 44: 814-837.
59. Morton M. Rubber Technology. New York: Van Nostrand Plublisher; 1973.
60. Roychoudhury A, De PP. Elastomer-carbon black interaction: Influence of elastomer chemical structure and carbon black surface chemistry on the bound rubber formation. J Appl Polym Sci 1995; 55: 9-15.
61. Nuguy N, Erman B. Property optimization in nitrile rubber composites via hybrid filler systems. J Appl Polym Sci 2001; 85: 2301-2316.
62. Mahapatra D, Arun B, Revathi P. Performance evaluation of high structure carbon black in different polymer blends. Rubber World 2004; 231: 33-42.
63. http://rtvanderbilt.com/FillersIntroWeb.pdf
64. http://en.wikipedia.org/wiki/Carbon_nanotube
65. McEuen PL, Fuhrer MS, Park HK. Single-walled carbon nanotube electronics, IEEE Trans. Nanotechnol 2002; 1: 78–85.
66. Prasek J, Drbohlavova J, Chomoucka J, Hubalek J, Jasek O, Adamc V, Kizek R. Methods for carbon nanotubes synthesis—review. J Mater Chem 2011; 21: 15872-15884.
67. http://en.wikipedia.org/wiki/Carbon_nanotube
68. Schaffer JP, Saxena A, Antolovich SD, Thomas J, Sanders H, Warner SB. The science and design of engeering materials: McGraw-Hill; 1999.
69. Callister W D. Material Science and Engineering: An Introduction. New York: John wiley and Sons, Inc; 2000.
70. Eitan A, Fisher FT, Andrews R, Brinson LC, Schadler LS. Reinforcement mechanisms in MWCNT-filled polycarbonate. Compos Sci Technol 2006; 66: 1159–1170.
71. Mittal V. Polymer Nanotube Nanocomposites: Synthesis, properties, and applications. Scrivener Publishing LLC; 2010.
72. http://en.wikipedia.org/wiki/Stone%E2%80%93Wales_defect
73. Avouris P. Carbon nanotube electronics. Chemical Physics 2002; 281: 429-445.
74. Baughman RH, Zakhidov AA, De Heer WA. Carbon nanotubes - the route toward applications. Science 2002; 297: 787.

75. Shaffer M, Sandler J. Carbon nanotube/nanofibre polymer composites. In: Advani SG, editor. Processing and properties of nanocomposites. World Scientific Publishing Company; 2006.

76. Niyogi, S, Hamon MA, Perea DE, Kang CB, Zhao B, Pal SK, Wyant AE, Itkis M. E, Haddon RC. Ultrasonic dispersions of single-walled carbon nanotubes. J Phys Chem B 2003; 107: 8799-8804.

77. Hilding J, Grulke EA, Zhang ZG, Lockwood F. Dispersion of carbon nanotubes in liquids. J Dispersion Sci Technol 2003; 24: 1-41.

78. Lu KL. Mechanical damage of carbon nanotubes by ultrasound. Carbon 1996; 34: 814-816.

79. Matarredonna O, Rhoads H, Li Z, Harwell JH, Balzano L, Resasco E. Disperison of single-walled carbon nanotubes in aqueous solutions of the anionic surfactant NaDDBS. J Phys Chem B 2003; 107: 13357-13367.

80. Shvartzman-Choen R, Levi-Kalishman Y, Nativ-Roth E, Yerushalmi-Rozen, R. Generic approach for dispersing single-walled carbon nanotubes: The strength of a weak interaction. Langmuir 2004; 20: 6085-6088.

81. Shvartzman-Cohen R, Nativ-Roth E, Baskaran E, Levi-Kalishman Y, Szleifer I, Yerushalmi-Rozen R. Selective dispersion of single-walled carbon nanotubes in the presence of polymers: the role of molecular and colloidal length scales. J Am Chem Soc 2004; 126: 14850-14857.

82. Moore VC, Strano MS, Haroz EH, Hauge RH, Smalley RE. Individually suspended single-walled carbon nanotubes in various surfactants. Nano Letters 2003; 3: 1379–1382.

83. Duro R, Souto C, Gomez-Amoza JL, Martinez-Pacheco R, Concheiro A. Interfacial adsorption of polymers and surfactants: implications for the propertiesof disperse systems of pharmaceutical interest. Drug Development and Industrial Pharmacy 1999; 25: 817-829.

84. Villmow T, Pötschke P, Pegel S, Häussler L, Kretzschmar B. Influence of twin-screw extrusion conditions on the dispersion of multi-walled carbon nanotubes in a poly(lactic acid) matrix. Polymer 2008; 49(16): 3500-3509.

85. Yue D, Liu Y, Shen Z, Zhang L. Study on preparation and properties of carbon nanotubes/rubber composites. J Mater Sci 2006; 41: 2541-2544.

86. Kim YA, Hayashi T, Endo M, Gotoh Y, Wada N, Seiyama J. Fabrication of aligned carbon nanotube-filled rubber composite. Scripta Mater 2006; 54(1): 31-35.

87. Sharma A, Tripathi B, Vijay YK. Dramatic improvement in properties of magnetically aligned MWCNT/polymer nanocomposites. J Membr Sci 2010; 361: 89-95.

88. Chae HG, Minus ML, Kumar S, Oriented and exfoliated single wall carbon nanotubes in polyacrylonitrile. Polymer 2006; 47: 3494-3504.

89. Kim GM, Michler GH, Poetschke P, Deformation processes of ultrahigh porous multiwalled carbon nanotubes/polycarbonate composite fibers prepared by electrospinning. Polymer 2005; 46:7346-7351.

90. Ci L., Suhr J, Pushparaj V,| Zhang X, Ajayan PM. Continuous carbon nanotube reinforced composites. Nano Lett 2008; 8: 2762-2766.

91. Dalton AB, Collins S, Razal J, Munoz E, Ebron VH, Kim BG, Coleman JN, Ferraris JP, Baughman RH. Continuous carbon nanotube composite fibers: properties, potential applications, and problems. J Mater Chem. 2004. 14:1-3.

92. Kumar S, Dang TD, Arnold FE, Bhattacharyya AR, Min BG, Zhang X, Vaia RA, Park C, Adams WW, Hauge RH, Smalley RE, Ramesh S, Willis PA. Synthesis, Structure, and Properties of PBO/SWNT Composites. Macromolecules, 2002. 35: 9039-9043.

93. Nah C, Lim JY, Sengupta R, Cho BH, Gent AN. Slipping of carbon nanotubes in a rubber matrix. Polym. Int 2010; 60: 42-44.

94. Feng C, Zhang H, Zhang Y. Nonlinear Viscoelasticity and Stress-Softening Behavior of Chloroprene Rubber Reinforced by Multiwalled Carbon Nanotubes. Polym Compos 2014; 10: 1-9.

95. Jiang HX, Ni QQ, Natsuki T. Design and evaluation of the interface between carbon nanotubes and natural rubber. Polym Compos 2010; 32: 2:236-242.

96. Kim Y, Minami N, Zhu WH, Kazaoui S, Azumi R, Matsumoto M. Langmuir-Blodgett films of single-wall carbon nanotubes: layer-by-layer deposition and in-plane orientation of tubes. Jpn J Appl Phys 2003; 42: 7629-7634.

97. Dresselhaus MS, Dresselhaus G, Saito R, Jorio A. Raman spectroscopy of carbon nanotubes. Phys Rep 2005; 409: 47-99.

98. Schroder DK. Semiconductor material and device characterization. John Wiley & Sons, Inc; 2006.

99. Choi S-S, Hwang K-J, Kim B-T. Influence of bound polymer on cure characteristics of natural rubber compounds reinforced with different types of carbon blacks. J Appl Polym Sci 2005; 98(5): 2282-2289.

100. Bokobza L. Multiwall carbon nanotube-filled natural rubber: Electrical and mechanical properties. Express Polym Lett 2012; 6: 213-223.

101. Choi SS. Improvement of properties of silica-filled natural rubber compounds using polychloroprene. J Appl Polym Sci 2002; 83: 2609-2616.

102. Muhr AH, Roberts AD. Rubber abrasion and wear. Wear 1992; 158, 213-228.

103. Tabsan N, Wirasate S, Suchiva K. Abrasion behavior of layered silicate reinforced natural rubber. Wear 2010; 269, 394-404.

104. http://iluvthailand.wordpress.com/2008/02/08/difference-between-gasohol-95-and-gasohol-91/

105. Klüppel M. The role of disorder in filler reinforcement of elastomers on various length scales, Adv Polym Sci 2003; 164: 1–86.

106. Sreeja TD, Kutty SKN. Acrylonitrile butadiene rubber/reclaimed rubber-nylon fiber composite. Adv Polym Tech 2001; 20(4): 281-288.

107. Sreeja TD, Kutty SKN. Studies on Acrylonitrile butadiene rubber-short nylon fiber composites. J Elastom Plast 2002; 34(2): 157-169.

108. Kok CM. The effects of compounding variable on the reversion process in the sulphur vulcanization of natural rubber. Eur Polym J 1987; 23: 611-615.

109. Ayala JA, Hess WM, Kistler FD, Joyce GA. Carbon-Black-Elastomer Interaction. Rubber Chem Technol. 1991; 64: 19-39.

110. Mark JE, Erman B, Eirich FR. Science and technology of rubber. London: Acadamic Press; 1994.

111. http://www.electronics-cooling.com/2001/11/the-thermal-conductivity-of-rubbers-elastomers/

112. Bag DS, DubeyR, Zhan N, Xie J, Varadan VK, Lal1 D, Mathur GN. Chemical functionalization of carbon nanotubes with 3-methacryloxypropyltrimethoxysilane (3-MPTS). Smart Mater Struct 2004; 13: 1263–1267.

113. Velasco-Santos C, Martinez-Hernandez AL, Brostow W, Casta VM. Influence of silanization treatment on thermomechanical properties of multiwalled carbon nanotubes: Poly(methylmethacrylate) Nanocomposites. J Nanomater 2011; 1-9.

114. Han Y; Huifang C, Dajun C. Hydrogen bond interaction in poly(acrylonitrile-co-methylacrylate)/attapulgite nanocomposites. Polym Eng Sci 2010; 50: 312-319.

115. Park JG, Cheng Q, Lu J. “Thermal conductivity of MWCNT/epoxy composites: the effects of length, alignment and functionalization. Carbon 2012; 50: 2083-2090.

APPENDIX

Table A1 Properties of P blends in MD and TD with various MWCNT loadings.

Properties	**MWCNT content**									
	0 phr		**2 phr**		**4 phr**		**5 phr**		**6 phr**	
	MD	**TD**	**MD**	**TD**	**MD**	**TD**	**MD**	**TD**	**MD**	**TD**
Tensile strength (MPa)	17.18±1.41	17.12±1.71	20.26±1.02	18.3±0.75	27.31±0.9	20.77±0.57	22.04±1.03	20.45±1.08	17.89±0.99	12.71±0.44
100% Modulus	0.86±0.03	0.84±0.01	1.98±0.29	1.67±0.05	3.09±0.15	2.12±0.21	3.12±0.22	2.92±0.08	3.41±0.31	2.94±0.17
300% Modulus	2.03±0.13	2.01±0.16	4.47±0.63	4.05±0.39	8.07±0.09	6.21±0.57	8.54±0.32	7.43±0.27	8.87±0.05	8.36±0.54
Elongation at break (%)	527.9±14.1	525.3±11.0	501.2±16.4	491.1±18.1	489.6±10.5	483.8±20.7	482.7±19.8	479.3±20.9	442.8±18.1	381.5±19.1
Tear strength (kN/m)	42.57±2.20	42.51±2.40	51.41±4.30	45.98±2.45	54.21±0.98	50.96±1.02	57.25±1.07	53.12±1.33	60.01±0.53	56.87±0.86
Electrical conductivity (S/m)	4.78E-11	4.81E-11	2.35E-09	5.88E-10	4.23E-04	2.74E-06	4.25E-04	5.49E-06	5.21E-04	1.68E-05

Table A2 Properties of C blends in MD and TD with various MWCNT loadings.

Properties	**MWCNT content**									
	0 phr		**2 phr**		**4 phr**		**5 phr**		**6 phr**	
	MD	**TD**	**MD**	**TD**	**MD**	**TD**	**MD**	**TD**	**MD**	**TD**
Tensile strength (MPa)	17.63±0.56	18.43±0.56	15.6±0.82	11.78±1.26	14.1±1.11	11.23±1.17	13.01±0.44	11.08±1.12	12.03±0.87	10.11±0.74
100% Modulus (MPa)	0.84±0.01	0.83±0.01	1.3±0.03	1.19±0.01	1.52±0.10	1.47±0.12	1.82±0.14	1.66±0.03	1.9±0.08	1.75±0.13
300% Modulus (MPa)	1.9±0.05	1.9±0.02	3.9±0.08	2.83±0.07	4.39±0.17	4.01±0.19	4.93±0.42	4.28±0.08	5.02±0.13	4.67±0.14
Elongation at break (%)	553.3±10.2	552.8±10.8	472±11.2	440.03±11.1	471.0±12.2	382±12.5	453.38±16.9	378.22±16.16	418±18.52	362.90±18.4
Tear strength (kN/m)	42.18±2.47	41.05±1.47	44.9±1.34	41.97±3.39	50.9±1.20	47.85±4.54	53.59±1.95	48.23±5.68	54.1±2.11	53.05±9.88
Electrical conductivity (S/m)	4.76E-12	5.18E-12	2.27E-10	5.24E-11	1.40E-06	3.34E-07	2.73E-06	7.14E-07	4.56E-06	1.91E-06

Table A3 Properties of P and C blends with various MWCNT loadings.

Properties	**Method**									
	P					**C**				
	0 phr	**2 phr**	**4 phr**	**5 phr**	**6 phr**	**0 phr**	**2 phr**	**4 phr**	**5 phr**	**6 phr**
Hardness (Shore A)	44.7±0.2	53.1±0.1	58.5±0.3	58.8±0.2	61.2±0.4	44.1±0.1	49.2±0.0	52.2±0.5	53.9±0.3	54.7±0.1
Abrasion loss (mm^3)	415.5±10.9	319.5±5.0	289.3±11.1	274.7±16.2	263.2±8.5	411.2±15.2	329.7±12.2	323.5±12.3	318.8±14.5	311.2±1.9
Thermal conductivity (W/mK)	0.187±0.002	0.223±0.001	0.374±0.004	0.259±0.004	0.258±0.001	0.185±0.001	0.207±0.001	0.226±0.002	0.241±0.001	0.242±0.001
Volume resistivity (Ohm/m)	2.78E+10	8.70E+04	7.20E+0.3	2.78E+03	1.69E+03	2.77E+10	2.73E+06	1.48E+05	4.42E+04	3.04E+04
Dichroic ratio	N/A	1.16±0.12	2.10±0.16	1.20±0.17	1.18±1.20	N/A	1.12±0.11	1.14±0.13	1.18±0.14	1.20±0.16
Oil resistance (Gasohol oil)	154.7±1.1	133.3±1.2	124.4±2.2	122.6±2.6	121.4±2.0	154.8±0.9	141.33±3.4	134.2±2.0	131.5±0.83	130.3±0.9
Oil resistance (Hydraulic oil)	41.5±0.6	26.3±2.3	21.5±2.7	20.7±1.3	19.8±2.2	41.9±0.1	37.2±2.0	32.3±4.4	31.1±3.3	31.7±2.1
Heat build-up (°C)	9.0±0.0	11.7±0.6	12.3±0.6	15.3±0.5	16.3±0.5	8.7±0.6	13.3±0.5	14.0±0.0	16.0±0.0	17.0±0.0
Dynamic compression set (%)	2.86±0.06	3.31±0.03	3.41±0.04	4.10±0.02	4.43±0.02	3.03±0.02	3.72±0.03	4.12±0.02	4.24±0.01	4.68±0.08

Table A4 Properties of mNR blends at various blend ratios in MD and TD.

Properties	**NR/NBR**									
	100/0		**70/30**		**50/50**		**30/70**		**0/100**	
	MD	**TD**	**MD**	**TD**	**MD**	**TD**	**MD**	**TD**	**MD**	**TD**
Tensile strength (MPa)	25.07±1.02	17.63±0.51	25.42±1.46	21.75±0.88	26.84±0.61	21.01±0.84	15.10±1.35	11.82±0.32	N/A	N/A
100% Modulus	2.35±0.02	2.09±0.01	2.98±0.01	2.43±0.04	3.07±0.02	2.55±0.04	3.09±0.01	2.57±0.05	N/A	N/A
Elongation at break (%)	483.1±10.2	498.9±9.1	475.3±17.01	494.0±14.0	473.2±10.58	481.67±10.67	343.7±8.5	375.5±15.0	N/A	N/A
Tear strength (kN/m)	88.73±2.46	79.22±3.12	71.21±1.41	68.24±1.35	53.92±0.45	52.02±1.14	48.5±3.01	46.63±0.52	N/A	N/A

Table A5 Properties of **mNBR** blends at various blend ratios in MD and TD.

Properties	**NR/NBR**									
	100/0		**70/30**		**50/50**		**30/70**		**0/100**	
	MD	**TD**	**MD**	**TD**	**MD**	**TD**	**MD**	**TD**	**MD**	**TD**
Tensile strength (MPa)	N/A	N/A	22.8±0.74	19.71±0.68	17.14±0.18	14.72±0.16	10.21±0.34	9.75±0.32	5.13±0.23	4.97±0.13
100% Modulus	N/A	N/A	2.68±0.03	2.26±0.04	2.84±0.03	2.35±0.06	2.89±0.05	2.40±0.07	3.07±0.04	2.86±0.04
Elongation at break (%)	N/A	N/A	458.8±10.28	460.3±16.5	471.7±11.31	483.9±9.02	341.0±8.48	380.2±14.0	200.0±10.0	220±16.0
Tear strength (kN/m)	N/A	N/A	64.88±2.56	60.63±2.92	47.12±0.95	44.09±1.11	43.05±2.55	40.83±2.43	38.71±1.84	34.71±0.84

Table A6 Properties of mNR and mNBR blends at various blend ratios.

Properties	Blend (NR/NBR)									
	mNR					mNBR				
	100/0	**70/30**	**50/50**	**30/70**	**0/100**	**0/100**	**70/30**	**50/50**	**30/70**	**100/0**
Hardness (Shore A)	52.0±0.0	54.5±0.0	56.1±0.3	55.4±0.2	N/A	N/A	52.5±0.4	53.2±0.2	53.5±0.3	56.2±0.2
Abrasion loss (mm^3)	296.6±8.5	275.9±7.2	268.1±8.1	230.7±5.0	N/A	N/A	293.2±4.5	290.6±4.3	247.8±1.9	130.8±15.2
Thermal conductivity (W/mK)	0.304±0.001	0.326±0.001	0.376±0.002	0.332±0.001	N/A	N/A	0.311±0.001	0.327±0.001	0.338±0.001	0.340±0.001
Dichroic ratio	2.20±0.14	2.10±0.11	2.11±0.16	1.80±0.13	N/A	N/A	1.78±0.09	1.62±0.13	1.48±0.08	1.37±0.15
Oil resistance (Gasohol oil)	166.7±6.7	133.5±3.4	115.5±2.6	93.6±2.1	N/A	N/A	153.9±4.8	133.2±2.8	100.0±3.5	64.3±2.6
Oil resistance (Hydraulic oil)	65.4±3.1	36.9±2.9	21.5±3.7	12.1±2.2	N/A	N/A	46.6±4.5	34.9±0.2	14.7±1.1	3.2±3.1
Heat build-up (°C)	10.0±0.0	11.0±0.0	13.0±0.0	15.0±0.0	N/A	N/A	12.0±0.0	15.0±0.0	16.0±0.0	17.0±0.0
Dynamic compression set (%)	3.11±0.04	3.16±0.03	3.44±0.05	4.61±0.07	N/A	N/A	3.44±0.04	3.56±0.03	3.62±0.02	3.65±0.05

Table A7 Properties of 50/50 NR/NBR blends containing MWCNT, OH-MWCNT and SiOH-MWCNT at different directions.

Properties	**Blend**					
	B_{MWCNT}		**$B_{OH-MWCNT}$**		**$B_{SiOH-MWCNT}$**	
	MD	**TD**	**MD**	**TD**	**MD**	**TD**
Tensile strength (MPa)	27.3±0.9	20.8±0.6	28.4±1.3	21.1±3.1	31.9±2.1	24.2±1.4
100% Modulus	3.09±0.05	2.12±0.21	3.17±0.07	2.16±0.03	3.79±0.17	2.24±0.10
300% Modulus	8.07±0.09	6.21±0.57	8.14±0.13	6.43±0.07	8.82±0.17	6.67±0.21
Elongation at break (%)	489.65±10.58	483.87±20.72	570.15±13.4	541.86±14.32	567.20±15.53	531.48±8.20
Tear strength (kN/m)	54.21±0.98	52.06±1.20	58.72±0.05	54.87±1.12	68.71±1.06	63.17±1.18
Electrical conductivity (S/m)	4.24E-04	3.22E-04	4.36E-04	3.28E-04	4.39E-04	3.33E-04
Storage modulust at 30 °C (MPa)	8.38±0.05	7.30±0.21	8.40±0.08	7.50±0.03	8.70±0.07	7.90±0.10

Table A8 Properties of 50/50 NR/NBR blends containing MWCNT, OH-MWCNT and SiOH-MWCNT.

Properties	Blend		
	B_{MWCNT}	$B_{OH\text{-}MWCNT}$	$B_{SiOH\text{-}MWCNT}$
Hardness (Shore A)	56.1±0.3	57.8±0.0	58.9±0.2
Abrasion loss (mm^3)	268.1±8.1	248.3±7.2	236.5±4.4
Thermal conductivity (W/mK)	0.376±0.011	0.368±0.021	0.373±0.023
Dichroic ratio	2.1±0.2	2.3±0.2	2.3±0.2
Oil resistance (Gasohol oil)	115.5±2.6	112.6±1.7	103.1±1.5
Oil resistance (Hydraulic oil)	24.5±3.7	19.2±2.9	15.6±3.1
Heat build-up (°C)	13.5±0.0	12.0±0.0	11.0±0.0
Dynamic compression set (%)	3.4±0.04	3.38±0.07	3.24±0.03

BIOGRAPHY

NAME	Mr. Pattana Kueseng
DATE OF BIRTH	November 2, 1983
PLACE OF BIRTH	Trang, Thailand
INSTITUTIONS ATTENDED	Prince of Songkla University, 2002-2006: Bachelor of Science (Rubber Technology) Mahidol University, 2006-2009: Master of Science (Polymer Science and Technology) Mahidol University 2009-2014 Doctor of Philosophy (Polymer Science and Technology)
RESEARCH GRANTS	The Office of the National Research Council of Thailand, 2007-2008 The Royal Golden Jubilee Ph.D. Program, The Thailand research Fund, Grant No.PHD/0013/2553, 2010-2014
EXPERIENCES	Mahidol University, 2008-2010: Teaching Assistant
HOME-ADDRESS	121 Moo 7, Bornamron, Kantang. Trang, 92110